

Predicting Temperature Patterns and Flow Behaviour of Poorly Constrained Geothermal fields: The Case of Songwe Extensional Basin (Tanzania)

Nnko, M.P.

DOI

[10.4233/uuid:f429112c-a2e2-4e53-9b7a-d05fdf7bf4c4](https://doi.org/10.4233/uuid:f429112c-a2e2-4e53-9b7a-d05fdf7bf4c4)

Publication date

2025

Document Version

Final published version

Citation (APA)

Nnko, M. P. (2025). *Predicting Temperature Patterns and Flow Behaviour of Poorly Constrained Geothermal fields: The Case of Songwe Extensional Basin (Tanzania)*. [Dissertation (TU Delft), Delft University of Technology]. <https://doi.org/10.4233/uuid:f429112c-a2e2-4e53-9b7a-d05fdf7bf4c4>

Important note

To cite this publication, please use the final published version (if applicable).
Please check the document version above.

Copyright

Other than for strictly personal use, it is not permitted to download, forward or distribute the text or part of it, without the consent of the author(s) and/or copyright holder(s), unless the work is under an open content license such as Creative Commons.

Takedown policy

Please contact us and provide details if you believe this document breaches copyrights.
We will remove access to the work immediately and investigate your claim.

**PREDICTING TEMPERATURE
PATTERNS AND FLOW BEHAVIOUR OF
POORLY CONSTRAINED GEOTHERMAL
FIELDS: THE CASE OF SONGWE
EXTENSIONAL BASIN
(TANZANIA)**



Martha Phineas Nnko

PREDICTING TEMPERATURE PATTERNS
AND FLOW BEHAVIOUR OF POORLY
CONSTRAINED GEOTHERMAL FIELDS: THE
CASE OF SONGWE EXTENSIONAL BASIN
(TANZANIA)

**Predicting temperature patterns and flow behaviour of poorly
constrained geothermal fields:
the case of the Songwe extensional basin (Tanzania)**

Dissertation

for the purpose of obtaining the degree of doctor
at Delft University of Technology
by the authority of the Rector Magnificus,
Prof.dr.ir. T.H.J.J. van der Hagen,
chair of the Board for Doctorates
to be defended publicly on
Thursday 27 March 2025 at 15:00 o'clock

by

Martha Phineas NNKO

Master of Science in Engineering Management,
University of Dar es Salaam, Tanzania
born in Ulanga, Tanzania

This Dissertation has been approved by the promotor.

Promotor: Prof. dr. G. Bertotti

Promotor: Prof. dr. D. Bruhn

Promotor: Dr. M. Brehme

Composition of the doctoral committee:

Rector Magnificus,

Chairperson

Prof. dr. G. Bertotti,

Delft University of Technology, promotor

Prof. dr. D. Bruhn,

Delft University of Technology, promotor

Dr. M. Brehme

ETH Zürich, Switzerland, promotor

This research received funding from the Netherlands Government through the NUFFIC Tanzania-Dutch Energy Capacity Building project (NICHE-TZA-260). The project had a strong capacity building component aspiring to provide knowledge and expertise to Tanzania counterparts in the wide field of geothermal energy studies.



Keywords: Geothermal energy, Geological modelling, Thermal modelling, Geochemical modelling, Natural state modelling, Production prediction

Printed by: Gilderprint

Cover by: GG

CONTENTS

SUMMARY	VI
SAMENVATTING	VII
LIST OF FIGURES	VIII
LIST OF TABLES	X
1 INTRODUCTION	1
1.1 GENERAL INFORMATION	1
1.1.1 Background of the Study	1
1.1.2 Geothermal Energy.....	2
1.1.3 Geothermal Energy in Tanzania.....	4
1.1.4 The Geology of Tanzania	4
1.2 SONGWE GEOTHERMAL PROSPECT	7
1.2.1 Geology	7
1.2.2 Hot Springs and Geochemistry	9
1.2.3 Hydrogeology and Possible Scenarios of Geothermal Prospect	11
1.3 RESEARCH GOAL	11
1.3.1 Geothermal Exploration	11
1.3.2 Research Questions	12
1.3.3 Research Approach and Thesis Outline	12
2 CONDUCTIVE THERMAL MODEL.....	15
2.1 INTRODUCTION	15
2.2 GEOLOGIC MODEL	16
2.2.1 Input Data and Architecture	16
2.2.2 Building the Model	17
2.2.3 Results	17
2.3 THERMAL MODEL	18
2.3.1 Approach, Boundary Conditions and Parameters	18
2.3.2 Building the Thermal Model	19
2.3.3 Results: 2D Model.....	20
2.3.4 Results: 3D model.....	22
2.3.5 Sensitivity Analysis	23
2.4 DISCUSSION	26
2.5 CONCLUSION.....	28
3 IMPLICATION OF GEOCHEMICAL STUDIES.....	29
3.1 INTRODUCTION	29
3.2 GEOLOGY AND STRUCTURAL GEOLOGY	31
3.2.1 Regional Geological Setting.....	31
3.2.2 Structural Geology of the Songwe Basin	33
3.3 METHODS AND MATERIALS	33
3.3.1 Sampling and Analysis.....	33
3.3.2 Geochemical Modelling.....	34
3.4 RESULTS	38
3.4.1 Thermal Springs Characterization	38
3.4.2 Rock Composition	39
3.4.3 Element Ratios in Thermal Water.....	40
3.4.4 Geothermometry.....	42
3.4.5 Mixing Model	45
3.4.6 Reservoir Fluid Chemistry	47
3.4.7 Mineral Saturation Indices	50
3.5 DISCUSSION	52
3.5.1 Hydrogeochemistry	52

3.5.2	<i>Reservoir Temperature Estimation</i>	52
3.5.3	<i>Water-Rock Interaction Modelling</i>	53
3.5.4	<i>Conceptual Fluid Flow Model</i>	55
3.6	CONCLUSION	57
4	NATURAL STATE NUMERICAL MODELLING	59
4.1	INTRODUCTION	59
4.2	METHOD	60
4.2.1	<i>Model Description - Geometry</i>	61
4.2.2	<i>Mesh</i>	61
4.2.3	<i>Rock Properties</i>	62
4.2.4	<i>Boundary and Initial Conditions</i>	62
4.2.5	<i>Calibration of the Model</i>	64
4.3	SIMULATION RESULTS AND DISCUSSION	64
4.3.1	<i>Updated Conceptual Model regarding Fluid Flow</i>	64
4.3.2	<i>Numerical Fluid Flow Model</i>	66
4.4	DISCUSSION	72
4.5	CONCLUSION	73
5	CONCLUSION	74
5.1	INTRODUCTION	74
5.2	TEMPERATURE, PERMEABILITY AND FLUID DISTRIBUTION	75
5.3	PRODUCTION PREDICTION	76
5.3.1	<i>Numerical Simulation with Well Placement</i>	76
5.3.2	<i>Production Simulation Results and Discussion</i>	77
5.4	RECOMMENDATIONS	79
	BIBLIOGRAPHY	81
	ACKNOWLEDGEMENTS	87
	CURRICULUM VITAE	89

SUMMARY

Energy plays a fundamental role in societies impacting everything from basic human needs like lighting, cooling and heating to complex industrial processes that significantly influence social development, economic growth, and national security particularly in terms of access and affordability for all citizens. The world's electricity demand grew by 2.2% in 2023 and is expected to rise at a faster rate by an average of 3.4% in 2026 (IEA, 2024). With the global climate warming, it is important to reduce our societal impact on Earth by using clean energy sources. One of the clean sources is geothermal energy which has a great potential to reduce dependency on the fossil fuels. Geothermal energy sources can deliver both, heat and electricity. Tanzania has a huge geothermal potential that has not yet been used and has only been explored to a limited extent. This thesis attempts to identify the geothermal potential of southwest Tanzania with appropriate drilling zones by assessing the main components of a geothermal system reservoir which are temperature, permeability and fluid flow at Songwe Tanzania. It is one of the identified potential development areas with very little information available.

The work flow begins with chapter 2 where a geological and thermal numerical model is set up to simulate the temperature at depth. The thermal model considers pure conductive heat flow to achieve a first idea of the temperature distribution in the different geological layers.

Chapter 3 describes the conducted field study at the thermal spring areas as well as the laboratory analysis of the samples in order to understand the geothermal fluid source by using geochemical modelling, obtain the reservoir temperature through geothermometer calculation and locate the up-flow and the outflow zones of the geothermal field.

In chapter 4 numerical simulations of fluid and convective heat flow are performed to allow understanding the heat transport by fluids and the hydrogeological behaviour of the geothermal reservoir by varying thermal and physical parameters.

Chapter 5 shows possible drilling locations for a first geothermal well in the study area, whereby areas of different productivity are distinguished.

SAMENVATTING

Energie speelt een fundamentele rol in samenlevingen die van invloed zijn op alles, van fundamentele menselijke behoeften zoals verlichting, koeling en verwarming tot complexe industriële processen die de sociale ontwikkeling, economische groei en nationale veiligheid aanzienlijk beïnvloeden, vooral in termen van toegang en betaalbaarheid voor alle burgers. De mondiale vraag naar elektriciteit groeide in 2023 met 2,2% en zal in 2026 naar verwachting sneller stijgen, met gemiddeld 3,4% (IEA, 2024). Met de mondiale opwarming van het klimaat is het belangrijk om onze maatschappelijke impact op de aarde te verminderen door gebruik te maken van schone energiebronnen. Eén van de schone bronnen is geothermische energie, die een groot potentieel heeft om de afhankelijkheid van fossiele brandstoffen te verminderen. Geothermische energiebronnen kunnen zowel warmte als elektriciteit leveren. Tanzania heeft een enorm geothermisch potentieel dat nog niet is benut en slechts in beperkte mate is verkend. Dit proefschrift probeert het geothermische potentieel van zuidwest Tanzania met geschikte boorzones te identificeren door de belangrijkste componenten van een geothermisch systeemreservoir te beoordelen, namelijk temperatuur, permeabiliteit en vloeistofstroom in Songwe Tanzania. Het is een van de geïdentificeerde potentiële ontwikkelingsgebieden waarover zeer weinig informatie beschikbaar is.

De werkstroom begint met hoofdstuk 2, waar een geologisch en thermisch numeriek model wordt opgezet om de temperatuur op diepte te simuleren. Het thermische model houdt rekening met zuivere geleidende warmtestromen om een eerste idee te krijgen van de temperatuurverdeling in de verschillende geologische lagen.

Hoofdstuk 3 beschrijft het uitgevoerde veldonderzoek in de gebieden met thermale bronnen, evenals de laboratoriumanalyse van de monsters om de geothermische vloeistofbron te begrijpen met behulp van geochemische modellen, de reservoirtemperatuur te verkrijgen door middel van geothermische berekeningen en de opwaartse en uitstroomzones van het geothermische veld te lokaliseren.

In hoofdstuk 4 worden numerieke simulaties van vloeistof- en convectieve warmtestromen uitgevoerd om inzicht te krijgen in het warmtetransport door vloeistoffen en het hydrogeologische gedrag van het geothermische reservoir door het variëren van thermische en fysische parameters.

Hoofdstuk 5 toont mogelijke boorlocaties voor een eerste geothermische put in het studiegebied, waarbij onderscheid wordt gemaakt naar gebieden met verschillende productiviteit.

List of Figures

Figure 1.1 The Geology of Tanzania and of surrounding countries (modified from Mtabazi, 2018). Red rectangle is the Songwe area.....	5
Figure 1.2 Geology map of the Songwe area (Hinz et al., 2018)	7
Figure 1.3 - Stratigraphic section of the Songwe Basin (Ebinger et al., 1989) Qns* are volcanistics lake sediments, Ns are fluvio-lacustrine sediments, Ob are basalt unit, Sb are Plivine basalts and picrites, K are Red sandstones, JR are Karoo sequences, Pu is a thin melanephelinite, Po is a 5m thick olivine basalt.....	8
Figure 1.4 - Stratigraphic cross section of the Songwe Basin (Delvaux et al., 1991)	9
Figure 1.5 Geologic map of Songwe hot spring area (red circle) and travertine deposits (highlighted in blue) modified after (Alexander et al., 2016).....	10
Figure 1.6 - Schematic geological conceptual models for Songwe hot springs (Alexander et al., 2016)	11
Figure 1.7 Research questions for this study.....	12
Figure 1.8 Research approach summary	13
Figure 2.1 Songwe geologic map (Hinz et al., 2018).....	16
Figure 2.2 Songwe 2D geologic model.....	17
Figure 2.3 Songwe 3D geological model (a); transparent 3D model showing spring fracture corrido corridors and Mbeya fault (b). The same colour code is used as in 2D model. X-axis is eastings, Y-axis is northings and Z-axis is the depth.	18
Figure 2.4 2D Temperature simulation results	20
Figure 2.5 Depth profile lines A, B and C.....	21
Figure 2.6 Temperature at depth in profiles A,B and C.....	22
Figure 2.7 Map view of temperature distribution at depths (from the surface) of 1km (panel a), 2km (panel b), 3km (panel c) and 4km (panel d). Curved lines are the lithological boundaries on map view, straight line on the top right is the Mbeya fault.....	23
Figure 2.8 Profile line D where temperature simulation results are observed.....	24
Figure 2.9 Sensitivity analysis using different values of heat flow as indicated in the legend.....	24
Figure 2.10 Effect of thermal conductivity on temperature distribution	25
Figure 3.1 Songwe geological map modified after (Alexander et al., 2016), showing thermal spring locations..	32
Figure 3.2 Schematic section across the Songwe half-graben. The overall geometry of the basin is obtained combining surface data from Alexander et al., (2016). The deep part of the basin is inferred from EAGER et al., (2018). The two reports provide a contrasting hypothesis for the position of the boundary between the Karoo and Red Sandstones (dashed line in our figure). The flow paths correspond to those predicted by Alexander et al., (2016).....	32
Figure 3.3 Geochemical modelling step using Phreeqc in Songwe geothermal area. 1a, 1b and 1c are for the model at surface temperature, while 2a, 2b, and 2c are for the model at reservoir conditions.....	35
Figure 3.4 Water type of thermal manifestations in the Songwe area from 1959 to 2019 based on anion concentrations	39
Figure 3.5 Relative concentration of Li-Cl-B of Songwe thermal manifestations from 1998 to 2019. (Ellis & Wilson, 1960; Nicholson, 1993).....	41
Figure 3.6 Relative concentrations of Na-K-Mg of Songwe thermal manifestations from 1959 to 2019 plotted in Giggenbach diagram for (a) high temperature systems (W. F. Giggenbach, 1988) and (b) lower temperature systems (< 200°C) (Giggenbach & Soto, 1992).....	44
Figure 3.7 Diagram of SiO ₂ vs log K ₂ /Mg of Songwe thermal water, concentration in mg/l, based on Giggenbach and Glover (1992). The curves provide information on equilibrium attainment for SiO ₂ and K-Mg geothermometers. Most thermal water plots near the quartz curve, suggesting that equilibria with quartz took place rather than with chalcedony.....	45
Figure 3.8 Mixing model of silica-enthalpy (based on chalcedony and quartz geothermometry temperature) and enthalpy-chloride (based on quartz geothermometry temperature). Silica concentration from previous geochemistry studies (see Table 3.1). The mixing lines on both diagrams are drawn from cold Songwe river water to the quartz solubility and to the steam line. Intersection points are based on the spring with higher concentration of silica (line A) and lower concentration (line B). Ikumbi springs were excluded from the mixing line because they were suspected as steam-heated waters.....	46
Figure 3.9 Linear relationship between Cl and B of Songwe thermal springs.....	47
Figure 3.10 The scheme of water-rock interaction for surface thermal springs (10a and 10b) and for estimated reservoir water (10c and 10d) at 125 °C (black ink) and 148 °C (white ink) when reacting with different lithology in the Songwe geothermal area. Lithologies are shown in different colors including porosity and permeability values. Arrows show the reaction pathway, covering the reaction with 1-3 layers and resulting saturation indices. The highlighted minerals in blue correlate with the highlighted minerals at surface of each thermal spring. (a) model outputs only focusing on calcite (calc.) and aragonite (arag.); it suggests the thermal springs are only in	

contact with Red Sandstone, and Ikumbi is also in contact with metamorphic rocks and Karoo group (longest arrow). Ikumbi springs react with all lithologies in the Songwe field, supported by the precipitation of analcime, muscovite and smectite. (b) model outputs including all mineral groups: Apt (apatite), Car (carbonates), Clay, WM (weathered metamorphics), and WV (weathered volcanics). (c) model outputs focusing on minerals measured and precipitated in the model reactions consisting of HAp (Hydroxyapatite), FAp (Fluoroapatite), Illite, Smec (smectite), Cl (chlorite), Non-Ca (nontronite-Ca), Non-Na (nontronite-Na), Cal (calcite) and Kao (Kaolinite). (d) model outputs of mineral groups percentage for the best fitting scenario. ^aThis study; ^bBeyer & Clutsom (1978).

Figure 3.11 Conceptual fluid flow model of the Songwe area after hydrogeochemical model interpretation. Showing fluid infiltration in the NE and supposedly SW, fluids rising along the fault and percolating within the sandstones before discharging in hot springs (Christopher, 2015). These are two different pathways, one is the Ikumbi which is a deep source and another one which is less deep; the two pathways do not cross in 3D	55
Figure 4.1 Meshed grid for the 3D geometry. The x-axis represents the GPS-easting coordinates, the y-axis represents the GPS-northing and the z-axis is the depth of the model	56
Figure 4.2 Boundary condition visualization. R=Rambo hot springs fractures; K=Kaguri hot springs fractures; I=Lyola hot springs fractures; M=Main hot springs fractures; 4=theoretical borehole location 4	63
Figure 4.3 Simulated reservoir temperature at geothermal gradient of 35°C/km (a) for the whole Red Sandstone volume and (b) for the theoretical borehole location 4 shown on figure 4.2b	64
Figure 4.4 General flow regime in the Songwe basin with two reservoir systems feeding the hot springs. The main upflow area is close to Rambo and Kaguri springs. Also Cl, T and pH concentrations as well as CO ₂ flux and soil temperature support the general fluid flow pathways. CO ₂ and soil temperature data from Alexander et al. (2016)	65
Figure 4.5 Conceptual flow model of the Songwe geothermal system with potential fluid pathways(b), geological set-up of the underground based on a summary of the presented investigations in this study(a)	66
Figure 4.6 Simulated temperature distribution and fluid flow direction(white arrows) in the model derived from the vertical sections (a)the thinnest part of the sediments towards the thickest part (d)	69
Figure 4.7 Simulated temperature distribution and fluid flow direction(white arrows) in the model derived from the vertical sections (c) and (d). The vertical sections are derived from profiles lines (c) and (d) respectively shown in figure 4.8. Vertical section (d) is located at the thickest part of the lithologies	69
Figure 4.8 3D model geometry showing lines a, b, c and d where vertical sections were derived from. Line (a) cuts through the thinnest part of the lithological layers and line (d) cuts through the thickest part	70
Figure 4.9 Fluid flow across different layers at a distance of 1700m below the surface. Top right is the basement, followed by Red Sandstone, Karoo and the Basement. More flow is observed on the Red Sandstone layer than other layers shown by longer arrows	70
Figure 4.10 Vertical section from the model simulation showing permeability distribution in the lithologies. The upper layer is the Neogene volcanics followed by Red Sandstone, Karoo and the basement	71
Figure 4.11 Map view of pressure distribution and fluid flow direction (white arrows) at different depths below the surface, as indicated in each figure. The NW-SE straight line in all figures is the map view of Mbeya fault followed by: (a) Neogene and Red Sandstone layer; (b) Red Sandstone, Karoo & basement; (c) Karoo & basement; (d) only basement Note that colour scales vary with pressure scales and depth from (a) – (d)	72
Figure 5.1 Production well locations shown by black rounded numbers 1, 2,3,4,5,6,7 and 8. A fixed injection well is shown by a blue rounded "IW"	77
Figure 5.2 Simulated production temperature at location 4 using a geothermal gradient of 35°C/km	79

List of Tables

Table 1.1 Reservoir temperature classification summary (Lee, 1996)	3
Table 2.1 Parameters adopted in modelling work from (a) Jones (2020) (b) Nyblade et al. (1990) (c) Didas et al. (2022) (d) Kuznik et al. (2013) (e) Mutabazi (2023) unpublished.....	19
Table 2.2 Temperature percentage increase at profile C with respect to profile B	22
Table 2.3 Temperature range at depth for the horizontal profiles.....	23
Table 2.4 Calculated linear vertical temperature gradients of different temperature profiles obtained by simulation of different values of heat flux	25
Table 2.5 Effect of thermal conductivity on temperature distribution.....	26
Table 3.1 Field parameter and chemical analysis of thermal manifestation in this study (2019) and other studies previously (Alexander et al., 2016; James, 1959; Kraml et al., 2008; Makundi and Kifua, 1985; Mnjokava, 2007; Nzaro, 1970; Pisarskii et al., 1998; SWEC	36
Table 3.2 Mineral composition and rock physical properties of selected rock formations in the Songwe graben	40
Table 3.3 Ratios of element concentrations in thermal manifestations in this study (2019) and former studies from: (Alexander et al., 2016; James, 1959; Kraml et al., 2008; Makundi and Kifua, 1985; Mnjokava, 2007; Nzaro, 1970; Pisarskii et al., 1998; SWECO, 1978)	41
Table 3.4 Estimation of reservoir temperature by different geothermometers for thermal manifestations in this study (2020) and former studies from: (Alexander et al., 2016; James, 1959; Makundi and Kifua, 1985; Pisarskii et al., 1998)	44
Table 3.5 Estimated chemical composition of reservoir fluid at 125 oC and 148 oC based on the chemical concentration of thermal springs using steam fraction calculation, K-Mg geothermometer and calcite dissolution equilibria calculation for pH.	49
Table 3.6 Scenario reactions for modelling the fluid-rock interactions in Songwe geothermal area.	51
Table 4.1 Assigned pressure and temperature values as boundary conditions on fracture corridors.....	63
Table 4.2 Simulated average reservoir temperature (whole Red Sandstone volume) at different geothermal gradients.....	67
Table 4.3 Fluid velocity distribution	70
Table 4.4 Permeability values used in the model	71
Table 4.5 Observed pressure values at different depths of Figure 4.5.....	72
Table 5.1 Production well scenarios and details.....	77
Table 5.2 Production well temperature at different locations.....	79
Table 5.3 Varying geothermal gradient at well location 4.....	79

1 INTRODUCTION

1.1 General Information

1.1.1 Background of the Study

Tanzania is one of the East African countries with a large amount of geothermal potential that has not been used yet and has only been explored to a limited extent. The national power system relies greatly on hydropower and natural gas. Willing to propose an alternative, the government of Tanzania has made geothermal development a priority (Mnjokava, 2015).

The achievements in neighbouring countries like Kenya which already has installed geothermal power with a total capacity of 865 MWe according to Omenda et al. (2021), serve as a great motivation for Tanzania to carry on with geothermal energy. Kenya has substantial geothermal resources and already producing fields along the Rift valley. The East African rift continues South of Kenya into Tanzania indicating the high geothermal potential of this country (Macharia et al., 2017).

Preliminary studies performed during the last ten years document the high potential of geothermal energy in Tanzania. The area around the city of Mbeya, located at the junction of two branches of the East African rift system has been identified as a first priority region from which two specific targets have been defined, the volcanic region of Ngozi and the half-graben of Songwe (Mnjokava, 2012).

In the frame of a large collaborative effort between Tanzania and the Kingdom of the Netherlands, NUFFIC, the Dutch organization for internationalization in education has sponsored the NICHE Tanzania-Netherlands Energy Project which researched the potential of renewable (geothermal) energy and the gas sector in Tanzania. In this frame, three PhD projects have been funded based at the University of Utrecht, University of Twente and Delft University of Technology, to investigate the potential of the Ngozi and Songwe domains. The project had a strong capacity building component aiming at providing knowledge and expertise to Tanzania counterparts in the wide field of geothermal energy studies. The knowledge was provided in terms of teaching geothermal energy related courses at the University of Dar es Salaam and consulting work with Tanzania geothermal company.

This study is the outcome of one of the PhD projects in the field of geothermal energy potential in Tanzania. The focus was on the Songwe basin as a model case, which can be applied to other potential locations in the rift, such as Ivuna, Kilambo, Mampulo, Kasimolo, Usangu basin, Lake Natron and Lake Manyara, to mention just a few.

1.1.2 Geothermal Energy

Geothermal energy is the heat from the Earth's interior which originates from the physical processes occurring inside our planet. In order to extract and utilize this large amount of heat, a carrier is required to transmit the heat towards accessible depths underneath the Earth's surface. Heat is first transferred by conduction from depth to the shallow subsurface and then by convection with fluids as the carrier. The fluid is mainly meteoric water that infiltrated into the Earth's crust in recharge areas, got heated, while percolating deeper through hot rocks, before it accumulated in permeable rock layers (reservoirs). Once heated, or even reaching boiled or supercritical conditions, fluids rise due to buoyancy effects and appear back at the surface in the form of hot springs, fumaroles, or similar manifestations (Barbier, 2002). Geothermal energy can be utilized by producing the hot fluids to the surface through wells. The hot fluids can be used directly for distributing heat or to generate electricity using turbines or binary power plants with secondary fluid cycles (Huddleston-Holmes & Hayward, 2011).

The use of geothermal energy depends mainly on the temperature of the fluids. A classification based on the reservoir temperature is the most common and can be estimated from geothermometry calculations in the exploration stage even before drilling (Hawkins & Tester, 2018). Low temperature geothermal resources (30-90°C) at shallower depths are mainly used for direct heat applications such as heating of buildings and chemical processing. Moderate temperature geothermal resources (90-150 °C) are suitable for both electricity generation and direct use. The high temperature geothermal resources (>150°C) are very useful for electricity generation (Pandey et al., 2018). There are a number of reservoir temperature classifications, which divide geothermal systems into low, intermediate and high temperature resources as shown in [Table 1.1](#)

Table 1.1 Reservoir temperature classification summary (Lee, 1996)

Source	Low-temperature resources (°C)	Intermediate-temperature resources (°C)	High-temperature resources (°C)
Benderitter and Cormy (1990)	< 100	100 - 200	> 200
Hochstein (1988)	< 125	125 - 225	> 225
Rybach (1981)	< 150	-	> 150
Muffler and Cataldi (1978)	< 90	90 – 150	> 150
Pandey (2018)	30 - 90	90 - 150	> 150

Furthermore, geothermal systems can be categorised by their geological, hydrogeological and heat transfer characteristics. The geological classification is defined by the distribution and characteristics of faults, fractures, lithology, stress field, and rock mechanics, while the hydrogeological classification defines the fluid flow and depends on the geochemistry of fluids and rocks, porosity, permeability and temperature distribution. The temperature distribution then mainly controls the heat transfer characteristics, which can be conductive or convective.

It is important to understand the geothermal system characteristics in order to successfully accomplish its commercial development. In general, three major pre-conditions need to be fulfilled for the successful installation of a geothermal power plant: sufficient heat, fluids and permeability. Based on that, geothermal systems are further divided into conventional and unconventional systems. Conventional (hydrothermal) geothermal systems have three main naturally occurring parameters, which are high subsurface temperatures, fluids and good permeability of the rock. Heat in conventional systems is transported mainly by fluids. Conventional geothermal systems include low enthalpy systems, medium enthalpy systems, high enthalpy systems with liquid-, vapour-dominated, or two-phase systems. Low enthalpy systems have lower temperatures, but a higher reservoir permeability. High enthalpy systems have high temperatures but a low permeability of the rock matrix and limited fractures in the system (Hawkins & Tester, 2018). Medium enthalpy systems show characteristics in between low- and high-enthalpy systems.

Nonconventional geothermal systems perform under extreme conditions because at least one of the major pre-conditions (heat, fluid, permeability) is not fulfilled. Some of the systems therefore only rely on conductive heat transport through rocks. Examples of nonconventional systems are supercritical or deep volcanic systems (450°C – 600°C), geo-pressured systems

(pressure gradient 210bar/km), enhanced geothermal systems (EGS) and advanced geothermal systems (AGS). Enhanced geothermal systems, for example, have high temperatures but lack natural rock permeability and/or fluid. Advanced geothermal systems use deep wells to extract heat energy from geologic formations through conductive heat transfer from the rocks to the fluid flowing in a closed loop system (Malek et al., 2022).

1.1.3 Geothermal Energy in Tanzania

Tanzania, among other East African countries, has a large resource potential of untapped geothermal energy (Teklemariam, 2005). The country is traversed by the East African rift system and related branches in north-south direction and has numerous domains with high heat flow of over 100mW/m² (Didas et al., 2022). Geothermal energy potentials in Tanzania are identified by hot springs located in the East African Rift System. The areas include the northern volcanic province of Kilimanjaro, Meru, Ngorongoro and the Rungwe Volcanic province in southwest Tanzania. Some coastal areas in the Rufiji basin, south of Dar es Salaam and to the north of Tanga region, also allocate hot springs attributed to rifting and intrusions (Mnjokava, 2013).

The total geothermal power potential is estimated to be 650MWe from 50 identified geothermal sites. From these sites, the Songwe area has an estimated geothermal energy potential of 100MWe (Mokveld & Eije, 2018). Therefore, the priority for exploration is currently given to the most promising geothermal areas, which are Ngozi and Songwe located in Mbeya, in southwest Tanzania. Geochemical, geophysical and field geology studies have been conducted in these two areas and are summarized below. However, a joint interpretation with a focus on potential drilling locations is still missing.

1.1.4 The Geology of Tanzania

The East African Rift (EAR) stretches from the Red Sea to Mozambique through Yemen, Eritrea, Djibout, Ethiopia, Kenya, Tanzania, Uganda, Rwanda, Burundi, the Democratic republic of Congo, Zambia, Malawi, Mozambique and Madagascar *Figure 1.1*. The rift branches into an Eastern and Western arm in Tanzania following pre-existing Proterozoic weak zones surrounding a stable Archean Tanzanian craton (Ebinger, 1989).

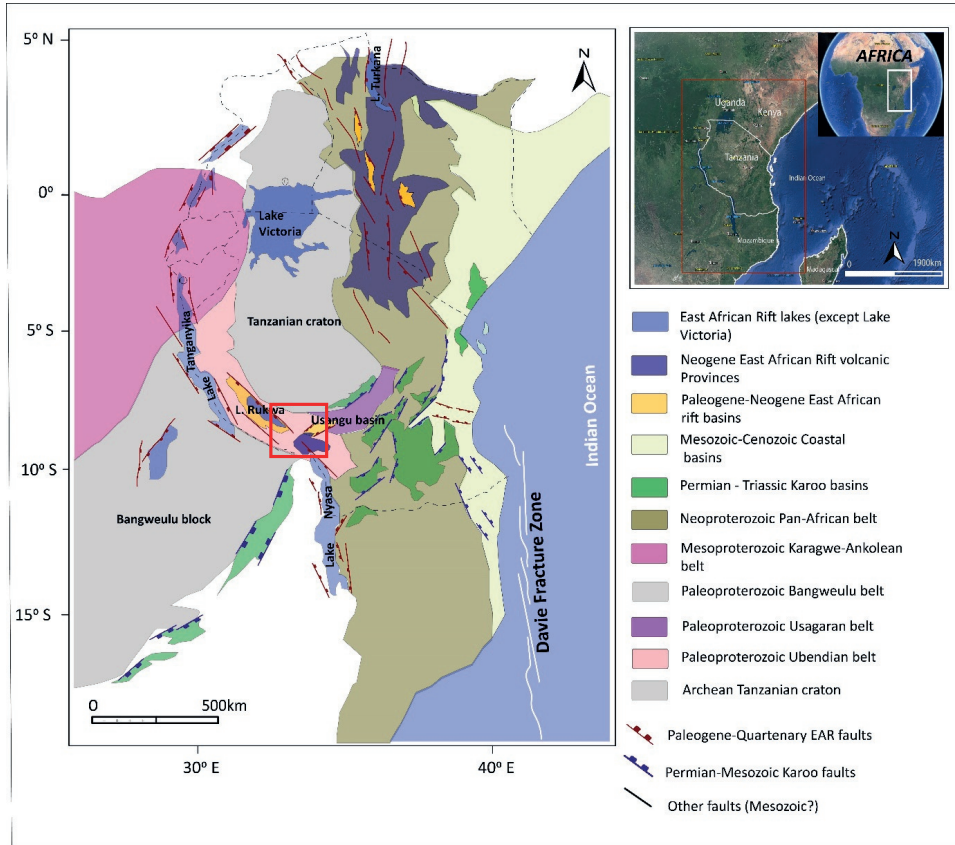


Figure 1.1 The Geology of Tanzania and of surrounding countries (modified from Mtabazi, 2018). Red rectangle is the Songwe area.

Tanzanian geology consists of three domains which are the oldest Archean Tanzanian craton, the Proterozoic mobile belts and Phanerozoic rocks. Archean rocks are visible in the central part of Tanzania and are composed of granitoids, granitic gneiss, greenstone complexes, migmatites, volcanics, amphibolites conglomerates, arenaceous argillaceous sediments turbidites and pelites (Borg et al., 1997). The Neoproterozoic Pan African Mozambique belt and Paleoproterozoic Usagaran belt build the eastern extent of Archean rocks in the Eastern part of Tanzania. The Mozambique belt is composed of varieties of rocks including meta-igneous (anorthosite), amphibolites and metasedimentary rocks which includes quartzites, pelites, graphitic schists and marbles (Johnson et al., 2003). Paleoproterozoic Usagaran rocks are exposed in the southern part of Tanzania craton and they consist of amphibolite, amphibolitized eclogites, semipelites, granulite metapelites, rare marbles and metavolcanics (Stern, 1994). The Western to Northern part of Tanzania is dominated by the Mesoproterozoic Karagwe ankolean

(Kibaran) and Paleoproterozoic Ubendian belt. The Karagwe ankolean (Kibaran) belt contains metavolcanics, conglomerate, metasedimentary rocks, granitoids, mafic and ultramafic layered complexes whereas the Ubendian belt consists of gneisses, eclogites, micaschists, quartzites, granulitic, metabasites, granites, metavolcanics, meta-anorthosite massifs and cordierite granulites (Fernandez-Alonso et al., 2012).

Phanerozoic sedimentary sequences and volcanic rocks are the youngest rock units in Tanzania. They are located in the rift structures formed as a result of Phanerozoic poly rift events that reactivated the pre-existing mobile belts (Delvaux & Hanon, 1991). The three recognized rifting phases in Tanzania are the Permo-Triassic (Karoo rifting), the Cretaceous and the Cenozoic rifting (Lambiase, 1989). The sedimentary sequences deposited throughout all the rifting phases consist of the Karoo Supergroup, the Red Sandstone Group and the Lake Beds respectively (Quennell et al., 1959). The main volcanic rocks comprise of large volumes of continental flood basalts, ignimbrites, nephelinite, phonolites, mugearites, rhyolites, trachytes and carbonatites (Baker et al., 1972).

The western branch of the rift passes along the western side of Lake Victoria and along the edge of the East Africa plateau (Mnjokava, 2014). It is composed of half grabens characterized by high angle normal rift faults oriented in NW-SE direction, it is seismically active but poor in magmatism (Koptev et al., 2015). The eastern branch runs NE-SW following the pre-existing Mozambique Mobile Belt, it is seismically less active and rich in magma compared to the western branch (Mulibo & Nyblade, 2016).

The western and eastern branches of the East African rift in Tanzania merge in the Rungwe volcanic province in the southern part of the country. The Rungwe area is volcanically active with typical volcanic rocks, such as basaltic, trachytic, tuffs and phonolitic lavas (Fontijn et al., 2012). The Songwe area (represented as red rectangle) in [Figure 1.1](#), focus of this study, is located in the southern part of the western branch of the East African Rift.

1.2 Songwe Geothermal Prospect

1.2.1 Geology

The Songwe basin is a NW-SE oriented and NE tilted half graben that rests on the Precambrian metamorphic basement reaching about 3 km depth along the Mbeya Range front fault [Figure 1.2](#)

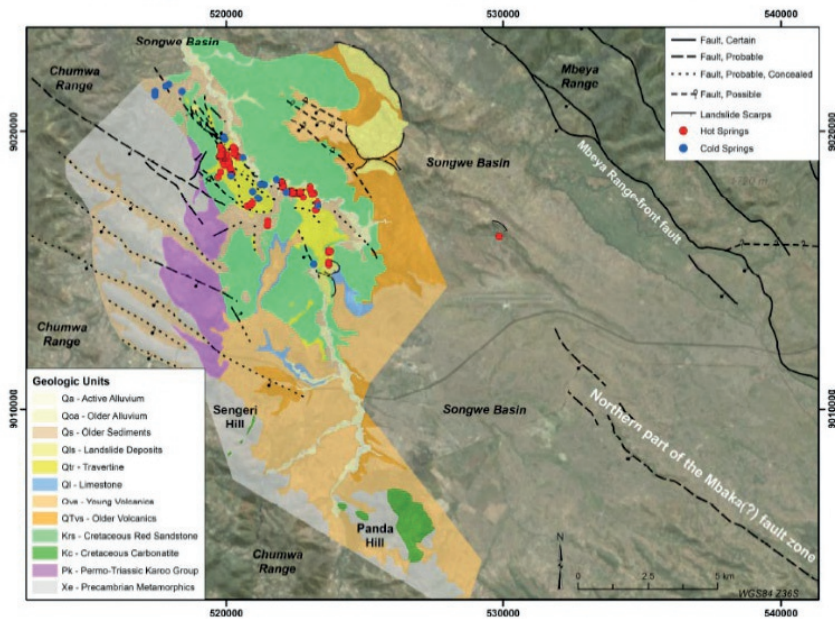


Figure 1.2 Geology map of the Songwe area (Hinz et al., 2018)

The stratigraphy of the Songwe basin overlying the complex basement consists of the Karoo supergroup, red sandstones, older volcanics, travertine, alluvium and the lake beds (Delvaux & Hanon, 1991; Ebinger, 1989; Roberts et al., 2004).

Roberts et al. (2004) present the most updated stratigraphy and age of the Red Sandstone group for the Songwe basin. Main units in the area of interest include the presence of both Cretaceous and Tertiary sediments. In a study by Ebinger et al. (1989), sediments overlying the complex basement in the Songwe basin were described in more detail [Figure 1.3](#). The Karoo sequence (JR) with a thickness of approximately 1500m and the red sandstones (K) with a thickness of more than 1500m related to the upper Jurassic-lower Cretaceous fluvio-lacustrine sequences (Dinosaur beds) cropping out along the western side of the Karonga basin located at the northern end of Lake Malawi. The white to tan fluvio-lacustrine sandstones and siltstones (Ns)

of Pliocene-Pleistocene age have a thickness much less than 200m with pebbles and boulders of the metamorphic basement and the volcanoclastic lake sediments (QNs*) of Pliocene-Holocene age are detached from the underlying Ns by an unconformity and are interbedded with felsic tuffs known as Mbeya tuffs [Figure 1.3](#).

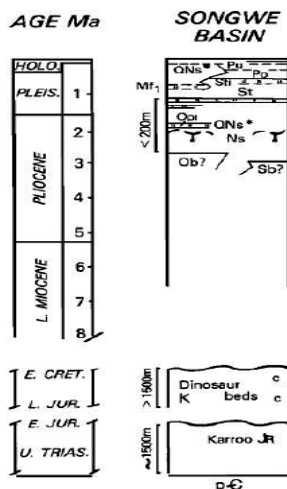


Figure 1.3 - Stratigraphic section of the Songwe Basin (Ebinger et al., 1989) Qns are volcanistics lake sediments, Ns are fluvio-lacustrine sediments, Ob are basalt unit, Sb are Pluvine basalts and picrites, K are Red sandstones, JR are Karoo sequences, Pu is a thin melanephelinite, Po is a 5m thick olivine basalt*

Delvaux & Hanon, (1991) gave details in a stratigraphic cross-section of the Songwe basin, based on studies at the Songwe and Ifisi rivers and Mbeya cement company exploratory wells. The cross-section shows that travertine deposits occur in Songwe and overlay the Basalt and the Older Lake Beds [Figure 1.4](#). They are deposited along the Songwe valley from hot spring discharge water [Figure 1.4](#).

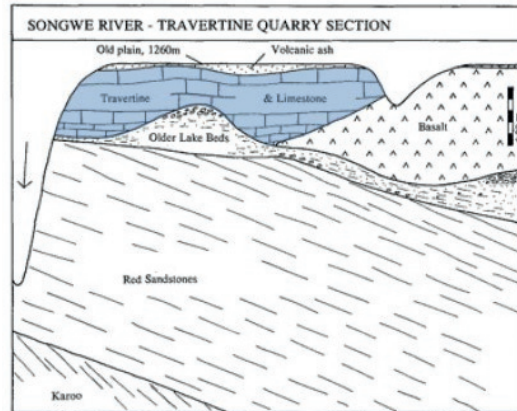


Figure 1.4 - Stratigraphic cross section of the Songwe Basin (Delvaux et al., 1991)

As shown in a structural geological study by Hinz et al., (2018), the Songwe basin is traversed by several important faults such as the southwest dipping Mbeya Range front fault, which is the largest structure in the northeast of the half graben. Also a series of west-northwest striking, south-southwest dipping faults in the Chumwa Range, southwest of the thermal springs, cut through Karoo Sandstones and the Cretaceous Red Sandstone. A NW-striking sinistral strike-slip fault system is mapped in the centre of the hot spring area [Figure 1.2](#).

In general, the geometry of the rift basins consists of half grabens constrained by unequal border faults with splits spread along the rift (Rosendahl et al., 1986). Faults in the western rifts have dip angles ranging from 45° to 75° with offsets that range from 1 to 7 km and lengths of about 80 to 120 km (Corti et al., 2007; Ebinger, 1989).

1.2.2 Hot Springs and Geochemistry

The most noticeable geothermal manifestations in Songwe are hot springs in the Songwe river/valley. The location of Songwe hot springs and the related travertine depositions are most likely controlled by faults. Hydrologically they are controlled by the location and water level of the Songwe River as well as the elevation of Lake Rukwa in the NW. The Songwe River originates from the metamorphic basement rock of the Chumwa Range to the S and SW of Songwe springs, it streams northward along the W side of Panda Hill before entering the Songwe hot springs area (Alexander et al., 2016). The outflow from the Songwe geothermal system is through hot springs at Rambo-Ilatile, Madibira, Kaguri and Iyola; with a natural

discharge between 50 and 75 Kg/s. The Songwe hot springs are of meteoric origin (Hochstein et al., 2000).

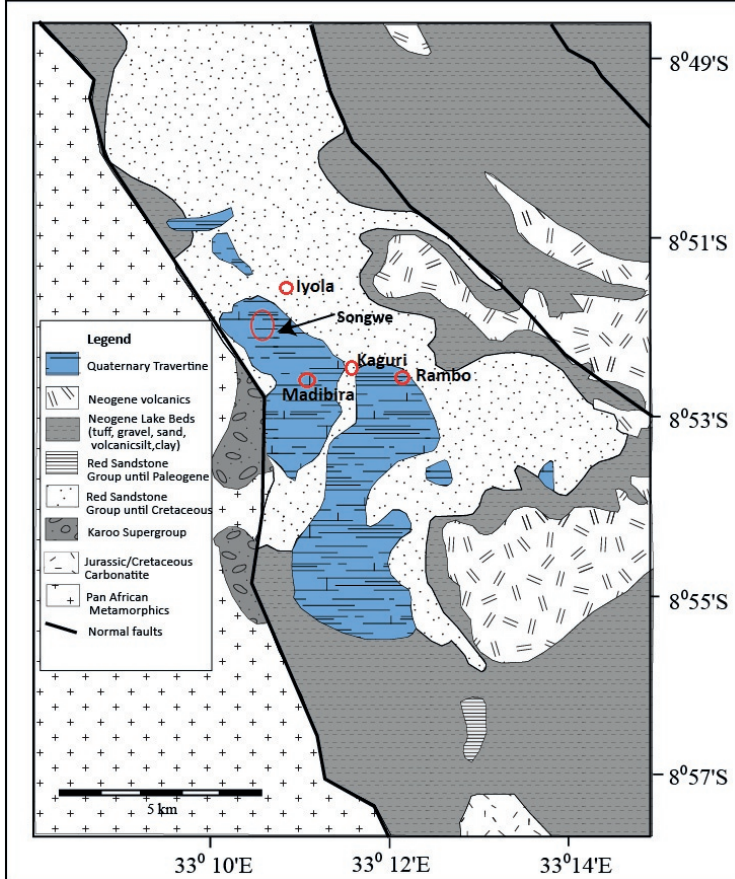


Figure 1.5 Geologic map of Songwe hot spring area (red circle) and travertine deposits (highlighted in blue) modified after (Alexander et al., 2016)

The hot springs discharge water at a temperature of 55-80°C (Bushy et al., 2016). According to a report by Luigi (2016), the water is mainly composed of Na-HCO₃ with an average salinity of 3271±115mg/kg. Mineral dissolution is mainly controlled by water-rock interaction driven by the conversion of CO₂ to HCO₃. Geothermometer temperatures indicate Giggenbach's Na-K temperatures of 250 ± 12 °C, Fournier's Na-K temperatures of 236 ± 13°C, and K-Mg temperatures of 128 ± 9°C. Silica geothermometers indicate temperatures of 96 ± 11°C, and quartz temperatures of 117 ± 9°C. The H₂-Ar and H₂-N₂ gas thermometers indicate a subsurface temperature of 139 ± 14°C. Thus, the geothermal gradient is expected to be within a range of 40-50 °C/Km in our study area, implying a circulation depth of 1.5 to 2.6 km.

1.2.3 Hydrogeology and Possible Scenarios of Geothermal Prospect

The most detailed study by Alexander et al. (2016) presented two alternatives of a hydrogeological conceptual model for Songwe (alternative A and B in [Figure 1.6](#)). In alternative A, recharge takes place in the SW, and fluids move then upward along two faults on the southwestern Songwe basin and discharge in springs at the surface. In alternative B, the main recharge area is in the Mbeya range in the NE. Fluids enter the subsurface through Mbeya Range front fault and flow upwards across the basin to the hot springs.

Alexander et al. (2016) concluded that alternative B is less possible than alternative A because of the lack of informed gas leakage in the half graben as well as the longevity of travertine deposition.

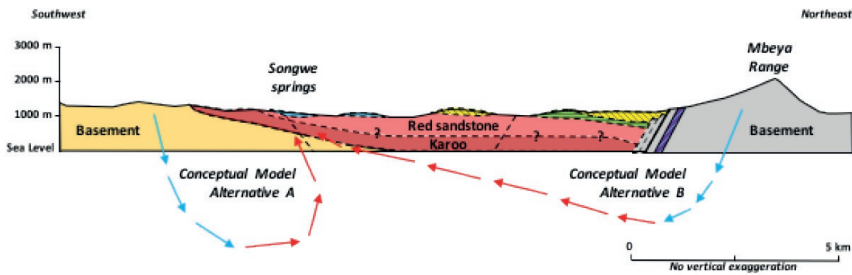


Figure 1.6 - Schematic geological conceptual models for Songwe hot springs (Alexander et al., 2016)

Geothermal systems similar to Songwe include Aristino geothermal field in Greece, a water dominated system with temperatures ranging from 51-99 °C in a fault controlled environment (Dalampakis et al., 2022). The Upper Rhine graben in Central Europe is also similar to Songwe in terms of its geological layering consisting of crystalline basement; Permian, Triassic and Cretaceous sandstones and Cenozoic sediments. Here, also fault zones serve as the main fluid pathways (Frey et al., 2022).

1.3 Research Goal

1.3.1 Geothermal Exploration

Geothermal exploration aims to locate a geothermal resource and identify appropriate drilling zones from the data obtained through field campaigns. It is a multidisciplinary approach, which includes geochemical, geological and geophysical methods (Sircar et al., 2015). Geological exploration seeks to identify different lithologies, structures, and the hydrogeological setting of the area. Geophysics helps in obtaining the geometry of the reservoir, locating the cap rock and giving structural images defining the geothermal system. Geophysical exploration methods that

are mostly used include electric/electromagnetic, magnetic, gravity and seismic measurements. Geochemical exploration aims to characterize geothermal fluids, determine their origin, locate recharge areas, understand fluid flow direction and estimate reservoir temperatures through sampling and analysis of water, gas, steam, and rocks from geothermal manifestations (Ochieng, 2016). The most important components in characterizing a geothermal reservoir include: studying the geochemistry of the surface and thermal springs, which is necessary for obtaining the reservoir temperature; assessment of faults and fractures which are responsible for controlling the fluid flow as well as the overall permeability of the lithology (Brehme et al., 2014). Understanding these components helps avoiding misallocation of a production borehole (Brehme, et al., 2016).

This study focuses on assessing the three main components of a geothermal system, which are reservoir temperature, permeability and fluid flow.

1.3.2 Research Questions

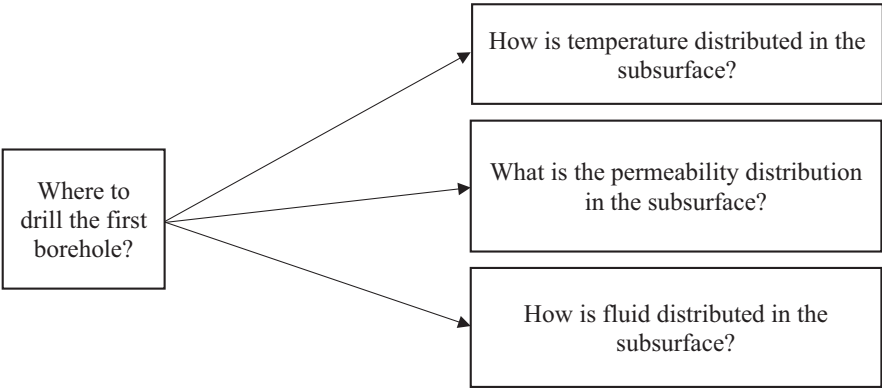


Figure 1.7 Research questions for this study

1.3.3 Research Approach and Thesis Outline

The area of interest in this study is a so-called green-field with very little information available. Most of the existing studies are limited to single studies on the geology, geochemistry and geophysics of Songwe. No well logs and seismic data are available, which would deliver important information on the reservoir. Also, none of the studies integrated the limited data in a joint interpretation to conclude with possible drilling locations. This is the ultimate goal of this study. With the available data, we investigate the permeability, fluid and temperature

distribution in the subsurface at an early stage of the geothermal exploration by using a combination of field work and numerical simulations.

As a first step, a geological and thermal numerical model was set up to simulate the temperature at depth. Input data are from literature and earlier studies in the area. The model considers pure conductive heat flow to achieve a first idea of the temperature distribution in the different geological layers. The software COMSOL was used to perform the numerical simulations.

In the next step, a field study at the thermal spring areas was conducted. Geochemical information from the surface manifestations of a geothermal field not only allows the estimation of reservoir temperature through geothermometers but also gives the source of the fluid, the up-flow and outflow zones (Brehme et al., 2021). We, therefore, collected water and surface rock samples from Songwe geothermal field and conducted laboratory analysis on the samples in order to understand the geothermal fluid source by using geochemical modelling, obtained the reservoir temperature through geothermometer calculation, and located the up-flow and the outflow zones of the geothermal field. Field work was conducted with support from Tanzania Geothermal Development Company and University of Dar es Salaam, school of geosciences and mining.

Furthermore, we performed numerical simulations of fluid and convective heat flow. These simulations allow understanding the heat transport by fluids and the hydrogeological behaviour of the geothermal reservoir. These processes are controlled by pressure and/or temperature gradients within a geothermal system. We used numerical modelling to quantitatively understand the fluid and heat flow processes by varying parameters such as thermal conductivity and permeability. Additionally, we placed possible drilling locations for a first geothermal well in the study area. By changing the drilling locations we were able to distinguish areas of different productivity. For this study we also used COMSOL to perform the numerical simulations.

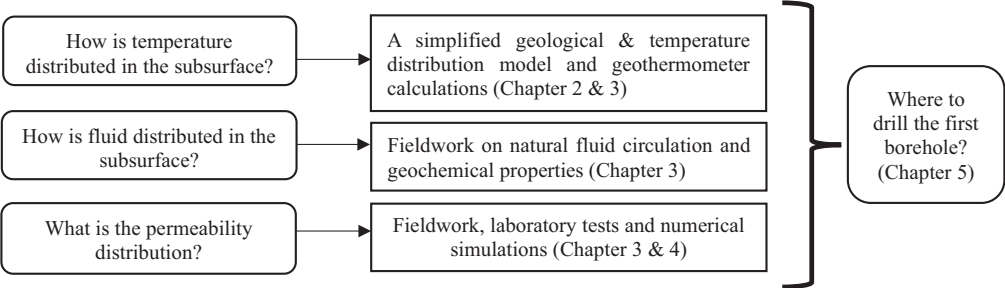


Figure 1.8 Research approach summary

2 CONDUCTIVE THERMAL MODEL

2.1 Introduction

In this chapter, we address the question of the temperature distribution of the subsurface of the Songwe prospect. The first step to achieve this is the construction of a 3D geological model of the area including the main sedimentological and structural heterogeneities present such as different lithological bodies as well as main fault zones. This geological model is based on the geological map and cross-sections presented by Hinz et al., (2018). In a second step, we built a numerical model simulating subsurface thermal processes. In our approach we assume solely conductive heat transfer, thereby neglecting the role of fluids which will be addressed in chapter four. This approach is normally used to provide initial assessment of distribution of temperature in the subsurface. Subsurface temperature is the main parameter in sedimentary basins for the prospection of geothermal energy. A similar approach was used, for example, in a study by Bonte et al. (2012), who presented a 3D temperature model of onshore Netherlands in order to calculate the temperature distribution of the basin fill, from which they identified temperature anomalies in the subsurface and discussed their causes. Similarly, Békési et al. (2020) presented an updated 3D temperature model of the onshore Netherlands using an updated temperature database aiming to account for thermal anomalies especially in areas with no available temperature data. Yang et al. (2022) established a steady state conductive temperature model to predict the temperature distribution in the underground during the early stage evaluation of the Beibu Gulf basin. A study of Gascuel et al. (2020) predicted distribution of temperature at depth for the Anticosti sedimentary basin with the aim of assessing deep geothermal resources with scarcity of data.

We first simulate different 2D thermal models, in order to get a preliminary understanding of temperature profiles over the subsurface and identify thermal anomalies of the area. We then simulate a 3D thermal model to observe temperature distribution over the whole volume. That way, we can also observe variations in temperature distribution along the fault strike and related to the position of sedimentary bodies. Eventually, we also performed a sensitivity study to account for the uncertainty of selected parameters, which are thermal conductivity and heat flow.

2.2 Geologic Model

2.2.1 Input Data and Architecture

Only little information is available on the geological structure of the Songwe prospect and, in particular, of its subsurface. Our geological model is therefore based on the available limited data. The area covered by the model is indicated in [Figure 2.1](#). The model is 12 km wide, 16 km long and reaches a depth of 3 km below sea level (referring to 4.5 km total depth).

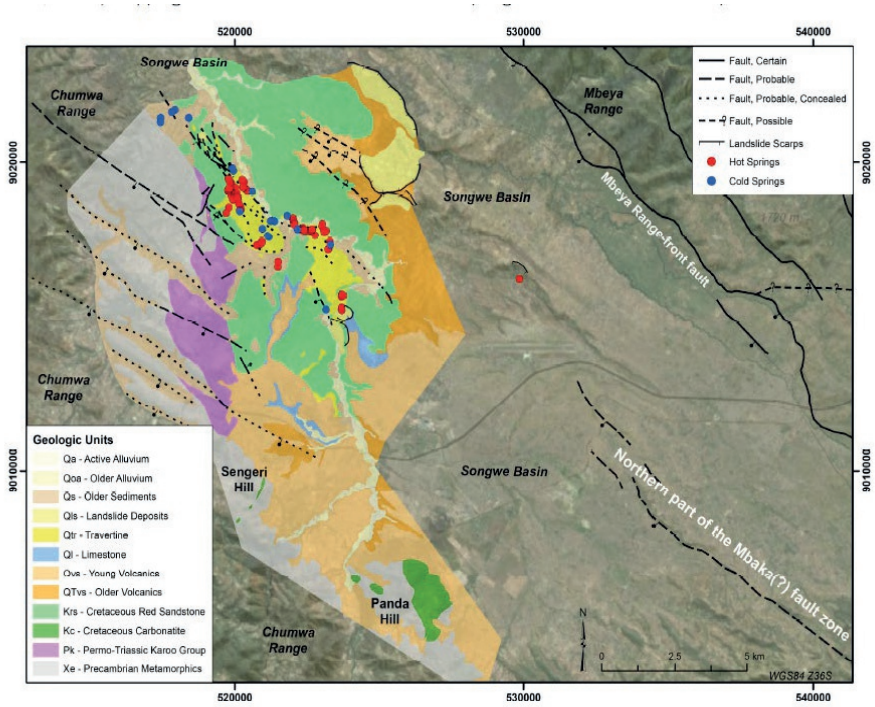


Figure 2.1 Songwe geologic map (Hinz et al., 2018)

The model in this study considers all different rock layers (see Chapter 1) with their geometry and thermal parameters as constant values or as functions of temperature or depth. The rock layers are defined in both 2D and 3D geometry domains as follows: Neogene volcanics is the youngest layer, followed by the Red Sandstone, the Karoo group and lastly the metamorphic basement as the oldest layer. For modelling purposes, we have discarded Quaternary sediments. Our geological model includes the Mbeya fault, which is the major fault of the Songwe half graben and the fracture corridors located in the SW of the area. In the model we simplify their natural complexity to three sections striking NW-SE [Figure 2.1](#)

2.2.2 Building the Model

The geologic model in this study is built in GeoModeller, a geological software that is used to describe lithologies and structures of an area using different data such as cross-sections, maps, wells, hydrological data. Data used to construct the Songwe geological models in this thesis are geological maps, cross-sections and the Digital Terrain Model. Geological maps and cross-sections were provided by the Tanzania geothermal development company. The Digital Terrain Model (DTM) was constructed using ArcGIS.

Important steps while building the geological model are as follows:

- Definition of the x, y and z limits of the study area to be modelled within a coordinate projection system
- Import of the Digital Terrain Model file for this area.
- Creation of a geological formation list with a stratigraphic pile, such that stratigraphic correlation between groups of formations can be assigned
- Digitization of the primary geological data for constraining the lithological contacts for the model
- We then compute the model in 2D and 3D.

2.2.3 Results

2.2.3.1 2D model

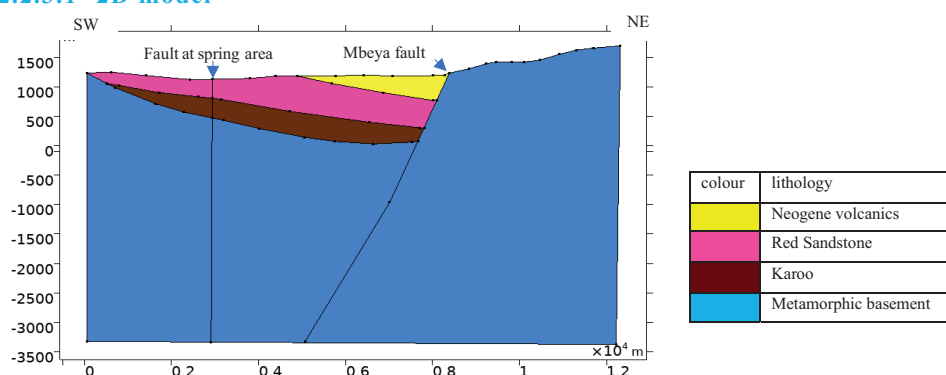


Figure 2.2 Songwe 2D geologic model

The 2D model *Figure 2.2* shows the SW dipping Mbeya fault and the sinistral strike-slip fault at the hot spring area. The sedimentary successions gently dip towards the Mbeya fault, namely, in NE direction. The Karoo sands at the bottom of the succession pinch-out towards the NE, while the thickness of the Red Sandstone increases. The Neogene volcanoclastic sediments at the top of the succession are limited to the central part of the area.

2.2.3.2 3D model

The 3D model *Figure 2.3* has been designed to better capture key geological features of the Songwe prospect, namely the changes in thickness and depth of the sedimentary bodies moving along strike, that is, parallel to the Mbeya fault. The x-axis on the model represents the GPS-easting coordinates, the y-axis represents the GPS-northing coordinates as per the geological map *Figure 2.1* and the z-axis represents the depth of the model. Two additional observations have been made compared to the 2D model:

- The thickness of Red Sandstone and Karoo layers decreases from the SE to NW
- The depth of the basement-sediment contact becomes shallower in the same direction

In addition, we have assumed that Neogene volcanics cover the entire area to the NW of the Mbeya fault due to the complicated topography of the area.

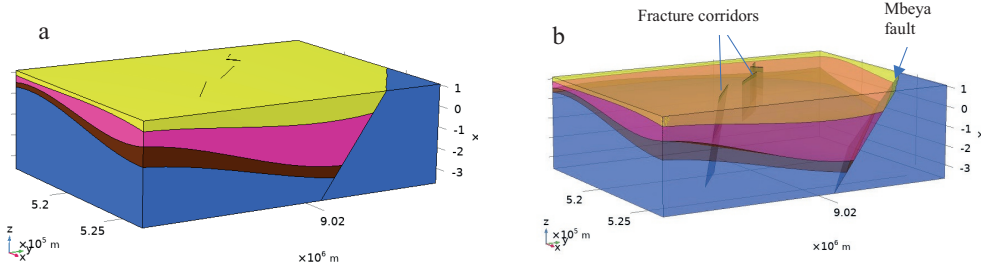


Figure 2.3 Songwe 3D geological model (a); transparent 3D model showing spring fracture corridor corridors and Mbeya fault (b). The same colour code is used as in 2D model. X-axis is eastings, Y-axis is northings and Z-axis is the depth.

2.3 Thermal model

2.3.1 Approach, Boundary Conditions and Parameters

Thermal modelling in this study is based on the steady-state conductive heat equation 2.1. Steady-state conduction can be assumed when the temperature conditions at the boundaries of the system do not change or when the heat flow is constant throughout the study area. Steady-state simulations are an appropriate strategy in areas with scarce measurements of geothermal gradient and heat flow (Kuznik et al., 2013). The conductive heat equation is:

$$\mathbf{q} = -\mathbf{k}\mathbf{A}\nabla T$$

2.1

Where \mathbf{q} is the heat transfer rate, \mathbf{k} is the thermal conductivity, \mathbf{A} is the area that heat transfer takes place and ∇T is the temperature gradient.

In our case, we model purely conductive heat transfer with the assumption that there is no fluid flow in the subsurface. Structures such as faults and fractures are present in the model but do not have their own physical properties and, therefore, do not contribute to thermal processes. The effect of the presence of fluids on the temperature distribution will be studied in chapter 4. Using the geological models described above, we perform 2D and 3D simulations.

The following boundary conditions have been applied to our model:

- Surface temperature at the top of the model is kept constant at 21°C.
- The lateral sides of the model are no-flow boundaries with no heat transfer
- Constant heat flow at the bottom of the model

Table 2.1 Parameters adopted in modelling work from (a) Jones (2020) (b) Nyblade et al. (1990) (c) Didas et al. (2022) (d) Kuznik et al. (2013) (e) Mutabazi (2023) unpublished

Parameter	
Surface temperature	21°C
Thermal conductivity ^(a) ^{(b)(c)(d)}	Neogene deposits 1-1.6 W/m/K (1 W/m/K is used in this study) Red Sandstone 1.230 – 3.665 W/m/K (2 W/m/K used in this study) Karoo 1.230 – 3.665 W/m/K (2 W/m/K used in this study) metamorphic basement 2-3 W/m/K (2.5 W/m/K in our preferred model)
Heat flow 3km below sea level ^(e)	51-62 mW/m ² (62 mW/m ² used in this study)

2.3.2 Building the Thermal Model

For our modelling work, we use the COMSOL Multiphysics version 5.6. It is a powerful modelling tool for solving different types of scientific as well as engineering problems. A major limitation of the software includes the inability to import the complex 3D geological model and therefore parametric surfaces were manually created to build the 3D geometry. From the 3D geological model x, y, z points are imported and thereafter parametric surfaces are manually created from the points to create lithological units and the faults. The 2D geometry is imported directly to COMSOL from the geological model.

2.3.3 Results: 2D Model

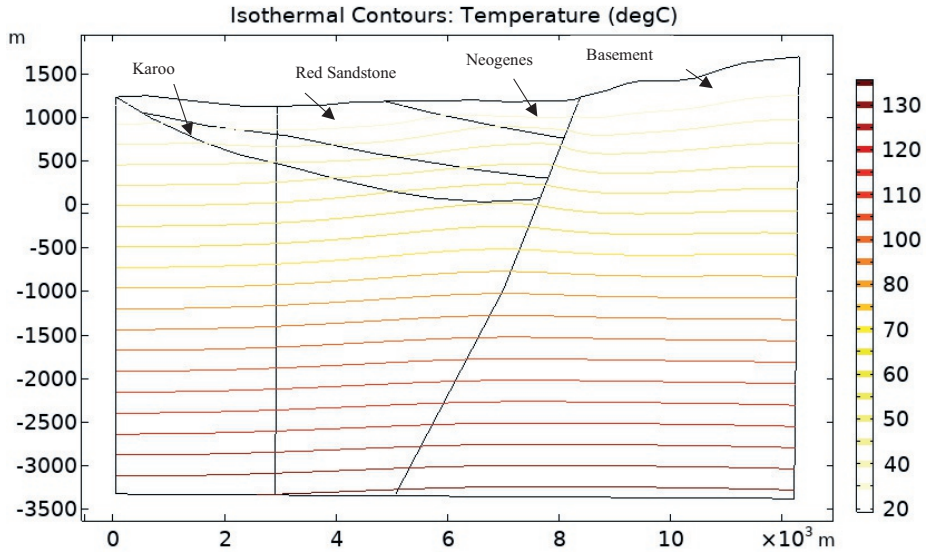


Figure 2.4 2D Temperature simulation results

The isotherms predicted by our model [Figure 2.4](#) are nearly horizontal over the entire surface. In the central part of the study area (between 5-8 km) a wide thermal anomaly is observed near the Mbeya fault which has the highest amplitude close to the surface and disappears moving downward. This anomaly is related to the presence of the Neogene volcanics layer at the top, which acts as an insulator due to its low thermal conductivity that prevents heat loss to the surface.

2.3.3.1 Thermal Profiles

To further investigate lateral and vertical changes in temperature distribution we extract temperatures from three vertical profiles (comparable to boreholes, [Figure 2.5](#)) crossing the Songwe graben at different positions. Profile A starts and remains in the metamorphic basement, profile B starts at the Red Sandstone and traverses Karoo sandstones and the metamorphic basement, while profile C cuts the entire succession from Neogene volcanics, Red Sandstone, Karoo sandstones and metamorphic basement.

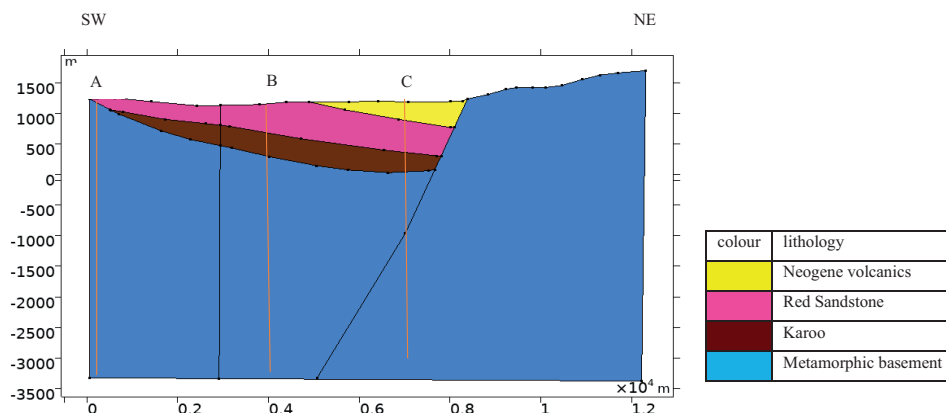


Figure 2.5 Depth profile lines A, B and C

Results show that temperatures range from 20° to 130°C. The profiles show similar trends of constantly increasing temperature with depth. This is a typical behaviour in fields with conductive heat transport. A slight variation is seen in profile C *Figure 2.6*, which displays temperatures significantly higher than those of the other profiles. We further analysed differences between profile C compared to profile B, by calculating the differences in percentage at selected depths. *Table 2.2* shows that the differences are greater near to the surface of the model and decrease as depth increases. In total, the differences range from 2 to 21%. The temperature behaviour of profile C confirms our interpretation that the thermal anomaly *Figure 2.4* results from the presence of Neogene volcanics that have a low thermal conductivity *Table 2.2*. These deposits act as partial insulators preventing heat loss.

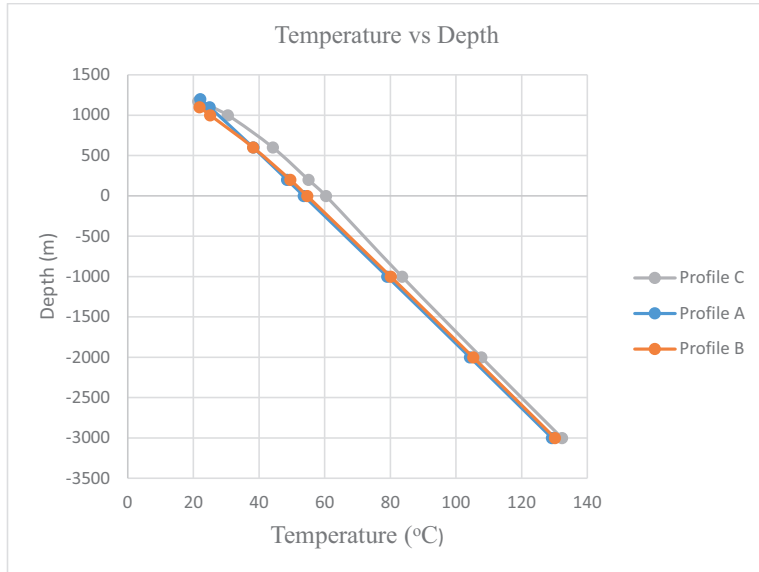


Figure 2.6 Temperature at depth in profiles A,B and C

Table 2.2 Temperature percentage increase at profile C with respect to profile B

Depth/Elevation (m)	Temperature increase on Profile C
1000	21%
600	16%
200	11%
0	10%
-1000	4%
-2000	2%
-3000	2%

2.3.4 Results: 3D model

2.3.4.1 Model Results

We display the results of our 3D model by showing temperature variations on horizontal surfaces at various depths below the surface [Figure 2.7](#).

Results show that temperatures range from 50° to 150°C. Despite its simplicity, our 3D model displays significant lateral changes in temperature. At all depths, an area of significantly higher temperatures is present in the eastern part of the model. This area corresponds to the location of the thickest pile of sediments in the Songwe graben. The magnitude of temperature changes at the corresponding depth is quantified in [Table 2.3](#)

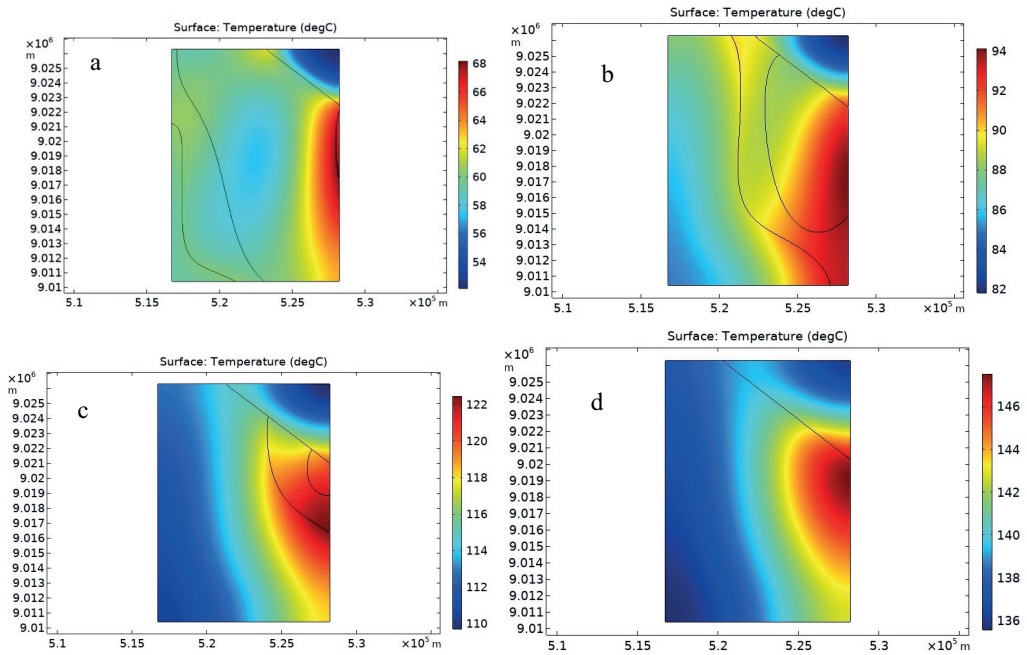


Figure 2.7 Map view of temperature distribution at depths (from the surface) of 1km (panel a), 2km (panel b), 3km (panel c) and 4km (panel d). Curved lines are the lithological boundaries on map view, straight line on the top right is the Mbeya fault.

Table 2.3 Temperature range at depth for the horizontal profiles

Horizontal profile	Depth from surface (Km)	Maximum temperature (°C)	Minimum temperature (°C)	Difference in Temp. (°C)
a	1	68.2	52.1	16.1
b	2	94.1	81.8	12.3
c	3	122	110	12.0
d	4	148	136	12.0

2.3.5 Sensitivity Analysis

2.3.5.1 Heat Flow

Because heat flux is the dominant process in conductive-dominated systems, we tested different heat flux scenarios in our model. In our model, we have assumed a heat flow of 62 mW/m² across the lower boundary of the model. In the sensitivity study, we use heat flow values of 51, 62 and 70 mW/m² to observe the effect on temperature distribution. With changing heat flow values, different temperature distributions were achieved. This is visualized through a vertical temperature profile at point D in the model. Temperatures are extracted from the vertical profile line D, shown in [Figure 2.8](#)

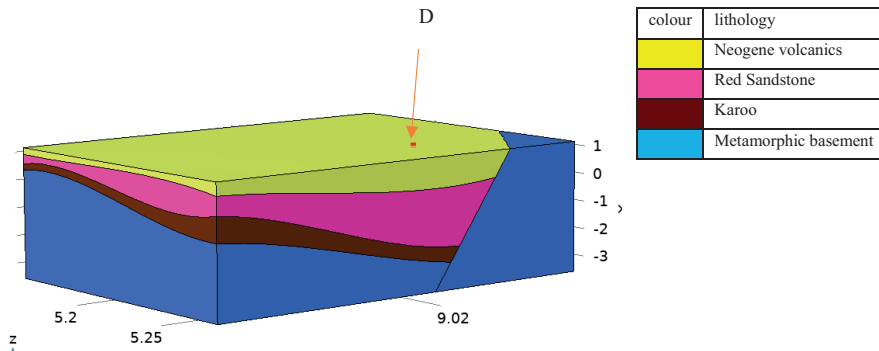


Figure 2.8 Profile line D where temperature simulation results are observed

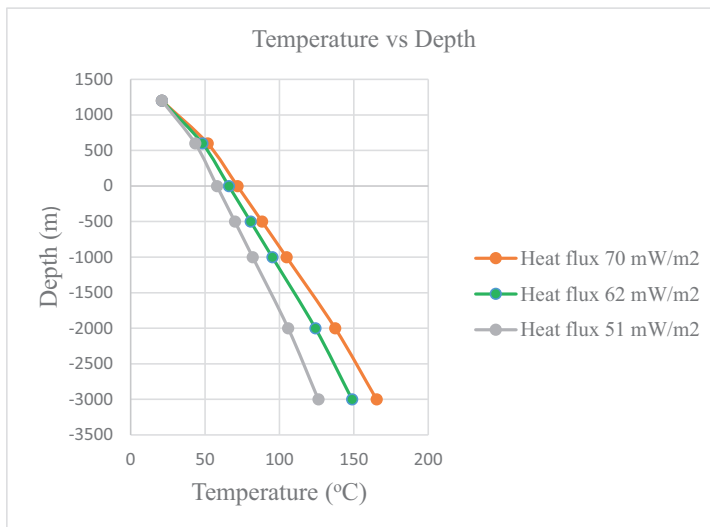


Figure 2.9 Sensitivity analysis using different values of heat flow as indicated in the legend

The temperature-depth curves in Figure 2.9 produced by the three heat flow scenarios lead to different geothermal gradients Table 2.4. The higher the heat flux, the higher the geothermal gradient.

Table 2.4 Calculated linear vertical temperature gradients of different temperature profiles obtained by simulation of different values of heat flux

Temperature profile line	Linear vertical temperature gradient
Heat flux 51 mW/m ²	25 °C/km
Heat flux 62 mW/m ²	30 °C/km
Heat flux 70 mW/m ²	34 °C/km

2.3.5.2 Thermal Conductivity of Red Sandstone

Because the Red Sandstone is the thickest sedimentary package in Songwe half graben and because it is the prospective geothermal reservoir, we have analysed its impact on temperature distribution by using different thermal conductivity values.

Building on studies by Nyblade et al. (1990) and Didas et al. (2022) which give a range of thermal conductivities on Red Sandstone between 1.230 and 3.665 W/m/K, we have chosen three representative values of 1.5, 2.0 and 3.0 W/m/K. Other parameters remain the same as in Table 2.1.

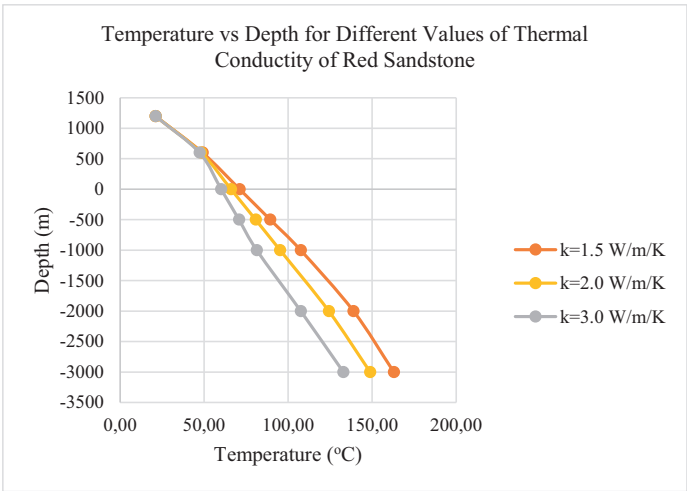


Figure 2.10 Effect of thermal conductivity on temperature distribution

Vertical temperature profiles were again observed at profile D. Temperatures extracted from profile D show that curves with higher temperatures are associated with lower thermal conductivity values Figure 2.10. Our results show that the highest temperatures are predicted for 1.5 W/m/K thermal conductivity for the Red Sandstone followed by 2 W/m/K and lastly 3 W/m/K.

Table 2.5 Effect of thermal conductivity on temperature distribution

Thermal conductivity value of Red Sandstone	Temperature gradient
1.5 W/m/K	34 °C
2.0 W/m/K	30°C
3.0 W/m/K	26 °C

Table 2.5 shows how thermal conductivity changes the geothermal gradient. By changing the thermal conductivity of the Red sandstone the thermal gradient also changes, lower thermal conductivity corresponds to a higher gradient and vice versa. This observation is comparable with the conclusions by Tang et al. (2019) that thermal conductivity affects the temperature distribution and therefore is an important parameter when exploring geothermal fields.

2.4 Discussion

This study presents baseline information on the subsurface temperature distribution for a large-scale geothermal field in the Songwe basin. As temperature is one of the essential requirements for geothermal energy development, it is important to understand how the heat flow and temperature distribution are affected by the geology. There are no temperature measurements done at Songwe basin that could be used to calibrate the model and compare the simulations results with the measured data. This study therefore mainly focused on characteristics of the temperature distribution by varying thermal parameters. Physical properties of the formation however are assumed to be constant with depth.

From the temperature simulation results, it can be observed that the isotherms in the subsurface are nearly horizontal, if the temperature field is controlled purely by conductive heat transport. Furthermore, we have observed from the 3D model that temperature does not only change with depth, but geological conditions such as lithological changes and stratum thickness also influence the temperature distribution. We have observed horizontal temperature changes that are related to the lateral changes of the lithological layers, which allow us to identify high-temperature areas.

The temperature gradients differ substantially between 2D and 3D simulations despite the fact that the same parameters were used in both models. Considering temperature gradients calculated from depth-temperature curves beneath the Neogene volcanics on profiles C and D, in the 2D and 3D models respectively, we observe a gradient difference of 5°C/km between the

two models, with the 3D model having the highest temperature gradient. This difference is due to the fact that lateral changes in lithological layers are not accounted for in the 2D model.

We can show with the sensitivity studies how the steady-state temperature field is affected by thermal conductivity of the rocks and the heat flux. This is in line with a study by Balkan et al. (2017), who showed that thermal conductivity is the main parameter in thermal modelling, as it leads to substantial changes in temperature even though the heat flux is constant.

In the 2D model, we have observed that low thermal conductivity of Neogene volcanics present in profile C slows the heat transfer from the subsurface to the surface thus causing higher temperatures in the subsurface. The amplitude of the anomaly decreases with depth, and at 2000 m below the surface it is reduced to 2%.

Therefore, when assessing geothermal resources in sedimentary basins, it is important to obtain site-specific parameters such as thermal conductivity and heat flux, because they have considerable influence on the resulting subsurface temperature distribution. The accuracy of these parameters has significant influence on the feasibility of the geothermal resource.

A steady-state conductive temperature for Songwe field is calculated to predict distribution of temperature in the subsurface because the area is still in an early evaluation phase. This method has been used previously for geothermal projects that were in the same early stage as indicated in studies by Yang et al. (2022), Espinoza-Ojeda et al. (2022) and McAilley & Li (2019). Temperature estimation during the exploration stage is crucial because it gives an understanding of where thermal anomalies are found in the subsurface as it was the case in a study by (Dalampakis et al., 2022), who identified thermal anomaly areas and calculated the geothermal gradients. Most of these studies had temperature data from exploration wellbores that were used to calibrate their numerical models, making their results more accurate. In contrast, in our study we could not calibrate the model using wellbore temperature data due to lack of such data. However, with the sensitivity study, we have been able to establish effects of the important parameters on the subsurface temperature distribution. The model can also be updated once the well data are available.

In general, the thermal model considering only conductive heat transport in a dry rock system serves as a reference for the interpretation of the actually observed temperatures in the geothermal field. Deviations from this reference model need to be interpreted in context of fluid flow and thermal transport by advection or convection, which would be important indicators for productive zones of geothermal systems. The effect of fluid flow is addressed in chapter 4.

2.5 Conclusion

This chapter serves as the first approach in trying to understand how temperature distribution can look like in the subsurface at exploration stage without any temperature and pressure measurements. It is the first time that a 2D and 3D temperature models for the Songwe basin have been established with actual geological information. The defined isotherms shape from the simulation results are useful when planning the exploitation of the geothermal field. The temperature distribution characteristics at Songwe basin are related to depth, lithological changes and stratum thickness with the thermal anomaly being found below the Neogene volcanics at the thickest part of the lithologies. In the conductive temperature distribution equation, temperature is mainly controlled by the heat flow and the thermal conductivity of the rocks. Therefore the determination of these two parameters are the key to temperature field simulation and the purpose of geological characteristics research.

3 IMPLICATION OF GEOCHEMICAL STUDIES

3.1 Introduction

Chapter 3 is a published peer reviewed journal publication studying the fluid composition, fluid distribution and temperature in the Songwe geothermal system (Asnin et al., 2022) where by the second author conducted field work and gave data input on the physical and thermal parameters of the rocks. The chapter contributes to all three research questions of the thesis, e.g. How is temperature distributed in the subsurface?, How is fluid distributed in the subsurface? and What is the permeability distribution? It uses field measurements, laboratory analysis of fluids and rocks and chemical simulations.

Geochemical investigations in the initial stage of geothermal field development typically aim for characterizing subsurface conditions in order to define drilling targets (Truesdell & Jones, 1974). The geochemical information is obtained from geothermal surface manifestations. They do not only support temperature estimations but also give general information on the geothermal system such as hydrogeochemical processes, upflow, and/or outflow zones (Henley, 1995). Techniques usually applied are geochemical sampling and characterization of spring and reservoir water as well as mixing models to identify fluid sources, 2-phase proportions or mixing during fluid rise to surface (Truesdell & Jones, 1974). Isotope studies help to identify the fluid source while geothermometers are used to estimate the reservoir temperature (Ellis & Wilson, 1960). Equilibrium calculations of fluids with minerals are used to predict scaling tendencies (Giggenbach, 1988). In this study the geochemical equilibration is used to identify the fluid source by comparing known precipitations to modelled fluid-rock interaction. By modelling the reaction of reservoir water with the different types of geological layers and comparing the results to measured minerals precipitated in that layer, we gain understanding of fluid pathways and sources.

Geochemical investigations related to geothermal energy exploration have been conducted in the Songwe field, Tanzania, since the late 1950s. Located in western Tanzania in the Rukwa Rift of the western branch of the East African Rift System (EARS) the Songwe geothermal area has a significant resource with medium to high temperature thermal springs with carbonate or travertine-rich deposits (Hochstein et al., 2000). The system is located 50km north of the Mbeya volcanic province.

James (1959) reported the first chemical analysis of thermal springs in the Songwe river valley. Using chemical data of the “Kaguri thermal spring” and gas samples of “Main hot springs”, the author suggests the gas-bearing springs are of volcanic origin. Nzaro (1970) also analysed the thermal springs throughout the valley with a focus on their relation to the block-faulted region of the rift system. Later, a Swedish consultant group SWECO (1978) carried out a geochemical sampling survey of surface manifestations in Tanzania, including the Songwe area, and considered it one of the high-temperature geothermal fields in Tanzania. (Makundi & Kifua, 1985) provided a chemical data inventory of thermal springs in the Mbeya prospect area. Applying the Na-K-Ca geothermometer, these authors argue that the estimated deep fluid temperature is ranging from 170°C near the Ivuna springs (80 km NW of Songwe) to 217°C at Songwe. The other geothermometers of thermal springs (chalcedony, K/Mg, Na/K geothermometer) suggest intermediate to high temperatures (100 – 255°C) in the Songwe reservoir although these springs are described as outflow zone (Hochstein et al., 2000; Mnjokava, 2007). Springs in outflow zones normally show low temperatures in contrast to the upflow zone of a geothermal system.

These various datasets and the yet uncertain understanding of the geothermal system in Mbeya area led to the implementation of the GEOTHERM technical cooperation program of BGR (Federal Institute for Geoscience and Natural Resources, Germany) that consisted of a geological, geochemical, and geophysical survey between 2006 and 2009 (Delvaux et al., 2010; Kalberkamp et al., 2010; Mnjokava, et al., 2010). Results show a structurally-controlled fluid flow and a close association of thermal springs with active strike-slip and normal faulting (Delvaux et al., 2010). Magnetotelluric and Transient Electromagnetic surveys conducted by Kalberkamp et al. (2010) show a low magnetic anomaly in the Songwe area indicating strong alteration in rocks. Thus, the GEOTHERM studies came up with the main conclusion that Songwe thermal springs are an outflow zone of Lake Ngozi volcanic hydrothermal system. Conversely, other authors distinguish between Songwe geothermal system and Ngozi volcano based on the recent studies on geology, geochemistry, and geophysics by TGDC (Tanzania Geothermal Development Co. Ltd) and UNEP (United Nations Environment Programme) in 2016 (Alexander et al., 2016; Hinz et al., 2018). These authors also conclude that many springs are not associated with large apparent faults.

In addition, major ion analyses and mineral composition of travertines in the Songwe area have been studied to understand its origin showing a close association of the travertine deposits with Neogene-Quaternary volcanism (Pisarskii et al., 1998). Additionally, U/Th travertine data suggest a link between volcanic and geothermal activities (Delvaux et al., 2010). It supports

the argument of Alexander et al. (2016) that Songwe Sr-rich travertines derive from volcanic rocks.

Even though a number of previous geoscientific studies have been carried out in the Songwe area, a detailed understanding of fluid flow pathways and related water-rock interaction has not been achieved yet. Taking advantage of the history of fluid geochemical data and geological mineral data of distinct lithologies, the purpose of this study is to update the interpretation of the Songwe geothermal system and add information on geothermal fluid pathways and sources. It comprises of 1) the reservoir temperature estimation and 2) interpretation of fluid flow pathways related to structural geology and 3) the modelling of water-rock interaction. We synthesize our results in a fluid flow model of the Songwe geothermal field.

3.2 Geology and Structural Geology

3.2.1 Regional Geological Setting

As part of the western branch of the EARS, Songwe geothermal resources are situated in the long valley of the Songwe basin. The Songwe basin is a sub-basin of the Rukwa Rift Basin, which is a half-graben flanked by uplifted Proterozoic metamorphic rocks of the late Ubendian shear belt (Kilembe & Rosendahl, 1992). Metamorphic rocks in Songwe area are composed of amphibolite, gneiss, schist, and mylonite (Sussman et al., 2018). The Proterozoic gneissic rocks consist of high-grade migmatitic metasediments (biotite-garnet gneisses) that are underlain by igneous rocks (hornblende-pyroxene gneisses and quartz-rich garnet pyroxene gneisses), and high-grade metamorphic rocks intruded by granodiorite and diorites (Harkin & Harpum, 1978; Macfarlane, 1966). These Proterozoic basement rocks are unconformably overlain by the Permo-Triassic Karoo group, Triassic Red sandstone, and Quaternary Volcanics *Figure 3.1*. In the western study area, the Permian-Triassic Karoo group is exposed at surface. These rocks are comprised of a series of glacial to periglacial strata, lacustrine, and fluvial deposits with conglomerates, siltstones and sandstone, carbonatic minerals and coal deposits (Alexander et al., 2016; Delvaux, 2001; Roberts et al., 2004; Semkiwa et al., 1998). EAGER (2018) suggests the Karoo layers in the Songwe basin are mainly comprised of sandstone and conglomerate with about 500 m thickness.

In the NW and the SE of the study area, the Red sandstone is widespread with 1300 - 1500 m thickness (EAGER, 2018). The rocks consist of quartz, K-feldspar, muscovite and apatite (Alexander et al., 2016; Roberts et al., 2004). The Red sandstones are loosely packed sediments, which are often overlain by massive travertine with 5 – 20 m thickness in the

surrounding of thermal springs and extend towards the western basin margin (EAGER, 2018). Additionally, fractures and pores in the Red sandstones are filled with carbonatic minerals. The Quaternary Volcanics are only deposited in the SE (Ikumbi) area and composed of trachyte and basalts (Alexander et al., 2016).

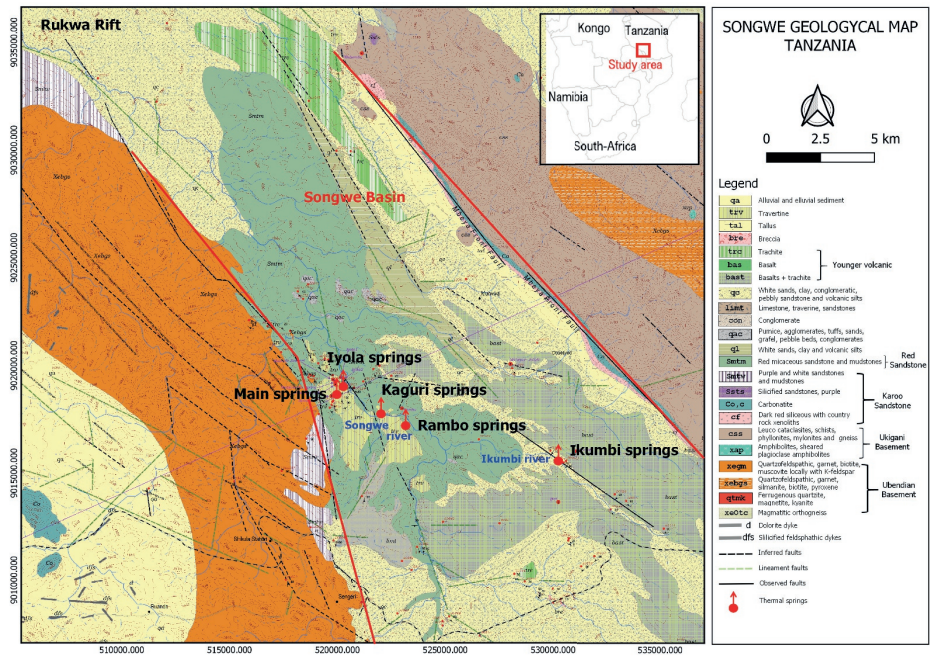


Figure 3.1 Songwe geological map modified after (Alexander et al., 2016), showing thermal spring locations.

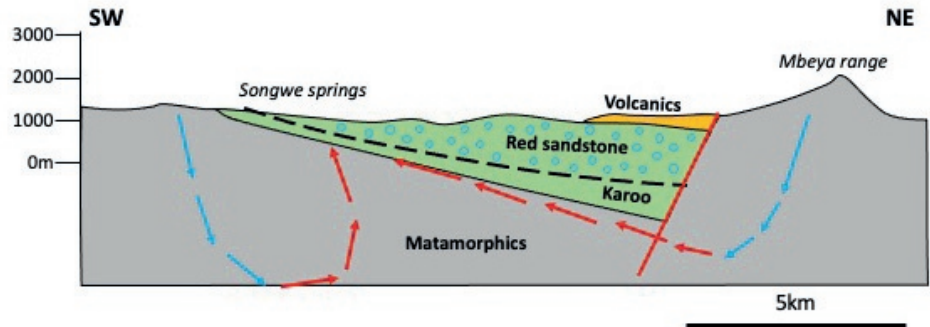


Figure 3.2 Schematic section across the Songwe half-graben. The overall geometry of the basin is obtained combining surface data from Alexander et al., (2016). The deep part of the basin is inferred from EAGER et al., (2018). The two reports provide a contrasting hypothesis for the position of the boundary between the Karoo and Red Sandstones (dashed line in our figure). The flow paths correspond to those predicted by Alexander et al., (2016).

3.2.2 Structural Geology of the Songwe Basin

The geological cross section of the Songwe basin shows the basic geological units e.g. Metamorphics as basement, overlain by Karoo Sandstones, Red Sandstones and partly volcanics [Figure 3.2](#). The Mbeya fault in the NE of the basin cuts these units and underlines the graben structure. Sandstones and Volcanics are only found within the graben system and dip towards NE. Previous fluid-flow models suggest an infiltration of rainwater at the NE and SW edges of the basin, which is then heated at depth and rises through the sandstones to surface.

Associated with a rifting system, the Songwe basin is situated in an active structural set-up. The set-up has been investigated in several studies by (Alexander et al., 2016; Delvaux et al., 2010; Ebinger, 1989; Hinz et al., 2018; Kilembe and Rosendahl, 1992; Theunissen et al., 1996). All studies suggest a transtensional regime with strike-slip and normal faults. The main strike direction of the structures is corresponding to the basin in NW-SE direction.

Various studies differ slightly in their interpretation but show two major faults within the Songwe basin (Alexander et al., 2016; Delvaux et al., 2010; EAGER, 2018). The Mbeya range fault is the NE boundary of the system and described as dextral strike slip or partly normal fault. Another major fault runs through the centre of the basin and is characterized as dextral strike-slip fault with a left step-over in the centre of the basin. This step-over zone is associated with fractures and accommodates most of the hot springs of the Songwe basin. Alexander et al. (2016) also suggested a fault at the SW boundary of the basin dipping as normal fault towards the basin. More recent studies by Hinz et al. (2018) additionally show fracture patterns and WNW striking, SW dipping normal faults within the basin. The detailed structural geology of the Songwe basin is subject of further studies by the authors of this paper and will be published in an additional format. Previous results confirm that the major dextral strike-slip fault in the basin centre provides locations of accompanying minor sinistral faults and a fracture pattern with normal displacement distributed over the basin.

3.3 Methods and Materials

3.3.1 Sampling and Analysis

Water samples

A total of 17 geothermal springs from five spring groups were sampled during the first week of November 2019. The sampling locations are shown in [Figure 3.1](#). During the field survey, deposits around the thermal manifestations were described and physicochemical parameters were measured in-situ using portable instruments, including water temperature (T), acidity

(pH), and specific electrical conductivity (EC). The sampling technique is applied according to hydrogeological procedures used by (Brehme et al., 2010). Water samples for chemical analysis were filtrated in-situ through 0.45µm filter and stored in two 30 ml polyethylene bottles. Hydrochloric acid was added into one of the batches to lower the pH < 2 for cation analyses, while the other batch taken for anion analyses remained untreated.

The major ions were analysed at the geochemical community laboratory of the Berlin Institute of Technology. Anion concentrations including Na⁺, K⁺, Fe^{2+/3+}, Ca²⁺, and Mg²⁺ were determined by AAS (Analytik Jena, novAA 400) and ICP-OES Thermo Jarrel Ash with a detection limit of 0.02 ppm, 0.04 ppm, 0.0007 ppm, 0.007 ppm, and 0.003 ppm, respectively. Cations Cl⁻, SO₄²⁻, F⁻, Br⁻, NO₃⁻ and PO₄³⁻, were determined using ion chromatography Dionex DX 120 with detection limit of 1.5 ppm, 2.5 ppm, 0.25 ppm, 0.75 ppm, 0.75 ppm, and 1 ppm, respectively. The HCO₃⁻ concentration was measured on-site using alkalinity titration.

The reliability of the major element analysis was evaluated based on ionic balance errors. An ionic balance error is calculated by comparing the molal concentration of anions and cations (meq). An ionic balance error ≤ 5% means that the accuracy of the chemical analysis is reliable (Nicholson, 1993). Practically, almost all data from the major elements analysis in 2019 are within the preferred ion balance error [Table 3.1](#) except for Kaguri 1 (6.6 %).

Surface rock samples

Rock samples were taken at areas of emerging thermal springs. In order to identify mineral compounds, the surface rock samples were analysed by X-ray diffraction (XRD) (Bruker D8 Advance diffractometer, with Cu Kα radiation and a Bragg-Brentano geometry) at the S-Rat Facilities Group of Delft University of Technology. About 1 gr of sample powder was deposited in PMMA holder L25, measured through XRD between coupled θ -2θ scan 10° - 110°, with a step size 0.030 ° 2θ, and counting time per step of 1 s. Data interpretation has been done using Bruker software DiffraSuite. EVA vs 5.2. The porosity of the samples is measured using a He-Pycnometer ("Ultra Pycnometer 1000"). Permeability is measured using a portable hand-held air permeameter from NER (<https://www.ner.com/site/systems/tinyperm3.html>). A rubber nozzle is pressed against the sample and withdraws air from it. The air is pulled from the sample and a microcontroller unit simultaneously monitors the syringe volume and the transient vacuum pulse created at the sample surface.

3.3.2 Geochemical Modelling

In order to understand the geothermal fluid source in the Songwe basin we use geochemical modelling method using PHREEQC version 3.6.2 (Parkhurst & Appelo, 2013) with the

Lawrence Livermore National Laboratory aqueous model database (llnl.dat) according to the scheme in [Figure 3.3](#). We test possible thermal water interaction with all lithologies of the study area at the surface temperature and reservoir temperature. First, for the reservoir temperature model, the hot spring composition was calculated back to a reservoir fluid composition using the steam fraction produced by boiling at two reservoir temperatures (125°C and 148°C) [Figure 3.3](#). In surface temperature models we first used measured chemical concentrations of the springs. In a second step, thermal water in springs and/or the calculated reservoir water react with different rock types of the study area to simulate water-rock-interaction in this specific lithology at different temperatures. This is done to test if the resulting fluid composition and precipitating minerals match with the measured values. The reaction in the equilibrium model gives saturation indices (SI) for different minerals. A negative SI suggests dissolution of the mineral while a positive SI suggests precipitation of the mineral (Brehme, et al., 2016). Modelled precipitated minerals in the surface temperature are compared to observed precipitated minerals at the hot springs. In the reservoir temperature model, modelled precipitated minerals are compared to measured minerals in the rocks. The composition of the rock was taken from XRD data and literature [Table 3.2](#). The best match indicates the real water-rock interaction and marks the lithology where the geothermal fluid originates. Thus, the reaction model improves our understanding of the water-rock interaction in the geothermal system and indicates the geothermal fluid source in the Songwe basin.

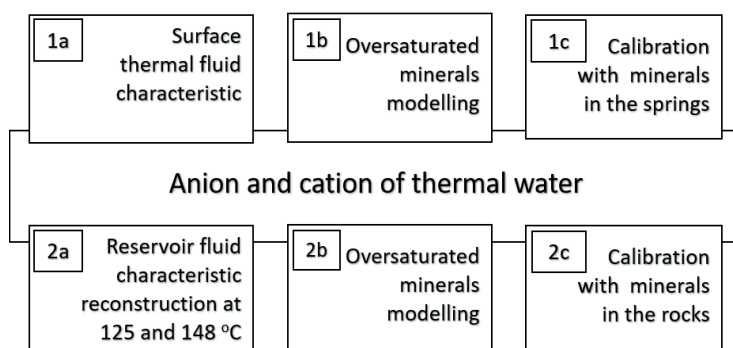


Figure 3.3 Geochemical modelling step using Phreeqc in Songwe geothermal area. 1a, 1b and 1c are for the model at surface temperature, while 2a, 2b, and 2c are for the model at reservoir conditions.

Table 3.1 Field parameter and chemical analysis of thermal manifestation in this study (2019) and other studies previously (Alexander et al., 2016; James, 1959; Kraml et al., 2008; Makundi and Kijua, 1985; Mnjokava, 2007; Nzaro, 1970; Pisarskii et al., 1998; SWECC

Springs	Sampling date	Southing/ Easting	Elevation (m)	T (°C)	Field pH	EC (µS/cm)	Na ⁺	K ⁺	Ca ²⁺	Mg ²⁺	SiO ₂	Fe ^{2+/3+}	Li ⁺	B ³⁺	As ³⁺	Al ³⁺	HCO ₃ ⁻	SO ₄ ²⁻	Cl ⁻	Ionic Balance
							mg/L													
Rambo old	11/5/2019	523088/9017787	1125	82.7	6.5	2650	867.7	81.1	19	7.91	-	0.0031	0.79	0.63	-	-	1831	176.84	222.58	1.9
Rambo middle	11/5/2019	523095/9017773	1124	70.2	6.7	2470	865.6	78.5	16	7.65	-	0.0011	0.78	0.62	-	-	1959	177.33	223.82	1.9
Rambo new	11/5/2019	523100/9017753	1124	82.9	4.8	2910	851.1	84.6	24	8.08	-	0.0049	0.77	0.62	-	-	1885	176.67	222.49	1.2
Kaguri 1	11/7/2019	521978/9018143	1078	70.9	8.6	2790	867.8	85.1	17	8.46	-	0.0068	0.74	0.60	-	-	1623	176.27	218.62	6.6
Kaguri 2	11/7/2019	522049/9018065	1080	48	8	2570	979.9	88.4	41	9.76	-	0.0113	0.73	0.61	-	-	2248	178.24	216.12	1.3
Kaguri 3	11/7/2019	522007/9018206	1079	62.9	5.8	2760	874.4	68.7	18	8.33	-	0.0129	0.70	0.59	-	-	2032	175.45	216.39	1.8
Main spring 1	11/5/2019	520034/9019037	1119	75	6.6	2640	840.4	88.5	47	13.9	-	0.0851	0.73	0.58	-	-	2123	174.52	195.14	1.7
Main spring 2	11/5/2019	520036/9019046	1127	75.5	6.2	2730	823.9	87.5	37	14.9	-	0.0046	0.72	0.57	-	-	1934	171.9	193.75	0.7
Main spring 3	11/5/2019	520046/9019135	1119	73.2	6.4	2870	862.1	90	37	16.3	-	0.0025	0.70	0.56	-	-	1922	171.56	192.59	3.1
Main spring 4	11/5/2019	520032/9019171	1127	68.7	6.5	2240	803.1	73.1	38	18	-	0.0019	0.69	0.55	-	-	1916	169.94	188.25	0.02
Iyola 1	11/5/2019	520249/9019413	1057	74.4	6.8	3600	818	107	61	23.7	-	0.0073	0.61	0.49	-	-	2166	168.83	175.78	0.6
Iyola 2	11/5/2019	520310/9019418	1064	62	6.4	2920	824	105	44	21.2	-	0.013	0.60	0.49	-	-	2026	168.01	178.63	0.8
Ikumbi 1	11/6/2019	529873/9016237	1211	43.9	7.1	420	116.1	46	12	4.78	-	0.0026	0.02	0.011	-	-	458	5.44	8.89	4.1
Ikumbi 2	11/6/2019	530101/9015910	1217	42	6.4	470	115.2	44.1	16	5.97	-	0.0005	0.02	0.004	-	-	439	5.04	7.94	0.8
Ikumbi 3	11/6/2019	530212/9015896	1214	38.2	8.2	450	119.4	45.6	15	5.85	-	0.0005	0.02	0.004	-	-	430	5.09	8.08	1.4
Ikumbi 4	11/6/2019	530291/9015840	1204	41.3	7.9	440	120.9	46.1	14	5.24	-	0.0018	0.02	0.023	-	-	439	5.48	9.12	0.01
Ikumbi 5	11/6/2019	530319/9015818	1210	37.1	7.5	410	116.8	45.9	15	5.44	-	0.0165	0.02	0.028	-	-	458	5.72	8.13	2.6
Rambo 2016 ^a	1/23/2016			80.2	7.6	3760	774	103	29.5	3.2	63	-	-	0.19	-	-	1976	430	217	11
Main spring 2016 ^a	1/19/2016	520042/9019043	1129	74.7	7.2	3830	745	113	20.9	15.6	72	-	-	0.17	-	-	2247	166	199	9.8
Rambo 1-2008 ^c	6/7/2006	523058/9017886	1127	72	nd	3700	806	83.4	10.4	7.9	68.1	0.011	0.758	0.725	0.143	0.007	-	139	181	65.7
Rambo 2-2008 ^c	6/7/2006	522966/9018008	1087	80.2	nd	3800	818	82	17.1	8	70.3	0.177	0.762	0.727	0.149	0.371	-	143	184	65.8
Rambo 3-2008 ^c	11/1/2006	522966/9018008	1088	65	7.1	3600	828	91.4	16.5	9.2	68.5	0.007	0.761	0.667	0.099	0.04	2350	146	196	7.9
Rambo 4-2008 ^c	6/7/2006	523025/9018021	1087	74.1	nd	3700	821	83.5	15.9	8.5	68.9	0.03	0.751	0.717	0.141	0.056	-	138	180	66.6

Table 3.1 (continued)

Springs	Sampling date	Southing/ Easting	Eleva tion (m)	T (°C)	Field pH	EC (µS/cm)	Na ⁺	K ⁺	Ca ²⁺	Mg ²⁺	SiO ₂	Fe ^{2+/3+}	Li ⁺	mg/L					Ionic Balance	
														B ³⁺	As ³⁺	Al ³⁺	HCO ₃ ⁻	SO ₄ ²⁻		Cl ⁻
Main spring 1-2008 ^c	11/3/2006	520022/9019159	1140	74	nd	3700	802	102	21	16.2	74.2	0.024	0.725	0.621	0.113	0.004	-	146	175	66.9
Main spring 2-2008 ^c	6/27/2007	520112/9018786	1156	60.3	6.7	3830	775	95.4	30.3	15.6	71.8	0.125	0.696	0.614	0.145	0.023	3061	154	197	19.9
Ikumbi 1-2008 ^c	7/1/2007	530101/9015912	1236	42.4	6.7	650	100	46.9	15.5	5.8	124	0.003	0.0175	-	0.0015	0.003	683	0.98	8.2	26
Ikumbi 2-2008 ^c	7/1/2007	529870/9016233	1216	44.1	6.9	640	106	48.7	12.1	4.5	133	0.003	0.0206	0.0051	0.0018	0.007	583	1.72	9	18
Ikumbi 3-2008 ^c	7/1/2007	530359/9015768	1226	38.5	7	670	102	48.3	15.5	5.7	126	0.01	0.0171	-	0.0016	0.005	559	0.91	8.3	15
Ikumbi 4-2008 ^c	7/1/2007	530357/9015794	1227	44.1	6.8	670	102	48.7	13.5	4.9	125	0.001	0.0206	-	0.0018	0.004	629	1.35	8.7	22
Rambo 1-2007 ^e	6/7/2006	523058/9017886	1127	72	8.3	3700	806	83.4	10.5	7.9	-	0.011	0.758	2.87	0.1433	-	1760	139	181	0.96
Rambo 2-2007 ^e	6/7/2006	523026/9018021	1087	74.1	8.3	3700	821	83.5	15.9	8.5	-	0.03	0.751	2.84	0.1408	-	1730	138	180	3.8
Rambo 3-2007 ^e	6/7/2006	522965/9018008	1087	80.2	8.5	3800	818	82	17.1	8	-	0.177	0.762	2.88	0.1485	-	1760	143	184	0.9
Main spring 1-2007 ^e	11/3/2006	520022/9019159	1140	74	7.9	3830	802	102	21	16.2	-	0.024	0.725	2.46	0.1128	-	1880	146	175	4.1
Main spring 1-1998 ^g	-	-	-	18	7.8	-	852	113	20	19.5	50	-	0.8	0.122	-	-	2067	163	199	0.5
Main spring 2-1998 ^g	-	-	-	65	7.9	-	870	109	20	14.6	47.5	-	0.85	0.114	-	-	1924	165	227	1.5
Main spring 3-1998 ^g	-	-	-	75	8.3	-	843	109	24.1	14.6	62.5	-	0.83	0.114	-	-	1828	164	223	2.7
Main spring 1985 ^d	-	-	-	73	6.9	-	790	102	49	19	85	-	-	-	-	-	2770	160	184	14
Rambo 1-1978 ^b	-	-	-	86	6.6	-	840	93	23	8	68	-	-	-	-	-	3580	170	215	25.6
Rambo 2-1978 ^b	-	-	-	83	7	-	860	90	23	8.2	61	-	-	-	-	-	2580	165	220	11.6
Rambo 3-1978 ^b	-	-	-	73	6.8	-	790	102	49	19	85	-	-	-	-	-	2870	160	184	15.4
Rambo 1970 ^f	-	518362/9019980	-	65	8.4	-	805	114	20	14.6	90	-	-	-	-	-	1721	163	223	2
Kaguri 1959 ^b	Dec-55	-	-	66	8.4	2721	835	114	24.9	5.83	90.1	-	-	-	-	-	1818	163	223	1.8

3.4 Results

3.4.1 Thermal Springs Characterization

Songwe geothermal springs can be divided into five groups, based on their location: Iyola, Main springs, Kaguri, Rambo, and Ikumbi. Except Ikumbi springs, they are located along the Songwe river, at the west side of the Songwe graben. The graben represents a NW-SE extended structure with a river and carbonate deposits surrounding the springs [Figure 3.1](#). Iyola springs (62 to 74°C) rise near to the river and from the riverbed below the water with gas bubbles [Table 3.1](#). SW of Iyola and 50m elevated, Main springs discharge from thick-blocky travertine rocks with temperatures of about 68 to 75°C. In the western-central part of the Songwe graben, Rambo springs discharge with higher temperatures ranging between 70 and 83 °C also from travertine rocks. Kaguri springs discharge close to Rambo but at a lower elevation in the riverbed with lower temperatures of 48 to 71°C. Approximately ~6 km southeast of Rambo springs along the Ikumbi river, Ikumbi springs rise, with the lowest temperature of 37 to 44°C in the study area. The most abundant rocks at Ikumbi springs are volcanic rocks.

The pH of the thermal springs is near neutral to slightly alkaline (5.8 – 8.3), except for ‘Rambo new’ spring which exhibits a slightly acidic pH (4.8) (Arnorsson et al., 1982; Reed & Nicolas, 1984; Truesdell & Jones, 1974; Wilson, 1961). The electrical conductivity (EC) ranges from 410 to 3600 $\mu\text{S}/\text{cm}$ in our measurements and 3830 $\mu\text{S}/\text{cm}$ in former studies. The highest EC occurs in the Iyola springs (in former studies in Main springs) with increased concentrations of all common ions, while Ikumbi springs show the lowest EC [Table 3.1](#) (Henley & Ellis, 1983; Minissale et al., 2019; Nicholson, 1993). The dominant anion in Songwe geothermal springs is HCO_3 , ranging from 430 to 2248 mg/L in our measurements compared to up to 3580 mg/L in former studies. Also, the $\text{Cl-SO}_4\text{-HCO}_3$ triangular diagram [Figure 3.4](#) shows, that all the springs plot in the HCO_3 apex. Interestingly, Ikumbi springs show high concentrations relative to SO_4 and Cl but contain the lowest absolute bicarbonate. Cl and SO_4 are the second most abundant anions with lower concentrations of 8 to 223 mg/L, and 5 to 178 mg/L (in former studies up to 227 and 430 mg/L), respectively. Cl concentrations appear within the range of common geothermal fluids of about <10 to 100,000 mg/kg (Nicholson, 1993). The most dominant cations in the springs are Na with up to 980 mg/L, and K, Ca, Mg, Li and Fe, with lower concentration of 44 – 107 mg/L (formerly up to 114 mg/L), 12 – 61 mg/L (formerly 10 - 49 mg/L), 5 – 24 mg/L (formerly 3 - 20 mg/L), 0.02 – 0.79 mg/L, and less than 0.02 mg/L (formerly up to 0.17 mg/L), respectively [Table 3.1](#). The low concentrations of these cations are common for

geothermal fluids. In high temperature fluids, Ca and Mg typically occur at low levels of about < ~50 mg/kg and 0.01 – 0.1 mg/kg, respectively (Nicholson, 1993).

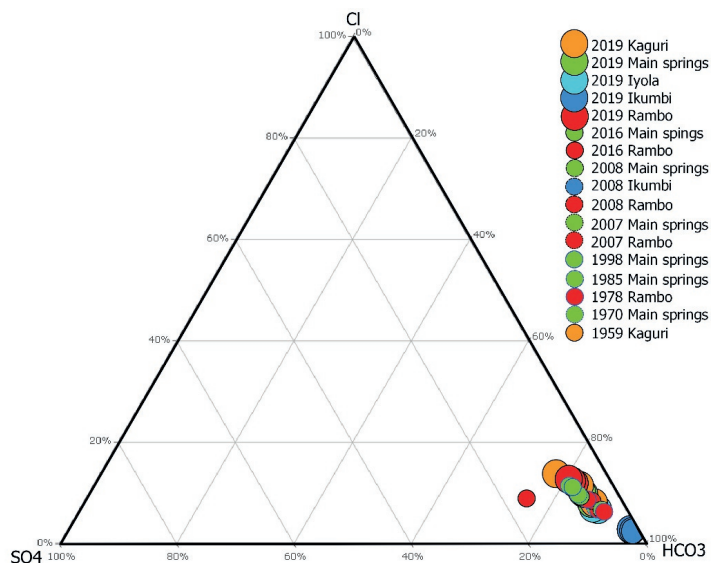


Figure 3.4 Water type of thermal manifestations in the Songwe area from 1959 to 2019 based on anion concentrations

3.4.2 Rock Composition

All geological layers have been observed during field work in 2019 mostly in unaltered conditions. XRD analysis show typical sandstone minerals for Karoo and Red Sandstone layers, e.g., quartz, feldspar, and muscovite. Several minerals have been detected in the Karoo Sandstone as indicators for high-temperature fluid-rock interaction, e.g., illite, smectite and kaolinite [Table 3.1](#). Fractures, observed especially in Red Sandstone and Karoo Sandstone outcrops, were filled with carbonates minerals. They form ~20% of the rock volume. Effective porosity and specific permeability measured in the laboratory show low values of maximum 21% porosity for the Red Sandstones and a maximum permeability of $1.3 \times 10^{-12} \text{ m}^2$ for Karoo Sandstones [Table 3.2](#). Geothermal manifestations mostly arise from travertines or Red Sandstone rocks, while Ikumbi springs are located within the Quaternary Volcanics in the east.

Table 3.2 Mineral composition and rock physical properties of selected rock formations in the Songwe graben

Name	Mineral composition	Porosity [%]	Permeability [m ²]
Proterozoic Metamorphics	K-feldspar, Ca-Al-pyroxene, FCO ₃ -apatite, titanite, amphibole, quartz, albite, and hematite (data from this study and Alexander et al., 2016).	-	2.2-6.9 x 10 ⁻¹⁴ (a)
Permo-Triassic Karoo Group	Quartz, muscovite, illite/smectite, kaolinite, K-feldspars, epidote, zircon, kyanite, pyroxene, chlorite, amphibole, calcite, and hematite (data from this study; Dypvik et al., 1990; Wopfner and Kaaya, 1991).	9.4 – 12.2 (a), 0.5 – 3.3 (c)	1.1 x 10 ⁻¹³ – 1.3 x 10 ⁻¹² (a)
Triassic Red Sandstone	Quartz, k-feldspar, muscovite, FCO ₃ -apatite, albite, nontronite-Ca, and nontronite-Na (data from this study; Alexander et al., 2016; Roberts et al., 2004).	15 – 21 (b)	8.4 x 10 ⁻¹³ (a)
Quaternary Volcanics	Quartz, albite, k-feldspar, illite, kaolinite, calcite, thenardite, Ca-Al-pyroxene, FCO ₃ -apatite, and amphibole (data from this study; Alexander et al., 2016; Mtelega et al., 2016)	-	-

^aThis study; ^bBeyer and Clutson (1978); ^cChristopher (2015).

3.4.3 Element Ratios in Thermal Water

The relative concentrations of lithium, chlorite and boron of Songwe thermal springs is shown in [Figure 3.5](#). Most of Songwe thermal springs plot close to the Cl corner, near the Cl-Li line and some close to older hydrothermal systems. Ikumbi springs show a slightly higher Cl relative to Li and B than other springs. All the springs plotting in [Figure 3.5](#) are consistent with the results of previous studies, except Rambo and Main springs in 2007 show a slight increase in B content (Giggenbach & Soto, 1992).

The Cl/B ratios show different trends for Ikumbi springs (89 – 616) compared to the other Songwe springs (103 – 111). Ikumbi springs also have a higher Cl/As ratio compared to the other springs. Our study shows that Kaguri and Rambo springs have high Na/Mg (>100) and Cl/Mg ratios (>14), a similar value to that presented in previous studies [Table 3.3](#).

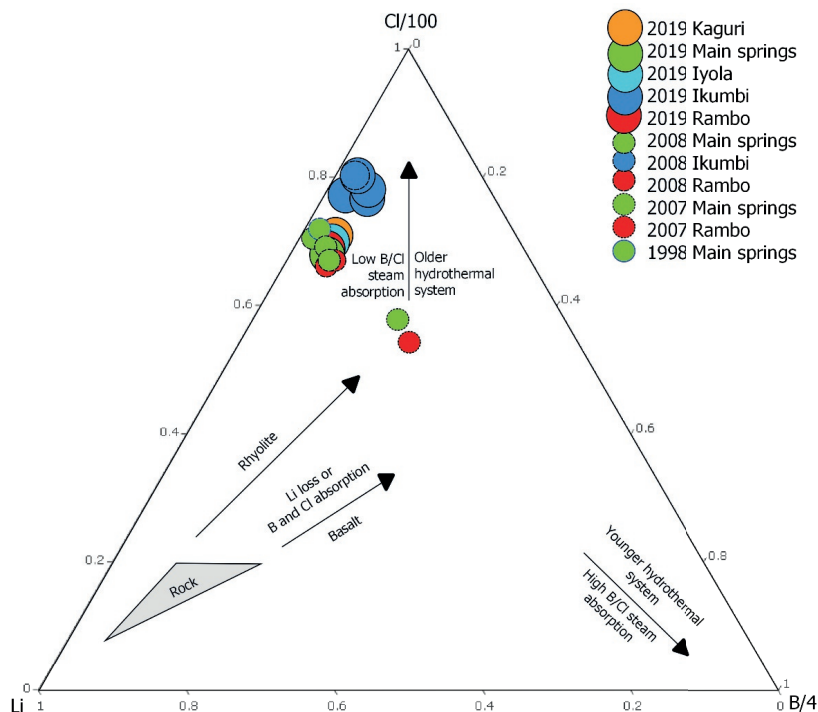


Figure 3.5 Relative concentration of Li-Cl-B of Songwe thermal manifestations from 1998 to 2019. (Ellis & Wilson, 1960; Nicholson, 1993)

Table 3.3 Ratios of element concentrations in thermal manifestations in this study (2019) and former studies from: (Alexander et al., 2016; James, 1959; Kraml et al., 2008; Makundi and Kifua, 1985; Mnjokava, 2007; Nzaro, 1970; Pisarskii et al., 1998; SWECO, 1978)

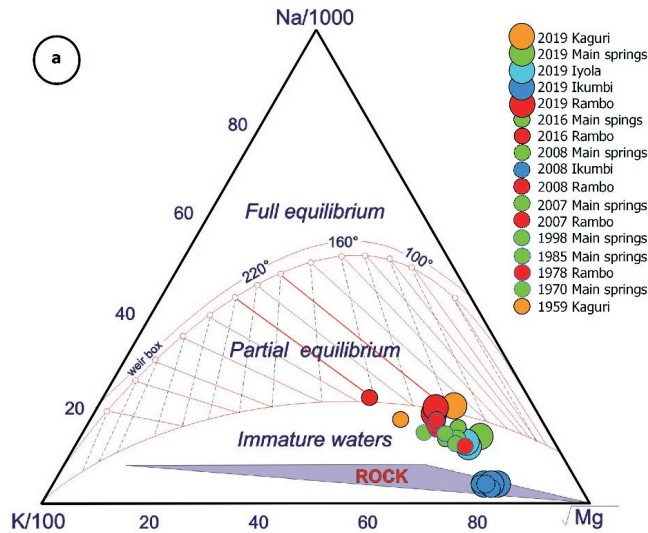
Springs	Sampling date	Cl ⁻ /B ³⁺	Cl ⁻ /As ³⁺	Na ⁺ /Mg ²⁺	Cl ⁻ /Mg ²⁺
Rambo old	11/5/2019	108		116	19
Rambo middle	11/5/2019	110		118	20
Rambo new	11/5/2019	109		113	19
Kaguri 1	11/7/2019	111		108	18
Kaguri 2	11/7/2019	108		106	15
Kaguri 3	11/7/2019	112		111	18
Main spring 1	11/5/2019	103		64	10
Main spring 2	11/5/2019	104		58	9
Main spring 3	11/5/2019	105		56	8
Main spring 4	11/5/2019	104		47	7
Iyola 1	11/5/2019	109		36	5
Iyola 2	11/5/2019	111		41	6
Ikumbi 1	11/6/2019	246		26	1
Ikumbi 2	11/6/2019	605		20	1
Ikumbi 3	11/6/2019	616		22	1
Ikumbi 4	11/6/2019	121		24	1
Ikumbi 5	11/6/2019	89		23	1

Rambo 2016 ^a	1/23/2016			256	46
Main spring 2016 ^a	1/19/2016			50	9
Rambo 1-2008 ^c	6/7/2006	76	2675	108	16
Rambo 2-2008 ^c	6/7/2006	77	2610	108	16
Rambo 3-2008 ^c	11/1/2006	90	4184	95	15
Rambo 4-2008 ^c	6/7/2006	77	2698	102	15
Main spring 1-2008 ^c	11/3/2006	86	3273	52	7
Main spring 2-2008 ^c	6/27/2007	98	2871	53	9
Ikumbi 1-2008 ^c	7/1/2007	543	11553	18	1
Ikumbi 2-2008 ^c	7/1/2007	19	10566	25	1
Ikumbi 3-2008 ^c	7/1/2007	19	10963	19	1
Ikumbi 4-2008 ^c	7/1/2007	19	10214	22	1
Rambo 1-2007 ^e	6/7/2006	22	2669	108	16
Rambo 2-2007 ^e	6/7/2006	497	2702	102	15
Rambo 3-2007 ^e	6/7/2006	607	2618	108	16
Main spring 1-2007 ^e	11/3/2006	597	3279	52	7
Main spring 1-1998 ^g	-			46	7
Main spring 2-1998 ^g	-			63	17
Main spring 3-1998 ^g	-			61	10
Main spring 1985 ^d	-			44	7
Rambo 1-1978 ^h	-			111	18
Rambo 2-1978 ^h	-			111	18
Rambo 3-1978 ^h	-			44	7
Rambo 1970 ^f	-			93	17
Kaguri 1959 ^b	Dec-55			151	26

3.4.4 Geothermometry

Solute geothermometers use variations of element concentrations in hot springs as a function of temperature to calculate the temperature of a geothermal system. Geothermometers are based on several assumptions including full equilibration and no-mixing, which not always meet realistic conditions (Fournier, 1977; Nicholson, 1993). HCO_3^- -waters, for instance, are often considered to occur far from the reservoir as a result of steam heating and condensation. However, depending on the geological setting, they can also represent deep reservoir fluids in non-volcanic but high temperature systems such as in Turkey and Africa (Nicholson, 1993). Therefore, the solute geothermometer calculations are still applied for Kaguri and Rambo springs, which have high surface temperatures, and high HCO_3^- concentrations. Additionally, the Na-K-Mg ternary diagram is used to estimate reservoir temperatures and shows that Kaguri and Rambo springs are partially equilibrated waters, which allows using them for geothermometer estimation *Figure 3.6*.

In the Na-K-Mg diagram, Rambo shows a distinctive span of Na-K temperatures over the years [Figure 3.6](#). Some samples plot in the range of 200 to 240 °C, exemplary for high-temperature systems, and some at 120 to 150°C exemplary for low temperature systems. In order to clarify the appropriate Na-K temperature for the study area, the Na-K geothermometer proposed by (Fournier, 1977; Giggenbach, 1988) is used. The results show that Kaguri and Rambo springs equilibrated at a subsurface temperature range of 216 to 232 °C [Table 3.4](#). Slightly higher temperatures have been proposed in previous studies: 217 to 256 °C for Rambo springs, 245 and 259 °C for Kaguri springs (Giggenbach, 1988; Hochstein, 1988). The Na-K-Ca geothermometer also shows high temperatures of >200 °C [Table 3.3](#). A Mg correction for the Na-K-Ca geothermometer, because Mg is very high in the Songwe thermal springs (up to 18 mg/L), then gives lower temperatures of 116 to 142 °C. Likewise, the K-Mg geothermometer suggests lower temperatures (125-148 °C) assuming interfering fast kinetic reactions with K and Mg, thus a faster re-equilibrium of the fluid. The low temperatures estimated by previous studies is confirmed by SiO₂ quartz geothermometry results, which predict that Songwe fluids equilibrated at 113 to 128 °C [Table 3.3](#). Although the chalcedony geothermometer predicts even lower temperatures of 82 to 104 °C, the correlation of SiO₂ content and C_{2K}/C_{Mg} indicates that mostly Kaguri and Rambo thermal waters are in equilibrium with SiO₂ quartz [Figure 3.7](#).



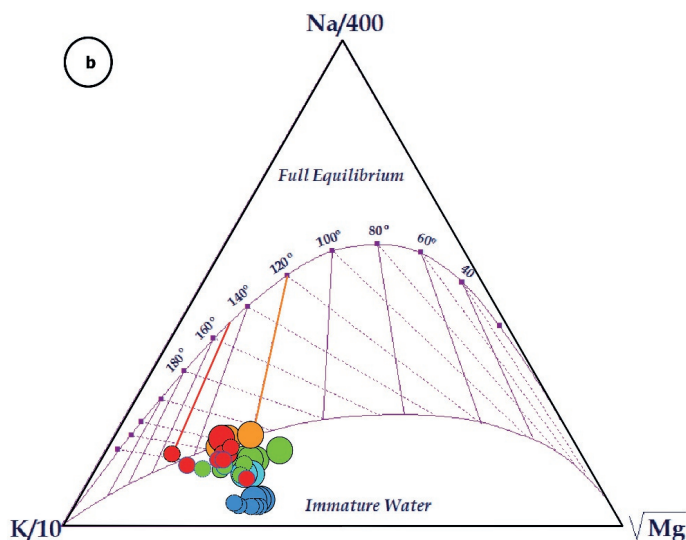


Figure 3.6 Relative concentrations of Na-K-Mg of Songwe thermal manifestations from 1959 to 2019 plotted in Giggenbach diagram for (a) high temperature systems (W. F. Giggenbach, 1988) and (b) lower temperature systems ($< 200^{\circ}\text{C}$) (Giggenbach & Soto, 1992)

Table 3.4 Estimation of reservoir temperature by different geothermometers for thermal manifestations in this study (2020) and former studies from: (Alexander et al., 2016; James, 1959; Makundi and Kifua, 1985; Pisarskii et al., 1998)

Springs	SiO ₂ Quartz (Fournier)	Chalcedony (Fournier)	Na-K (Giggenbach)	Na-K (Fournier)	Na-K-Ca	Na-K-Ca Mg correction	K-Mg
	°C						
Rambo old			227	211	209	137	125
Rambo middle			225	209	209	142	125
Rambo new			232	217	210	136	126
Kaguri 1			231	215	213	136	125
Kaguri 2			224	208	201	137	126
Kaguri 3			216	197	199	116	125
Rambo 2016 ^a	113	84	256	243	224	163	148
Rambo 1-2008 ^c	117	88	235	220	220	12	126
Rambo 2-2008 ^c	118	90	233	217	213	24	125
Rambo 3-2008 ^c	117	89	240	226	220	16	126
Rambo 4-2008 ^c		89	234	219	215	15	125
Rambo 1-2007 ^d			235	220	220	139	126
Rambo 2-2007 ^d			234	219	215	134	125
Rambo 3-2007 ^d			233	217	213	138	125
Rambo 1-1978 ^f	117	88	241	226	216	49	129
Rambo 2-1978 ^f	111	82	236	221	213	42	128

Rambo 3-1978 ^f	128	101	254	240	216	-23	119
Kaguri 1959 ^b	128	104	259	245	229	113	141

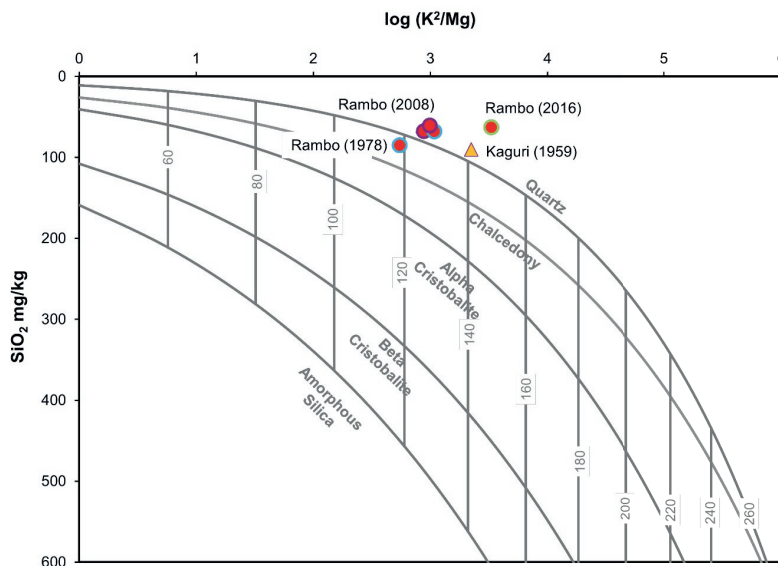


Figure 3.7 Diagram of SiO₂ vs log K₂/Mg of Songwe thermal water, concentration in mg/l, based on Giggenbach and Glover (1992). The curves provide information on equilibrium attainment for SiO₂ and K-Mg geothermometers. Most thermal water plots near the quartz curve, suggesting that equilibria with quartz took place rather than with chalcedony.

3.4.5 Mixing Model

Geothermometer application for mixed thermal waters can influence the reliability of the estimated temperature. Thus, two mixing models were applied to evaluate the subsurface temperature of the Songwe area, estimated by solute geothermometers. Figure 3.8 shows the silica-enthalpy model (Truesdell & Jones, 1974) for Rambo, Main springs, Kaguri and Ikumbi thermal springs. The mixing line is based on the sample with the highest and lowest silica content. The estimated temperature of the mixed thermal springs is between 100 °C and 124.5 °C based on the silica (chalcedony)-enthalpy mixing model, but the silica (quartz)-enthalpy mixing model shows higher temperature between 128.5 °C and 148.3°C. The chlorite-enthalpy mixing model results in a temperature of 142.5°C. Additionally, another evidence for mixing processes in our geothermal waters is shown by the relationship between Cl and conservative species B in Figure 3.9 . All the thermal springs show a linear relationship between Cl and B.

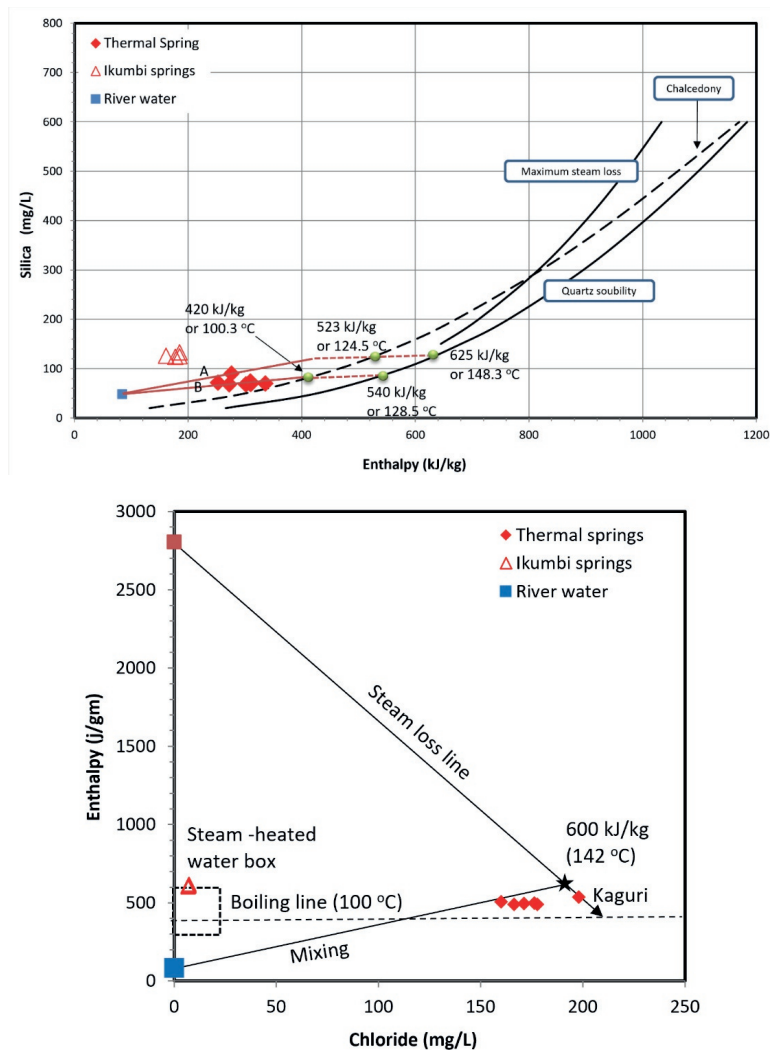


Figure 3.8 Mixing model of silica-enthalpy (based on chalcidony and quartz geothermometry temperature) and enthalpy-chloride (based on quartz geothermometry temperature). Silica concentration from previous geochemistry studies (see Table 3.1). The mixing lines on both diagrams are drawn from cold Songwe river water to the quartz solubility and to the steam line. Intersection points are based on the spring with higher concentration of silica (line A) and lower concentration (line B). Ikumbi springs were excluded from the mixing line because they were suspected as steam-heated waters.

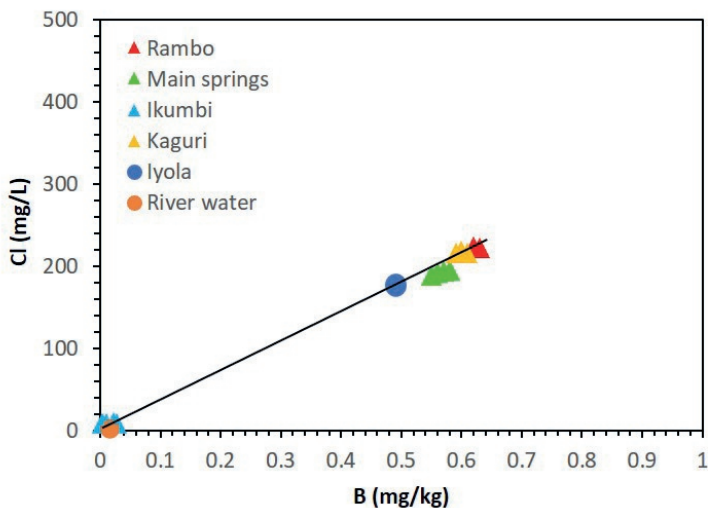


Figure 3.9 Linear relationship between Cl and B of Songwe thermal springs.

3.4.6 Reservoir Fluid Chemistry

The fluid characteristics for the reservoir temperature were reconstructed using one representative spring water composition out of each group: Rambo old, Kaguri 1, Main spring 2, Iyola 1 and Ikumbi 4. Concentrations of all species were calculated for 125 °C and 148 °C, representing the Songwe deep reservoir temperature, based on K-Mg geothermometer results. At these temperatures, it is assumed that the steam separates from the fluid phase during boiling and ascent to the surface. After the steam fraction is subtracted from the reservoir fluid, the liquid phase has a smaller mass and increased concentration of elements. Therefore, all solute concentrations of the reservoir fluid in Table 3.5 are lower than thermal springs at surface.

The pH of the reservoir fluid can be estimated using mineral equilibria reaction. Carbonate and especially calcite dissolution equilibria are commonly used to get a close approximation of the reservoir pH. First, carbonate equilibria are used in this study since Songwe thermal springs are dominated by bicarbonate evolving from the dissociation of dissolved carbon dioxide into bicarbonate and hydrogen in equilibrium governing described (Nicholson, 1993):



The XRD data of rock samples in all springs, also show calcite minerals, thus, we additionally applied the calcite dissolution equilibria. The calcite method gives a lower pH value (5.8 – 6.3) than the carbonate method (6.0 – 6.2, Table 3.5). The differences in pH from both methods are the consequence of carbonic species concentration in the sample. The pH also differs depending

on temperature. For the calcite equilibria, the lower pH (5.8) occurs at 148 °C which increases with decreasing temperature (125 °C: 6.3). The bicarbonate method has a reverse trend. Based on the assumption that pH varies with temperature and a neutral pH 7 observed at surface, a pH of ~5.5 at higher reservoir temperatures at depth is expected (Nicholson, 1993). In our case, the pH calculation with calcite dissolution equilibria shows more reliable results.

Table 3.5 Estimated chemical composition of reservoir fluid at 125 oC and 148 oC based on the chemical concentration of thermal springs using steam fraction calculation, K-Mg geothermometer and calcite dissolution equilibria calculation for pH.

Springs	T surface (°C)	pH springs in the field	T Reservoir (°C)	Steam fraction	pH (H ₂ CO ₃)	pH (CaCO ₃)	mg/L							
							Na ⁺	K ⁺	Ca ²⁺	Mg ²⁺	Fe ^{2+/3+}	HCO ₃ ⁻	SO ₄ ²⁻	Cl ⁻
Rambo old	82.7	6.5	125	0.08	6.1	6.1	800.3	74.8	17.5	7.3	0.0029	1688.7	163.10	205.3
Kaguri 1	70.9	8.6	148	0.12	6.0	6.2	763.1	71.3	16.7	6.9	0.0027	1610.3	155.5	195.8
			125	0.10	6.1	6.0	782.8	76.8	15.3	7.6	0.0061	1464.1	159	197.2
Main spring 2	75.5	6.2	148	0.14	6.0	6.0	746.1	73.2	14.6	7.3	0.0058	1395.4	151.6	187.9
			125	0.09	6.0	6.1	739.7	79.6	33.7	13.6	0.0042	1759.7	156.4	176.3
Iyola 1	74.4	6.8	148	0.13	5.8	6.2	714.7	75.9	32.1	12.9	0.0040	1677.6	149.1	168.1
			125	0.09	5.9	6.1	742.8	97.2	55.4	21.5	0.0066	1966.8	153.3	159.6
Ikumbi 4	41.3	7.9	148	0.13	5.7	6.2	708	92.6	52.8	20.5	0.0063	1874.8	146.1	152.1
			125	0.15	6.4	6.1	103.2	39.3	11.9	4.5	0.0015	374.67	4.7	6.9
			148	0.19	6.3	6.2	98.2	37.5	11.4	4.3	0.0015	356.7	4.5	6.6

3.4.7 Mineral Saturation Indices

In order to calculate mineral saturation indices, the Phreeqc program Parkhurst & Appelo (2013) is used to identify possibly precipitating minerals, shown by positive saturation indices. Our model represents thermal water at surface temperature and at reservoir temperature reacting with different lithologies in the study area. Input data are thermal spring compositions and calculated reservoir fluid compositions at temperatures of 125 °C and 148 °C including pH, Na, K, Ca, Mg, Fe, HCO₃, SO₄, and Cl [Table 3.1 and Table 3.5](#). The primary minerals of each lithology in the Songwe area are from XRD data of rock samples and literature [Table 3.2](#). There are eight scenarios modelled for the hot spring cluster at surface conditions: scenario I-V for Rambo, Kaguri, Main springs, and Iyola, and scenario VI, VII and VIII for Ikumbi springs, including volcanics observed at shallow depth [Table 3.6](#). At reservoir conditions, scenario I-V were modelled for reservoir fluids reconstructed from all springs, but scenario VI-VIII for Ikumbi springs only. In scenario I and IV, the thermal water reacts with a single lithology (Metamorphic rocks or Red Sandstone). While in scenario II, III, V, VI, VII and VIII, a mixture of lithologies from oldest to youngest (Metamorphic, Karoo, Red Sandstone, Volcanic) reacts with the water simultaneously. The reaction delivers a new fluid composition and oversaturated minerals, which precipitate at reservoir depth. The results are then compared to sampled water and mineral compositions as calibration data, to test which rocks the reservoir water has been in contact with. The resulting oversaturated minerals were divided into groups: weathered volcanics, clays, apatites, weathered metamorphics, and hydrothermal minerals. In the surface temperature model, the modelled oversaturated minerals are compared to minerals encountered at the hot springs and the real hot spring water composition to understand reservoir water flow pathways and its interaction with rocks. In more detail, minerals precipitating at hot springs derive from dissolved solids in the reservoir water, attained through water-rock interaction at depth. Our model can show at which rock layer the finally precipitating minerals have been dissolved.

Table 3.6 Scenario reactions for modelling the fluid-rock interactions in Songwe geothermal area.

Lithology	Mineral composition (input)	Scenario					The calibration minerals	
		Scenario I Thermal water + Metamorphics	Scenario II Thermal water + Metamorphics and Karoo	Scenario III Thermal water + Karoo and Red Sandstone	Scenario IV Thermal water + Red Sandstone	Scenario V Thermal water + Metamorphics, Red Sandstone and Karoo	T surface	T Reservoir
Proterozoic Metamorphics	K-feldspar, Ca-Al-pyroxene, FeCO_3 -apatite, titanite, amphibole, quartz, albite, and hematite (data from this study and Alexander et al., 2016).	Scenario I Thermal water + Metamorphics	Scenario II Thermal water + Metamorphics and Karoo	Scenario III Thermal water + Karoo and Red Sandstone	Scenario IV Thermal water + Red Sandstone	Scenario V Thermal water + Metamorphics, Red Sandstone and Karoo		Apatite
Permo-Triassic Karoo Group	Quartz, muscovite, illite/smectite, kaolinite, K-feldspars, epidote, zircon, kyanite, pyroxene, chlorite, amphibole, calcite, and hematite (data from this study; Dypvik et al., 1990; Wopfinger and Kaaya, 1991).			Scenario III Thermal water + Karoo and Red Sandstone	Scenario IV Thermal water + Red Sandstone	Scenario V Thermal water + Metamorphics, Red Sandstone and Karoo	Calcite and aragonite	Illite, smectite, kaolinite, chlorite, calcite
Triassic Red Sandstone	Quartz, k-feldspar, muscovite, FeCO_3 -apatite, albite, nontronite-Ca, and nontronite-Na (data from this study; Alexander et al., 2016; Roberts et al., 2004).			Scenario III Thermal water + Karoo and Red Sandstone	Scenario IV Thermal water + Red Sandstone	Scenario V Thermal water + Metamorphics, Red Sandstone and Karoo		Apatite, nontronite
Quaternary Volcanics	Quartz, albite, k-feldspar, illite, kaolinite, calcite, thenardite, Ca-Al-pyroxene, FeCO_3 -apatite, and amphibole (data from this study; Alexander et al., 2016; Mtefela et al., 2016)					Scenario VIII Thermal water + Red Sandstone and Volcanics	Analcime, Chabazite-Ca, Muscovite, Smectite	Illite, kaolinite, calcite, thenardite, apatite

3.5 Discussion

3.5.1 Hydrogeochemistry

The results show that all the thermal springs in the Songwe area have a Na-HCO₃ water type. This is related to the presence of bicarbonate in the reservoir rocks. At Ikumbi springs, located within volcanic rocks, the HCO₃ can also form near surface when CO₂ gas and steam condenses into cold water (steam heated water). The enthalpy-chloride model also shows that Ikumbi thermal waters plot in the steam heated water area *Figure 3.8*.

Kaguri, Rambo, Main springs, Iyola and Ikumbi have a similar water type, but different fluid pathways or a change of lithology at depth, shown by different element ratios. Element ratios can be used to identify the common source of reservoir fluids and identify physicochemical processes in a geothermal system (Nicholson, 1993). Relatively high Na/Mg and Cl/Mg ratios are typical for high temperature fluids, that reach the surface rapidly defining the upflow zone of the system (Nicholson, 1993). The ratios suggest that Kaguri and Rambo are situated in the upflow zone and are directly fed from the reservoir. This is in good agreement with high surface temperatures observed in both springs. Thus, Songwe thermal springs form a geothermal area with an independent geothermal (heat) source and are not an outflow of the Ngozi volcanic geothermal system as suggested by previous studies (Delvaux et al., 2010; GeothermEx & Colin Harvey, 2013). During their rise to the surface, there is a chance that Songwe springs might mix with cold groundwater in the upflow zone. It can be seen in *Figure 3.9* that shows a linear relationship between Cl and B. As a conservative species in geothermal fluids, Cl content will increase continuously during progressive water-rock interaction.

The alkali metal Li, which is least affected by secondary absorption processes, is typically used together with conservative elements B and Cl for evaluating a possible origin of geothermal fluids (Giggenbach & Soto, 1992). Our results suggest that Songwe thermal springs were formed through absorption processes with low B/Cl magmatic vapor input and originate from an older hydrothermal system. Tritium data (Kraml et al., 2010) have been used to explain that Songwe thermal springs have very low (0.00 ± 0.02) tritium, suggesting relatively high residence times in the subsurface.

3.5.2 Reservoir Temperature Estimation

Classical geothermometers have been applied to Songwe geothermal springs which yield a wide range of temperatures from previous geochemistry studies. Makundi & Kifua (1985) argued that as part of the Mbeya volcanic area, Songwe is a high enthalpy system with temperatures of

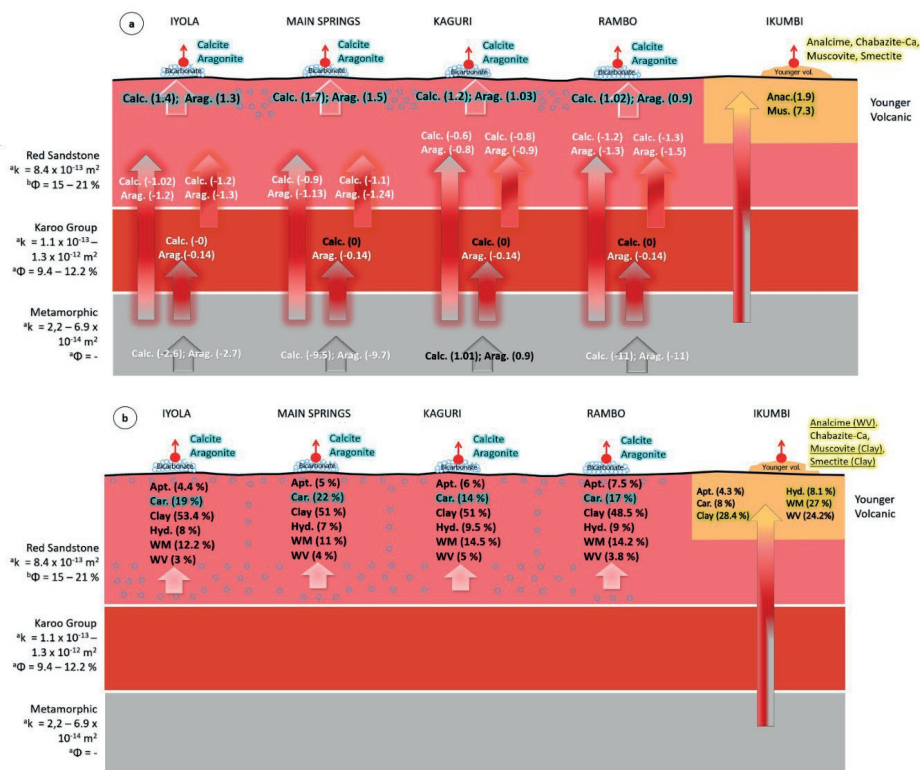
217 °C based on the Na-K-Ca geothermometer. However, the Na-K-Ca geothermometer shows unreliable high temperatures because it is applied to HCO₃ waters in a low temperature system (Pope et al, 1987). Likewise, this study shows overestimated Na-K geothermometer results because Kaguri and Rambo springs not being fully equilibrated and kinetic reactions including Na and K causing a slow re-equilibration [Figure 3.6](#) (Giggenbach, 1988; Hochstein, 1988). In contrast, this study suggests that Songwe is a low to medium enthalpy geothermal system. K-Mg geothermometers and Na-K-Ca_(Mg correction) ([Table 3.4](#)) give reasonable approximations of reservoir temperatures in the range of 125 to 148 °C. This is in good agreement with Alexander et al., (2016) who also predicted lower temperatures (112 ± 16 °C) based on K-Mg, Silica and quartz geothermometers.

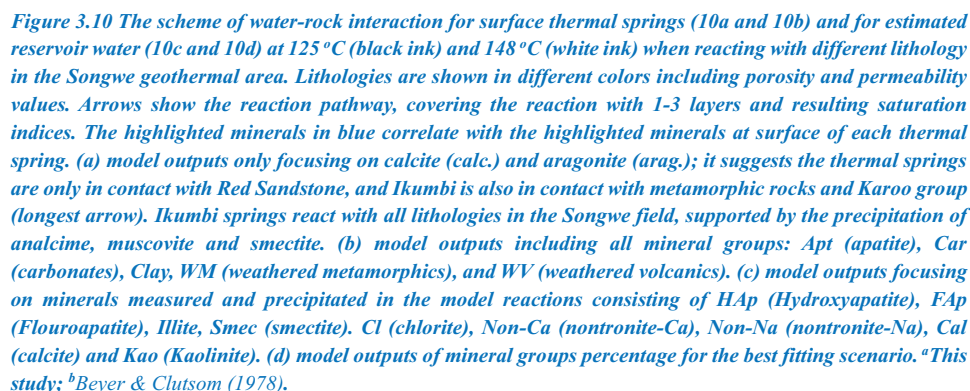
The silica-enthalpy and enthalpy-chloride mixing models show that the temperature of possible parent fluid in the study area are in the range of 100 to 149.5 °C. Those numbers are higher than those obtained by the quartz geothermometer [Figure 3.8](#) and [Table 3.3](#), which suggests that most of the hot water is mixing with cooler water from shallow aquifers and/or that conductive cooling takes place during the ascent of the geothermal fluid to the surface.

3.5.3 Water-Rock Interaction Modelling

Each of our hydrogeochemical models results in possibly precipitating mineral groups, while percentage and composition differ. A comparison with the mineral composition of the reservoir rocks and minerals precipitated at surface we obtained best fits of our models. The best fitting scenarios are summarized in [Figure 3.10](#), including saturation indices and percentages. Lithologies are shown in colored layers including porosity and permeability values. Arrows show the reaction pathway, covering reactions with 1-3 layers and resulting saturation indices. The highlighted minerals in blue and yellow correlate with the observed minerals at each thermal spring. [Figure 3.10\(a\)](#) focuses on carbonate precipitation, [Figure 3.10\(b\)](#) also shows other precipitating minerals at surface temperature. At Rambo, Kaguri, Iyola, and Main springs only carbonate minerals were detected at surface, while at Ikumbi mainly analcime, muscovite, and smectite have been detected. The best fitting model, showing carbonate precipitation in the model and in real case at Rambo, Iyola, Kaguri, and Main springs is when the fluid reacts only with Red sandstone (scenario IV). For Ikumbi, scenario VI (reaction with Metamorphics, Karoo, Red Sandstone and Volcanics) results in the best fit. [Figure 3.10\(b\)](#) presents the final results of the model, showing that Iyola, Main springs, Kaguri and Rambo spring water is mainly dissolving minerals from the Red Sandstone, resulting in massive carbonate precipitation at surface. Also, Ikumbi waters have been in contact with all lithologies, resulting

in the precipitation of Analcime, Chabazite-Ca, Muscovite, and Smectite. [Figure 3.10\(c\) and \(d\)](#) show the reaction results at reservoir condition. The precipitation of measured minerals is only found in modelled reactions of scenario II, III and V for Iyola, Main springs, Kaguri and Rambo and scenario III, IV, VI, VII and VIII for Ikumbi. The best fitting model for Rambo, Iyola, Kaguri and Main springs at 125 °C and 148 °C is when the reaction involves the fluid, Karoo and Red sandstone (scenario III). It shows the most secondary minerals precipitating (group of apatites, clays and hydrothermal minerals) in the modelled reaction and the measured minerals. Scenario VI is the best fitting model for Ikumbi where the group of apatites, clays and weathered volcanics precipitate in the modelled reaction confirmed by measured data. This is consistent with the Li-Cl-B data of Ikumbi [Figure 3.5](#) that show a slightly higher Cl content relative to Li and B than other springs indicating that Ikumbi migrated from fluid in the old basement rock.





through faults and fractures in the basin. Water-rock interaction during the rise leads to secondary hydrogeochemical processes that change the chemical composition of thermal water.

Both models suggest that during ascent fluids reach more permeable lithologies like the Karoo and Red Sandstones. Due to higher permeability fluids now also percolate laterally within the sandstones and have a longer reaction time with these carbonate rich rocks. They eventually rise towards the surface at minor fracture sets, as observed at Rambo, Kaguri, Main springs and Iyola. Ikumbi water additionally is in contact with volcanic rocks overlaying the sandstones. Both hydrochemical models, calibrated with reservoir or surface temperature show, that these fluids are dominated by water-rock-interaction in the Red Sandstone *Figure 3.11*

During ascent of the fluids, temperature and pressure drops, resulting in cooling and degassing of CO₂. Degassing results in decreased solubility of HCO₃ and calcite/aragonite oversaturation, causing massive travertine deposits. High HCO₃ and Na concentrations in all spring waters support the theory of carbonate dissolution from the Red Sandstone layer as the most common water-rock interaction in the Songwe basin.

Conventional geothermometry predicts reservoir temperatures in the range of 125 to 148 °C. The hydrochemical model at reservoir condition shows that thermal fluids react with Karoo and Red Sandstone in the study area. The higher the reservoir temperature, the deeper the lithology in contact with thermal fluids.

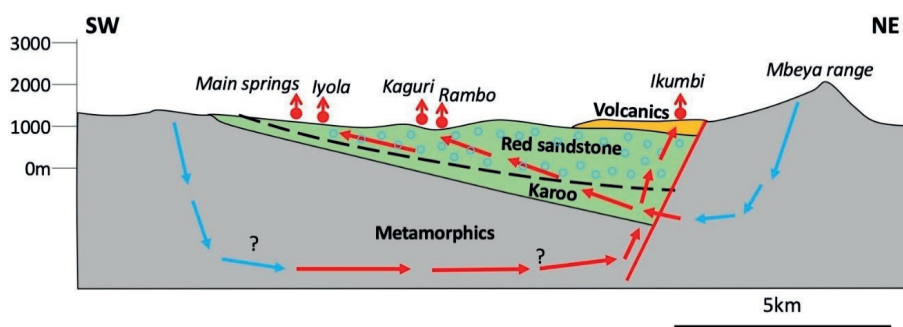


Figure 3.11 Conceptual fluid flow model of the Songwe area after hydrogeochemical model interpretation. Showing fluid infiltration in the NE and supposedly SW, fluids rising along the fault and percolating within the sandstones before discharging in hot springs (Christopher, 2015). These are two different pathways, one is the Ikumbi which is a deep source and another one which is less deep; the two pathways do not cross in 3D

3.6 Conclusion

This study presents a fluid source model of the Songwe geothermal system using data on the composition of thermal spring fluids, primary minerals of lithologies, and a water-rock reaction model. The medium to high temperature thermal waters of neutral pH and Na-HCO₃ type are driven by advective flow through interconnected fault/fracture networks. Fluid-rock interaction within permeable zones causes re-equilibrium of fluids with rocks, in fast kinetic reactions of mainly Mg with K, as well as Na and Ca with Mg correction. The K-Mg and Na-K-Ca (Mg correction) geothermometer shows an equilibrium temperature for the reservoir fluid between 125 and 148 °C. The reconstruction of the chemical fluid composition under reservoir condition and at surface temperatures are used to identify water-rock reaction scenarios most suitable for mimicking measured minerals in the rocks and for imitating minerals precipitating at the surface (i.e. calcite, aragonite, analcime, muscovite, and smectite). There are three best fitting reaction scenarios for fluid-rock interaction for different conditions and it can be used to identify the thermal water source: scenario IV for Kaguri, Rambo, Iyola, and Main springs, at surface temperature and scenario III at reservoir temperature and scenario VI for Ikumbi springs at both conditions. The thermal springs have been in contact with Red Sandstone only at surface temperature, but at the higher temperatures, thermal water also reacts with deeper lithologies like Karoo and Red Sandstone. Ikumbi is in contact with all lithologies including Younger Volcanics. These results are supported by relatively high Na/Mg and Cl/Mg ratios at Rambo and Kaguri, as well as partial equilibration of thermal spring water, which suggests that Rambo and Kaguri is directly fed from reservoir and located in the upflow zone of the Songwe geothermal system. The other springs are located at the outflow zone that are generally controlled by NW-SE trending faults and fractures.

4 NATURAL STATE NUMERICAL MODELLING

4.1 Introduction

This chapter answers the research questions “What is the permeability distribution?” and “How does fluid flow in the subsurface?” To answer this research question, we use a combination of numerical modelling and knowledge from the previous chapters.

Geothermal reservoir modelling enables the understanding of the heat transport and hydraulic behaviour of the geothermal reservoir based on various laws such as conservation of heat, conservation of mass and Darcy’s law. The model is calibrated using real data from field and laboratory measurements. Geothermal modelling involves collecting and studying data, developing a conceptual model, creating and calibrating the natural state model, which is used to generate the production model (O’Sullivan, 2014). All of these steps are part of this thesis with field and laboratory data presented in Chapter 3 and the conceptual model presented in Chapter 1 and an updated version in Chapter 3. The conceptual model is further improved using detailed structural geological data and presented with the numerical modelling in this chapter.

In this chapter, we develop a natural state numerical model for Songwe geothermal system. A natural state model is a reservoir model of a geothermal system prior to any production. It is the mathematical representation of the physical behaviour of the geothermal system, for which a computer model is set up with the available data on fluid properties and heat as input as well as the permeability structure of an actual reservoir, in order to simulate the system before exploitation (Jalilinasrabad et al., 2021; Rachmat et al., 2019). We use the updated conceptual model based on the new geochemical and structural geological data and the constructed three-dimensional geological model (presented in chapter 2), taking into consideration the geologic structures such as faults and stratigraphic boundaries of the Songwe basin with their lateral changes in thickness so that their effect is well represented to create a natural state model to give insights into the permeability distribution and natural fluid flow.

The initial assumption for the simulations of natural state is that the system is firstly assumed to be cold and then heating of the system starts over time. The state of the pre-production approximation is attained on the assumption that the temperatures and pressures in the reservoir are in equilibrium (Bjarkason et al., 2019). Pre-production data such as exploration well data

and surface features are used to calibrate natural state models (O’Sullivan, 2014). In our case, we use the geothermometer reservoir temperature to calibrate Songwe natural state model due to lack of well data.

The scopes of most of the existing studies such as Alexander et al. (2016); Bushi et al. (2016); Hinz et al. (2018); Marini Luigi (2016); Roberts et al. (2004) are limited to single aspects of the geology, geochemistry, and geophysics of Songwe basin as stated in details in chapter 1. None of the previous studies integrated the available data to give a combined interpretation.

4.2 Method

We model the Songwe sedimentary basin using numerical modelling method by coupling fluid flow and heat transfer. We use Darcy’s law described in equations 4.1

$$\frac{\partial}{\partial t}(\varphi\rho) + \nabla \cdot (\rho u) = Q_m \quad 4.1$$

$$u = -\frac{k}{\mu}\nabla p \quad 4.2$$

where φ is the porosity ρ is the fluid density, u is the Darcy’s velocity, Q_m is the mass source (SI unit: $\text{kg}/(\text{m}^3 \cdot \text{s})$), k is the permeability, μ is fluid’s dynamic viscosity, p is fluid’s pressure in the pore.

We model the heat transfer in porous media by convection and conduction whereby the temperature equation 4.3 links to the convection-diffusion equation with thermodynamic properties to cater for both solid matrix and fluid properties.

$$(\rho C_p)_{\text{eff}} \frac{\partial T}{\partial t} + \rho_f C_{p,f} u \cdot \nabla T + \nabla \cdot q = 0 \quad 4.3$$

$$q = -k_{\text{eff}} \nabla T \quad 4.4$$

Where by $(\rho C_p)_{\text{eff}}$ is the effective volumetric heat capacity at constant pressure ($\text{J/m}^3\text{C}$), ρ_f is the fluid density (Kg/m^3), $C_{p,f}$ is the fluid's heat capacity at constant pressure (J/(kg.K)) and k_{eff} is the effective thermal conductivity of the matrix (W/(m.K)). Heat transfer by convection is represented by the second term on the left side of equation 4.3 whereas heat transfer by conduction is shown by the third term on the same equation.

4.2.1 Model Description - Geometry

A 3D geometry with dimensions of 12 km in width, 16 km in length and 4.7 km depth is used for modelling in this study with minimized complexity that excludes the topography of the area as described in chapter 2. Structures such as faults are incorporated in the 3D geometry as 2D elements, they include the fault along the Mbeya Range from which meteoric water enters the Songwe basin according to the conceptual model described in chapter 3, and also faults in the centre of hot springs area.

4.2.2 Mesh

The domains in a 3D geometry are discretized into small simple shapes such as tetrahedral, prism, pyramid or hexahedral, known as mesh elements. The geometry boundaries are discretized into quadrilateral or triangular boundary elements whereas the edges are discretized into edge elements *Figure 4.1*. In this study, the maximum element size is 557m and minimum element size is 23.9m.

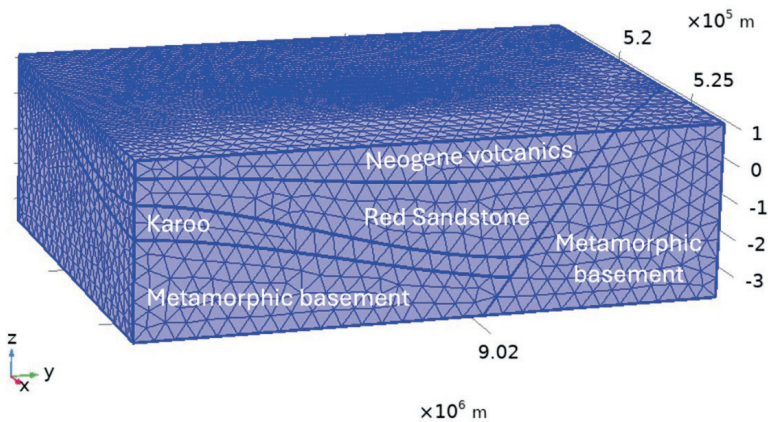


Figure 4.1 Meshed grid for the 3D geometry. The x-axis represents the GPS-easting coordinates, the y-axis represents the GPS-northing and the z-axis is the depth of the model.

4.2.3 Rock Properties

In natural state numerical simulation, the choice of material properties plays an important role in obtaining the best match to the geothermal field. For this study, thermal properties are obtained from literature as described in chapter 2, while permeability values are adopted from chapter 3.

4.2.4 Boundary and Initial Conditions

Setting boundary and initial conditions is pre-requisite for the stability of the model results. Boundary conditions characterise natural recharge, manifestations, regional or lateral flows, inflows, and outflows of the aquifers. Thermal boundary conditions describe fixed values of temperature, heat flow and adiabatic conditions.

We have adopted the conceptual model described in chapter 3 to define the fluid flow direction in which we apply Dirichlet boundary conditions, whereby we define pressure on the side boundaries of the model geometry shown in *Figure 4.2(a)* as per equation 4.5.

$$P = p_{\text{suf}} - (z\rho g)$$

4.5

where P (Pa) is pressure at depth, z (m) is the model's depth, p_{suf} (Pa) is the pressure at surface, ρ is the density of fluid and g is the gravity acceleration (m/s^2)

We similarly apply this boundary condition for the hot springs by assigning pressure values on fracture corridors, because these are locations where hot water discharges from the geothermal system to the surface. We calculate air pressure at hot springs altitudes and assign the pressure to the fault corridors *Table 4.1*.

In all rock formations, hydrostatic conditions are similarly defined using equation 4.5 as the initial condition. To account for rain infiltration in the model as a recharge according to our conceptual model explained in chapter 3, we assign a precipitation rate of 285mm/year on the NE of the Mbeya fault based on the annual rain fall data for Songwe.

For the heat transfer, we define heat flow on the side boundaries of the model geometry as per equation 4.6 to allow the possibility of heat transfer across boundaries, as fluid flows in the same direction as per our conceptual model. We use a geothermal gradient in the range of 25 - 40 °C/km. Consequently, the top and bottom boundaries are insulated. We similarly use equation 4.6 to define initial temperature in all domains. The top boundary is fixed with a surface

temperature of 21 °C except for the upper part of the faults that represent hot springs, which have fixed temperatures of the respective hot springs [Table 4.1](#)

$$T = T_{\text{surf}} - (zT_{\text{grad}})$$

4.6

where T_{surf} is the surface temperature (°C), T_{grad} is the temperature gradient (°C/ km), T is the temperature at a certain depth(°C) and z is depth (km).

The heat source of our model is the vertical temperature gradient (°C/ km).

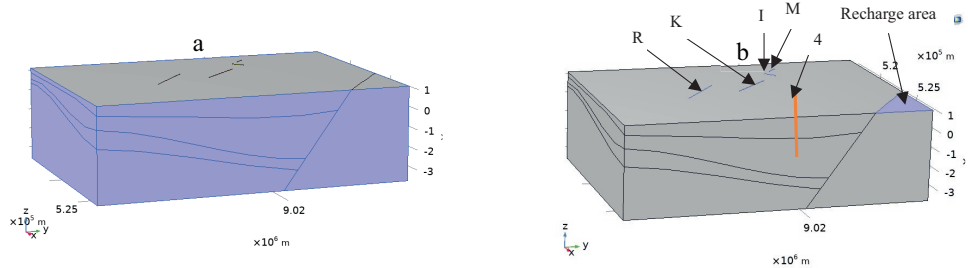


Figure 4.2 Boundary condition visualization. *R*=Rambo hotsprings fractures; *K*=Kaguri hotsprings fractures; *I*=Iyola hotsprings fractures; *M*=Main hotsprings fractures; *4*=theoretical borehole location 4.

Dirichlet boundary condition, where pressure and heat are defined allowing movement of fluid and heat (a); pressure value assigned allowing fluid flow in fracture corridors (b)

Table 4.1 Assigned pressure and temperature values as boundary conditions on fracture corridors

Fracture corridor	Altitude (m)	Air pressure at altitude (Pascal)	Temperature (°C)
Iyola springs	1057	89,488.90	74
Main springs	1127	88,746.47	75
Rambo springs	1124	88,778.18	83
Kaguri springs	1080	89,244.40	71

4.2.5 Calibration of the Model

The aim of the natural state simulation is to replicate the temperature and pressure distribution prior to any exploitation (Jalilinasrabady et al., 2010; Rachmat et al., 2019). Additionally, Jalilinasrabady et al. (2010) recommend the natural state numerical simulation model to be run over a time that enables the geothermal system to go to the steady state without any recharge or production wells. In this study we simulate the model without any artificial recharge or discharge for 150 years. The equilibrium is attained at approximately 80 simulation years *Figure 4.3*.

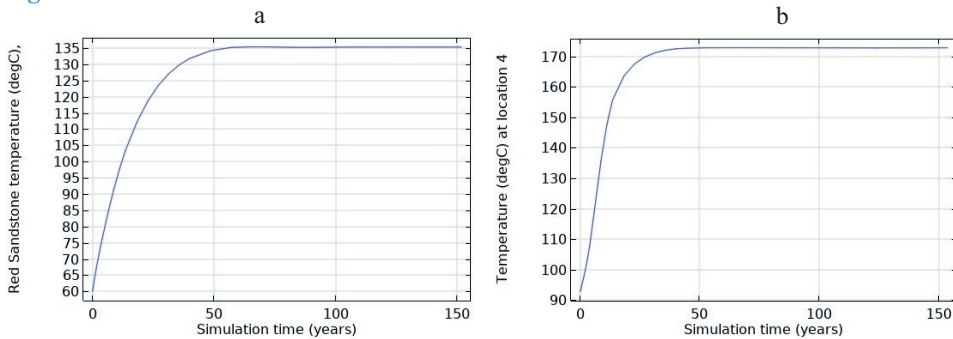


Figure 4.3 Simulated reservoir temperature at geothermal gradient of 35°C/km (a) for the whole Red Sandstone volume and (b) for the theoretical borehole location 4 shown on figure 4.2b

We performed the natural state calibration of the model by carrying out several iterative processes, which involved changing the geothermal gradient values in order to obtain a good fit between the model and the geochemical calculation. Specifically, our focus in this study was to obtain a good fit between the reservoir temperature of the model and the calculated geothermometer temperature (125-148 °C) based on field measurements. The natural state simulation results (reservoir temperature) are then compared with calculated reservoir temperatures from geothermometers.

4.3 Simulation Results and Discussion

4.3.1 Updated Conceptual Model regarding Fluid Flow

The present state of stress observed in faults of the model region has a compressive component in the NNE-SSW direction, and fractures are open parallel to that direction. Most of them have a strike-slip component although not always recognizable in the field. Large strike-slip faults observed by earlier studies have not been confirmed by this study. All structures observed are conductors allowing fluid to flow.

A differentiation of water types across the area led to the conclusion that the Ikumbi springs belong to a different reservoir system and the Songwe system is separated from the Ngozi volcanic system. Ikumbi spring waters are strongly influenced by mixing with shallow groundwater, in place or infiltrating through the Mbeya fault, and therefore show lower salinities. Their fluid pathways cross the younger volcanic deposits in the Songwe graben, and therefore the water contains less HCO_3^- and has a different Cl/B ratio (Asnin et al., 2022). The other springs belong to a common flow system, while the upflow of the geothermal system is at the Rambo springs and the remaining springs are mainly fed by lateral flow. The Main springs show patterns, e.g. high Fe, K, Ca concentrations, of a longer contact of water with the Karoo sandstones. The discharge in hot springs is associated with massive travertine precipitation with several hundreds of m in thickness (personal communication with TGDC). The carbonate minerals are dissolved from Red Sandstone layers and precipitate as soon as temperature and pressure drop at the surface.

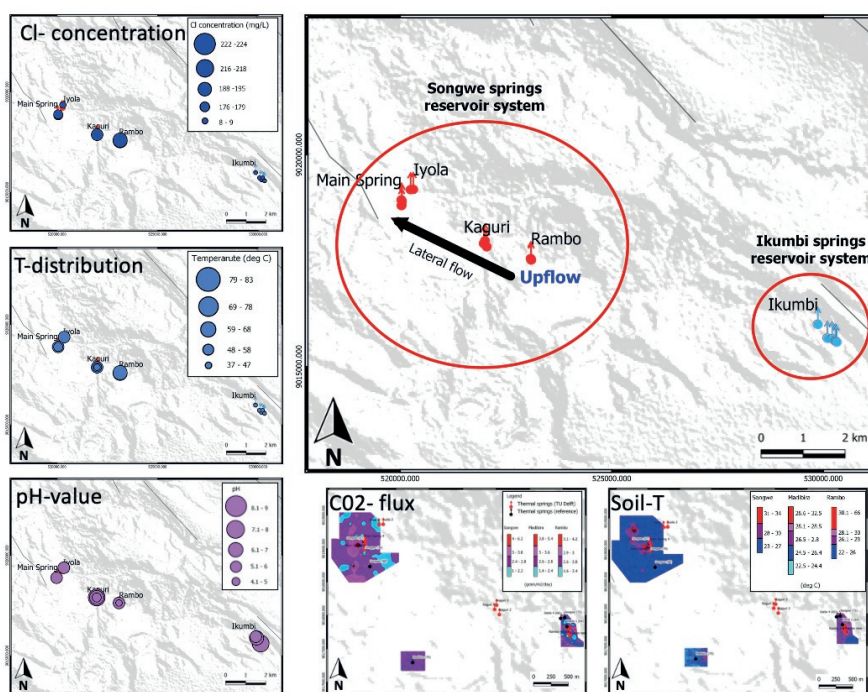


Figure 4.4 General flow regime in the Songwe basin with two reservoir systems feeding the hot springs. The main upflow area is close to Rambo and Kaguri springs. Also Cl, T and pH concentrations as well as CO₂ flux and soil temperature support the general fluid flow pathways. CO₂ and soil temperature data from Alexander et al. (2016)

In general, the central graben area has sufficient conductive structures, as also described by earlier studies, to allow deep geothermal waters to rise. Hinz et al. (2018) suggest that the

Mbeya fault and strike-slip faults SE of the springs serve as recharge areas leading to artesian hot spring flow. Asnin et al. (2022) conclude that the waters are in strong contact with Red Sandstone layers, which also show the highest permeability.

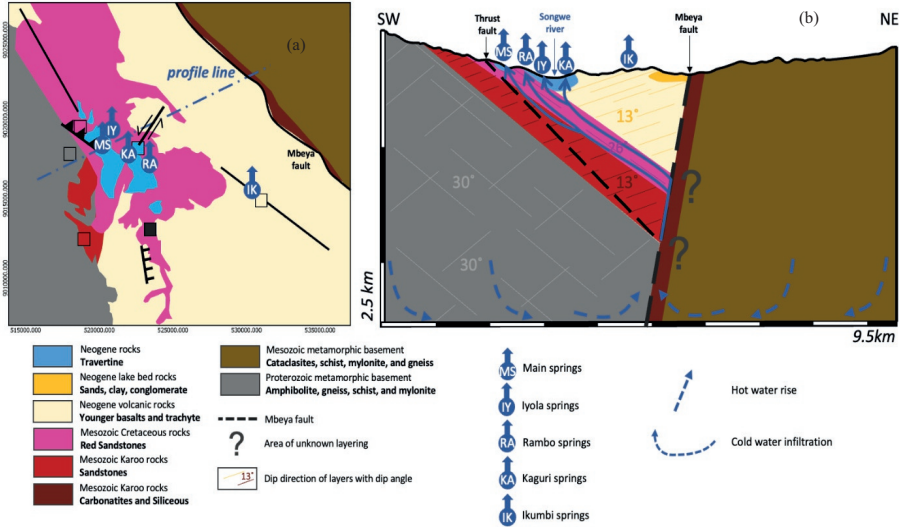


Figure 4.5 Conceptual flow model of the Songwe geothermal system with potential fluid pathways(b), geological set-up of the underground based on a summary of the presented investigations in this study(a)

4.3.2 Numerical Fluid Flow Model

The model iteratively estimates the natural conditions, while subsurface data play a crucial role in creating a realistic conceptual model. As previously mentioned, the geothermal gradient was the key parameter for adjustment in the model in order to match the reservoir temperature of the model with that of the geochemical calculation.

A study by Didas et al. (2022) gives a geothermal gradient of 20–43°C/km for the Songwe basin, while an unpublished study of Mutabazi (2023) gives a geothermal gradient range of 28–54°C/km. We simulate the reservoir temperature using different values of geothermal gradients as per Table 4.2. The model can successfully reproduce the geothermometer average reservoir temperature (125–148°C) at geothermal gradients of 32–39°C/km, with other parameters remaining constant. The model also shows reservoir temperatures up to 172°C at specific locations where the reservoir is at 2km depth or more.

Table 4.2 Simulated average reservoir temperature (whole Red Sandstone volume) at different geothermal gradients

Geothermal gradient (°C/km)	Reservoir temperature (°C)
26	106
30	119
32	125
35	135
37	142
39	148
40	152

Figure 4.7 shows the fluid flow and temperature distribution on the vertical sections (a), (b), (c) and (d) taken from lines a, b, c and d respectively shown on *Figure 4.8*. We observe both lateral and upward movement of fluid. Lateral movement is mostly observed on the Red sandstone layer in vertical sections (a), (b) and (c) whereas upward movement is greatly observed in vertical section (d). Fluid flows laterally in the Red Sandstone from the thinnest part towards the thickest part and then moves upwards. Calculated velocity distribution of the lithologies in *Table 4.3* shows higher fluid velocity in the Red Sandstone compared to other lithologies *Figure 4.9*. This is attributed to the permeability distribution where by Red Sandstone has the highest permeability as shown in *Table 4.4* and *Figure 4.10*. Fluid flow is therefore attributed to lateral changes of the lithological layers as well as their permeability.

Temperature on the other hand is observed to be higher on the thinner part of the lithological layers and tend to decrease as they become thicker *Figure 4.7(a), (b), (c) and (d)* respectively. This may be due to the thinner part having a bigger portion of the underlying basement which has higher thermal properties compared to the sedimentary rocks. The much greater temperature difference in vertical section (d) between the bottom and the upper part of the model may have contributed to the upward fluid movement in the Red Sandstone.

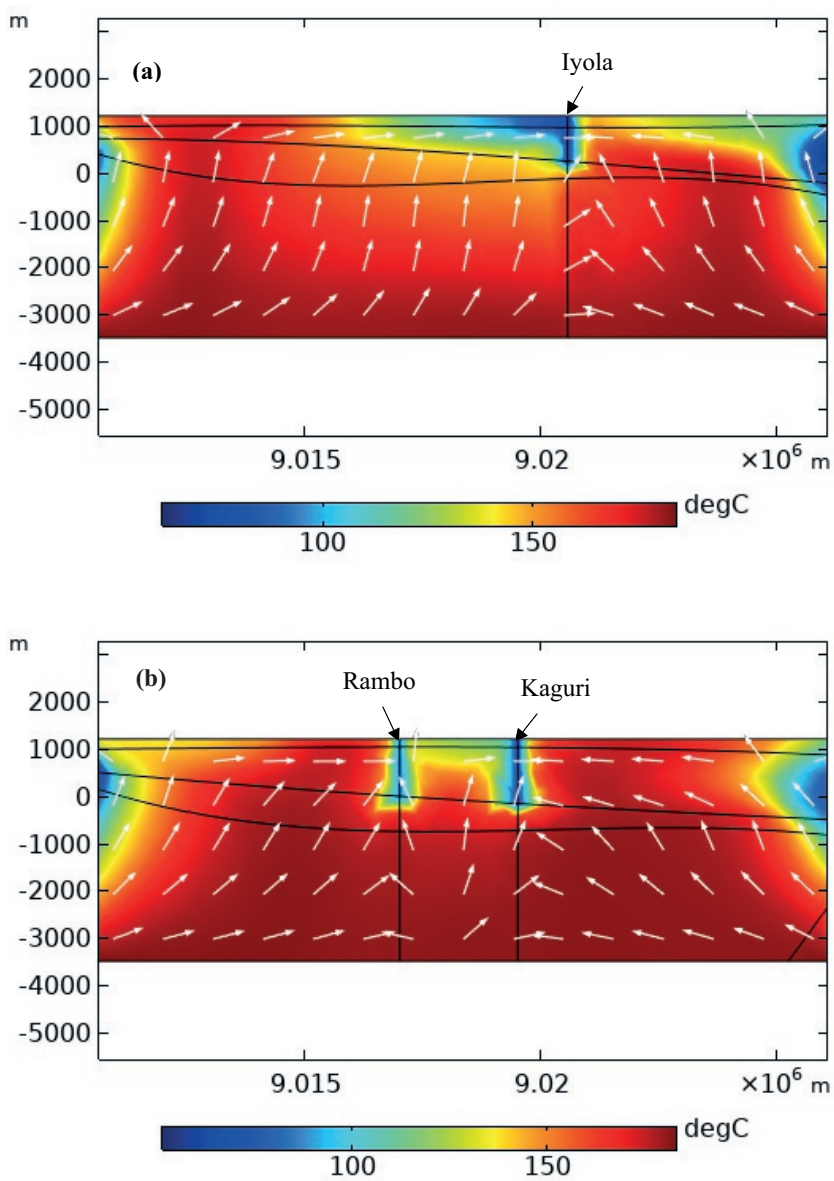


Figure 4.7 Simulated temperature distribution and fluid flow direction(white arrows) in the model derived from the vertical sections (a) and (b) from profile lines (a) and (b) respectively shown on figure 4.8. Vertical section (a) being at the thinnest part of the model lithologies.

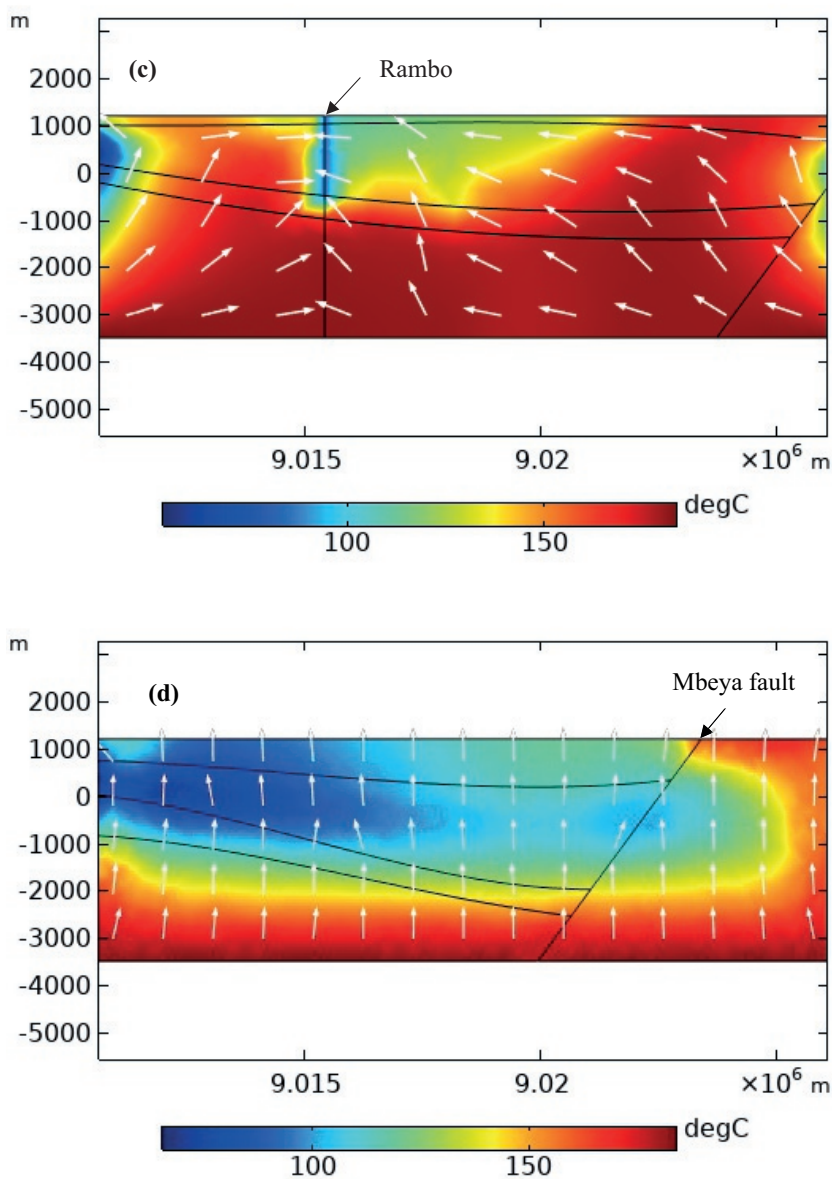


Figure 4.7 Simulated temperature distribution and fluid flow direction(white arrows) in the model derived from the vertical sections (c) and (d). The vertical sections are derived from profiles lines (c) and (d) respectively shown in figure 4.8. Vertical section (d) is located at the thickest part of the lithologies.

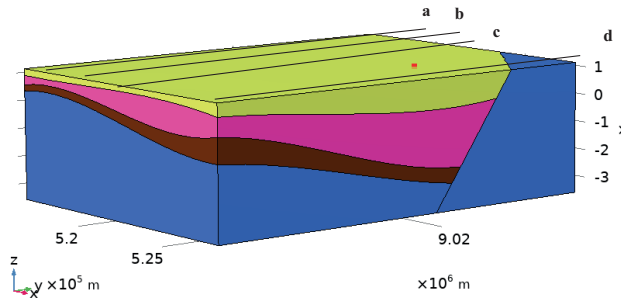


Figure 4.8 3D model geometry showing lines a, b, c and d where vertical sections were derived from. Line (a) cuts through the thinnest part of the lithological layers and line (d) cuts through the thickest part.

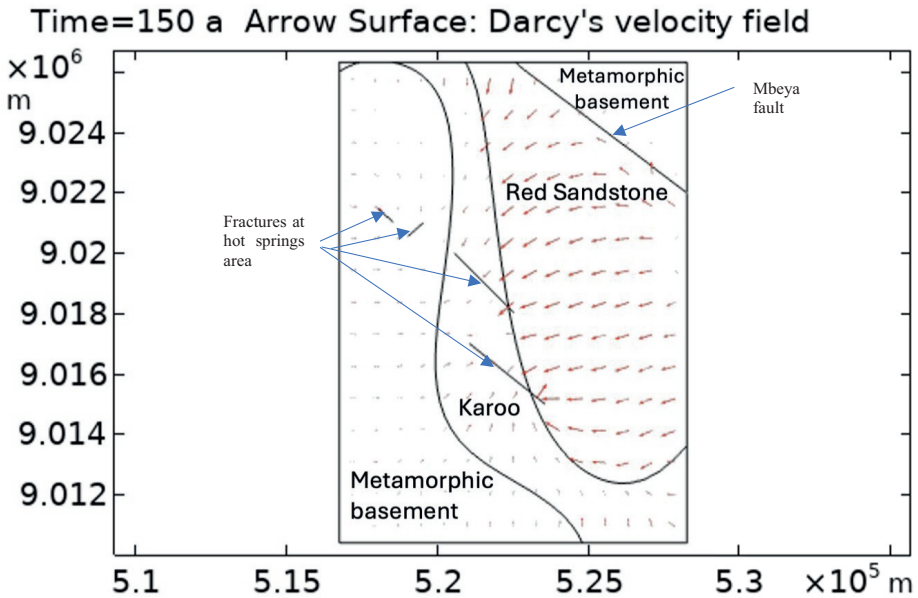


Figure 4.9 Fluid flow across different layers at a distance of 1700m below the surface. Top right is the basement, followed by Red Sandstone, Karoo and the Basement. More flow is observed on the Red Sandstone layer than other layers shown by longer arrows.

Table 4.3 Fluid velocity distribution

Lithology	Fluid velocity(m/s)
Neogene volcanics	1.8×10^{-7}
Red Sandstone	1.0×10^{-5}
Karoo	2.6×10^{-6}
Basement	2.0×10^{-6}

Table 4.4 Permeability values used in the model

Lithology	Permeability (m^2)
Neogene volcanics	1×10^{-14}
Red Sandstone	8.4×10^{-13}
Karoo	1.1×10^{-13}
Basement	4.55×10^{-14}

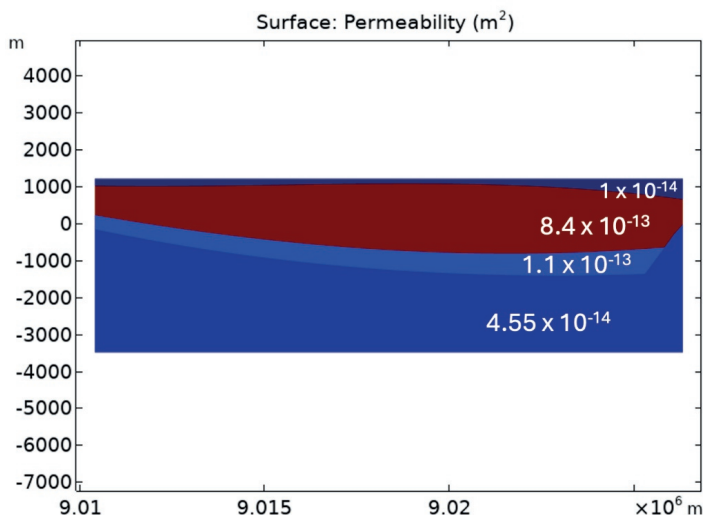


Figure 4.10 Vertical section from the model simulation showing permeability distribution in the lithologies. The upper layer is the Neogene volcanics followed by Red Sandstone, Karoo and the basement

Figure 4.11 shows pressure distribution in the model at different depths. The blue colour represents the area with the lowest pressure while the red colour represents the areas with the highest pressure, and the greenish to yellowish colours are medium pressure areas as indicated in the colour legends. The lowest pressure areas are where the hot springs fracture corridors are located. Moving away from the fracture corridors pressure tends to increase. Pressure also increases as depth increases, this is observed by increasing pressure values from (a) to (d) as shown in Table 4.5. This fact explains the size change of the low pressure area (blue colour) as the low pressure area is quite prominent in higher pressures at greater depths. The area is greater because the difference in pressure caused by the fractures is greater in high pressure areas compared to the top where the pressure is lower.

Table 4.5 Observed pressure values at different depths of Figure 4.5

Subfigure	Minimum pressure (Pa)	Maximum pressure (Pa)
(a)	8.87×10^4	1.4×10^7
(b)	8.88×10^4	1.7×10^7
(c)	3.69×10^6	3.15×10^7
(d)	4.48×10^6	4.13×10^7

In addition, we observe fluid flowing towards the corners of the model as well as towards the fracture corridors in *Figure 4.11(a)*, while in (c), (d) and (e) fluid flows only towards the fracture corridors. This may be caused by the fact that (a) is in the upper part of the model where pressure is much lower than the deeper of the model where (c), (d) and (e) are located. Fluid flow in the subsurface is greatly controlled by pressure.

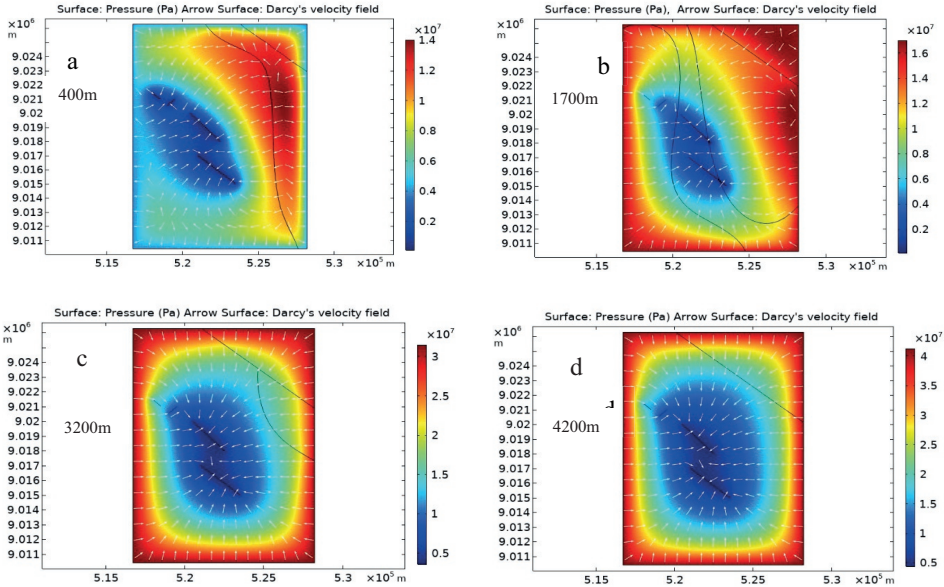


Figure 4.11 Map view of pressure distribution and fluid flow direction (white arrows) at different depths below the surface, as indicated in each figure. The NW-SE straight line in all figures is the map view of Mbeya fault followed by: (a) Neogene and Red Sandstone layer; (b) Red Sandstone, Karoo & basement; (c) Karoo & basement; (d) only basement. Note that colour scales vary with pressure scales and depth from (a) – (d).

4.4 Discussion

Boundary conditions used in this study rely on the described updated conceptual model for Songwe basin. The side boundaries of the model for instance are kept open and hydrostatic pressure as well as temperature gradient are defined so as to allow fluid to flow across them.

Other studies that used hydrostatic pressure as the initial boundary condition are such as Sutopo et al. (2019), Pradhipta et al. (2019), Vereina (2005), Niaraq et al. (2021) and Jalilinasrabady et al. (2010). However, the natural state models from these studies were calibrated using temperature and pressure values from well data, which we are lacking in our study, instead we have calibrated the model using reservoir temperature calculated from geothermometers. Different results may be obtained once the natural state model for Songwe is calibrated using well data such as temperature and pressure logs.

The topography of the Songwe basin has all four lithologies exposed to the surface at different locations and elevations. However, the top surface of our 3D model is simplified and smoothened into having only the Neogene volcanics and the metamorphic basement layers due to the complexity of the geometry that could not be integrated into the software. This simplification may have slightly increased the values of the output temperatures due to different thermal properties of the Neogene volcanics that are assumed to cover the top surface. From chapter 2, we have observed how thermal conductivity of the rocks plays a significant role on the output temperature, therefore Neogene volcanics having the lowest value of thermal conductivity may likely cause a temperature increase at depth in the model. Similarly, not all structures such as faults and fractures have been included in the model, because there has not been an intensive study on the structures and how they are interconnected. This may also have affected the simulation results. Thermal and physical properties of the rocks are assumed to be constant at depth which may have affected the results.

Nevertheless, the model serves its purpose of describing how fluid flow is controlled by pressure distribution, lateral changes of lithological layers and faults as well as permeability distribution in the subsurface, which had not been addressed and established in the previous studies of the Songwe geothermal system.

4.5 Conclusion

This chapter presents for the first time a numerical model for Songwe basin at an exploration stage analysing the fluid, permeability and temperature distribution in the subsurface. Fluid distribution in the subsurface is attributed to pressure, permeability and structures such as faults where by both lateral and vertical fluid flow is observed. Furthermore, the uncertainty of the vertical temperature gradient has been greatly reduced as we have established a range of 32 °C/km - 39°C/km.

5 CONCLUSION

5.1 Introduction

Understanding a geothermal system is crucial for the success of its commercial development. Three main requirements for a productive geothermal system are adequate heat, fluids and permeability. Defining locations where these three requirements are met at drillable depth in the subsurface is thus the task of conceptual and all further reservoir models. Locating a geothermal resource and finding suitable drilling areas are the main purposes of geothermal exploration.

In this study, we chose an approach combining field studies and numerical simulation. The field studies focused on sampling and analysis of water from the hot springs as well as surface rocks in order to investigate the fluid source, reservoir temperature and the physical properties of rocks such as permeability. From these studies, we could draw first conclusions on the reservoir temperature and the fluid source. The numerical simulations then extrapolate the temperatures to depth, where we lack direct measurements.

In chapter 2, an extensive literature study on previous work and geological mapping in the field disclosed the distribution of geological layers and location of hot springs, while the static geological and thermal modelling extrapolated this information to depth and combined all information to a temperature distribution at depth. Chapter 3 combines hydrogeochemical field work and modelling. During fieldwork, all hot springs were analysed on fluid properties, and porosity, permeability and mineral composition was measured on all rock types. Based on these data, geothermometer calculations derived possible reservoir temperatures, while the hydrogeochemical model identified fluid pathways and fluid sources of the hot spring water. This chapter concluded with a conceptual fluid flow model. In chapter 4, an updated conceptual model is presented for the Songwe geothermal area integrating all data and knowledge from previous chapters. Additionally, a thermal-hydraulic model is set up based on the new conceptual model, which shows the fluid flow directions with velocities and permeability distribution in the reservoir.

Previous work, conducted before this thesis, was limited to single studies on the geochemistry, geophysics or geology of Songwe and without wellbore and seismic data. In this study, we have now integrated all available, but still limited data, including new geological and geochemical information acquired during fieldwork to better constrain the heat distribution, fluid flow and

permeability of the Songwe geothermal field at an early stage of exploration, and to use the interpretation to determine possible drilling locations.

5.2 Temperature, Permeability and Fluid Distribution

This thesis focused on assessing the temperature, fluid flow and permeability for the Songwe geothermal system and subsequently proposing a location where to drill the first borehole.

The assessed temperature of the Songwe basin subsurface, where isotherms are nearly horizontal, increases almost linearly with depth (chapter 2). Additionally, we have characterized the importance of rock layers for the temperature distribution. For instance, we have recognized the importance of the Neogene volcanics layer causing higher temperatures at depth. Fluid flow is not considered in the thermal model, heat transfer is based purely on conduction. Also, well data would have been of great help for constraining the thermal model. With all these limitations, the study (chapter 2) still serves as a first attempt to locate higher temperature areas, which are so important for geothermal well targeting.

The Songwe area is quite favourable for geological mapping, with little vegetation and topographical changes giving access to outcrops at various points. The combination of field and literature data then provided good input for the temperature model. The limited time and multipurpose field work provided fewer datapoints than wished for. Songwe is a low- to medium temperature geothermal system with reservoir temperatures between 125°C-148°C, as constrained by our geothermometer studies (chapter 3). With these temperature constraints and determination of the thermal model (chapter 2), uncertainty on the temperature gradient of the geothermal system could be significantly reduced compared to previous studies, as we have found a range of 32 °C/km - 39°C/km (chapter 4).

Fluid flow in the subsurface is controlled by pressure and structures such as faults and fractures, with the recharge area being the NE of the Mbeya fault. While the recharge was described before by Alexander et al. (2016), constraints on the main flow paths and the upflow regions were missing and are now determined in this study with geochemical analyses performed from field data. For this purpose, we sampled several hot springs of different type that had not been sampled before.

The fast and simple sampling technique allowed for the immediate development of a conceptual model. We identify an upflow region in the Rambo hot springs area and the outflow at the remaining hot springs (chapter 3). According to the new conceptual model constructed on the basis of all available information (chapter 3), the fluid source and main flow in the rock layers is in the Red Sandstone due to its high permeability compared to other lithologies. Because of the limitation to one single sampling trip, however, no seasonal effects are accounted for and the model is restricted to 2D and does not include TH-processes.

The numerical model in chapter 4 includes for the first time the permeability distribution and fluid velocities in 3D (chapter 4) for the region. The direction of fluid flow in the subsurface of the Songwe basin is both vertical (from the basement towards the surface) and lateral (through the Red Sandstone and Karoo). The vertical movement is influenced by pressure distribution as well as the open structures such as faults and fractures, while the lateral movement is influenced by the permeability distribution (chapters 3 & 4). The combination of conceptual and numerical models allowed to include various field data and resulted in a detailed image of the subsurface permeability distribution, fluid velocities and fluid flow direction. As no well data are included in the model yet, the extrapolation to the subsurface is uncertain and based on a simplified geometry.

5.3 Production Prediction

5.3.1 Numerical Simulation with Well Placement

After the determination of temperature distribution and fluid flow in the subsurface in chapters 2-4, the question remains where to place the first borehole in the Songwe geothermal field? For this, a prediction of reservoir performance is important, including an assessment if the reservoir can sustain fluid productivity at the required temperature for a certain period. To address this issue, a model was set up to determine where the highest temperatures can be reached, and a sufficient volume of hot water can be produced for the sustainable production of geothermal energy.

In order to find the optimal location for a first production borehole, we simulate several production scenarios. We use the natural state model developed in chapter 4 to predict future production scenarios. We use the same boundary conditions as the natural state model described in section 4.2.4, additionally we place production and injection wells assigning a mass flow rate of 20 kg/s in both wells and simulate for a period of 30 years. We place the production well at

different locations of the Songwe basin as indicated by black rounded numbers on [Figure 5.1](#) and simulate the production temperature. The location of the injection well close to the natural recharge area remains fixed (shown by a blue round “IW” in [Figure 5.1](#)). The different locations of the producer represent different distances to the injection borehole, different lithologies and locations of lower or higher fracture density [Table 5.1](#).

Table 5.1 Production well scenarios and details

Well	Well depth (m)	Lithology	Distance to Injector (m)	Fractured zone
1	700	Red Sandstone	5500	Yes
2	700	Red Sandstone	4000	No
3	700	Red Sandstone	2000	No
4	700	Red Sandstone	500	No
5	700	Karoo & Basement	6800	Yes
6	700	Basement	5657	Yes
7	700	Basement	4472	Yes
8	700	Red Sandstone	4031	No

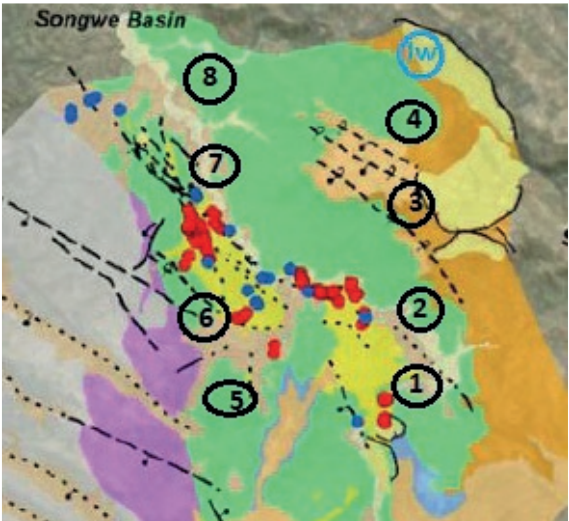


Figure 5.1 Production well locations shown by black rounded numbers 1, 2,3,4,5,6,7 and 8. A fixed injection well is shown by a blue rounded “IW”.

5.3.2 Production Simulation Results and Discussion

[Table 5.2](#) shows the calculated temperature output from the production well for each location of the model. Production well 4 has the highest and number 7 has the lowest output temperature

compared to the rest. Comparing between the highest and lowest temperature locations, we observe that the production well 4 is located on the thickest part of the Red Sandstone unit which is closer to the Mbeya fault and further away from the hot springs, whereas the production well 7 is located much closer to the hot springs and above the thinner part of the Red Sandstone. Simulated production temperatures are observed to increase when the production wells are placed towards Mbeya fault, where there is a thicker layer of the Red Sandstone and farther from the hot springs. Furthermore, production temperatures are predicted to remain stable in all the 30 years as for the case of location 4 shown in [Figure 5.2](#), this is dependent on the applied boundary conditions and the production rate. Additionally, we varied the temperature gradient from the range we obtained in chapter 4 (32-39°C/km) and observed the output temperature for production well location 4, which is the well with the highest output temperature [Table 5.3](#). We observe that production temperature is very dependent on the geothermal gradient therefore in order to obtain realistic production temperatures its exact value should be established.

Thickness and depth of the Red Sandstone has shown to be important for the sustainability of the production temperature, as it prevents early cool-down. In contrast, hot springs cool down the subsurface during the model life time due to open structures beneath them that allow heat to be dissipated to the atmosphere by convection. Also, the hot springs represent the outflow (see chapter 4) in the geothermal system, where the fluid already lost temperature during ascent.

Our modelling approach is limited by the applied boundary conditions, since we miss data such as water head, pressure and temperature data from exploration wells. Also, fluid flow rate data is lacking. The geometry is also simplified and also not all structures are included in the model. Nevertheless, the simplified production scenarios show consistent reservoir temperatures. The conduction based model in chapter 2 resulted in a geothermal gradient of 25-34°C/km, which are reservoir temperatures of 113-147°C. Chapter 3 calculated reservoir temperatures of 125-148°C using geothermometers, which correlates with a geothermal gradient of 28-34°C/km. In chapter 4, fluid flow and thus convection were introduced into the model. With a geothermal gradient of 26-40°C/km the reservoir temperatures are at 106-152°C. All reservoir temperatures are average temperatures over the whole Red Sandstone body while production temperatures are temperatures at specific well location. Temperatures at specific locations were mainly tested in chapter 5. However, the model in chapter 4 shows 172°C at a theoretical well location 4, at that same location the production model in chapter 5 results in 180°C production temperature using a geothermal gradient of 35°C/km in both models. The difference between the two

temperature values may be caused by the fact that no wells exist in the model from chapter 4 and therefore associated well parameters such as mass flow rate are not taken into account instead the temperature is measured from a simple line whereas in chapter 5 well features exist and the associated well parameters are taken into account in the production temperature.

Table 5.2 Production well temperature at different locations

Location on the map (Figure 5.1)	Output temperature (°C)
1	169
2	170
3	175
4	180
5	165
6	158
7	153
8	176

Table 5.3 Varying geothermal gradient at well location 4

Temp.grad.(°C/km	32	35	39
Prod.temp. at location 4 (°C)	166	180	198

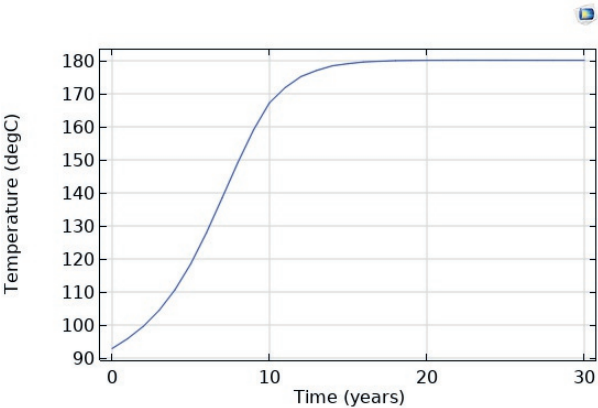


Figure 5.2 Simulated production temperature at location 4 using a geothermal gradient of 35°C/km

5.4 Recommendations

Based on the current state of knowledge, the first drilling location may be considered at the thickest part of the Red Sandstone and far from the hot springs such as location 4 from Figure 4.4 in order to obtain higher production temperatures and prevent early cool down. Moreover, in order to further constrain the location and the produced temperature, the mass flow rate of the reservoir fluid should be obtained.

And as stated in the previous chapters, studies in this thesis have been carried out with limited data on the subsurface, physical and thermal properties of rocks. For instance, fractures and faults affect heat and temperature distribution therefore they need to be investigated in detail. Similarly, uniform permeability has been assumed throughout the rock units while in nature it is more likely to have zones of channelized flow. In order to determine this heterogeneity, much more detailed mapping and downhole measurements are required.

BIBLIOGRAPHY

- Alexander, K. B., Cumming, W., & Marini, L. (2016a). Geothermal Resource Assessment Report Ngozi and Songwe Geothermal Prospects, *Tanzania Final Report-September 2016*.
- Alexander, K. B., Cumming, W., & Marini, L. (2016b). Technical Review of Geothermal Potential of Ngozi and Songwe Geothermal Prospects, Tanzania.
- Alexander, K., Cumming, W. B., & Marini, L. (2016). Geothermal resource assessment report: Ngozi and Songwe Geothermal Prospects, Tanzania. In *Final Report dated September 2016 to UNEP/ARGeo and TGDC*.
- Arnorsson, S., Sigurdsson, S., & Svavarsson, H. (1982). The chemistry of geothermal waters in Iceland. I. Calculation of aqueous speciation from 0° to 370°C. *Geochimica et Cosmochimica Acta*, 46, 1513–1532.
- Asnin, S. N., Nnko, M., Josephat, S., Mahecha, A., Mshiu, E., Bertotti, G., & Brehme, M. (2022). Identification of water–rock interaction of surface thermal water in Songwe medium temperature geothermal area, Tanzania. *Environmental Earth Sciences*, 81(21). <https://doi.org/10.1007/s12665-022-10594-4>
- Baker, B. H., Mohr, P. A., & Williams, L. A. J. (1972). *Geology of the Eastern Rift System of Africa* (pp. 1–68). <https://doi.org/10.1130/SPE136-p1>
- Balkan, E., Erkan, K., & Şalk, M. (2017). Thermal conductivity of major rock types in western and central Anatolia regions, Turkey. *Journal of Geophysics and Engineering*, 14(4), 909–919. <https://doi.org/10.1088/1742-2140/aa5831>
- Barbier, E. (2002). Geothermal energy technology and current status: an overview. In *Renewable and Sustainable Energy Reviews* (Vol. 6). www.elsevier.com/locate/rser
- Békési, E., Struijk, M., Bonté, D., Veldkamp, H., Limberger, J., Fokker, P. A., Vrijlandt, M., & van Wees, J. D. (2020). An updated geothermal model of the Dutch subsurface based on inversion of temperature data. *Geothermics*, 88. <https://doi.org/10.1016/j.geothermics.2020.101880>
- Beyer, L. A., & Clutson, F. G. (1978). Density and porosity of oil reservoirs and overlying formations from borehole gravity measurements, Gebo Oil Field, Hot Springs County, Wyoming. In *Oil and Gas Investigation Chart*. <https://doi.org/10.3133/oc88>
- Bjarkason, E. K., O'Sullivan, J. P., Yeh, A., & O'Sullivan, M. J. (2019). Inverse modeling of the natural state of geothermal reservoirs using adjoint and direct methods. *Geothermics*, 78, 85–100. <https://doi.org/10.1016/j.geothermics.2018.10.001>
- Bonte, D., Wees, J.-D. van, & Verweij, J. M. (2012). Subsurface temperature of the onshore Netherlands: new temperature dataset and modelling. *Netherlands Journal of Geosciences*, 491–515.
- Borg, G., Borg, G., & Shackleton, R. M. (1997). The Tanzania and NE-Zaire Cratons-in de Wit and Ashwal-Greenstone Belts (OUP) Geoarchaeological provenance studies on base and precious metals in prehistoric and ancient times View project Archean gold deposits View project *The Tanzania and NE-Zaire Cratons*. <https://www.researchgate.net/publication/310799213>
- Brehme, M., Deon, F., Haase, C., Wiegand, B., Kamah, Y., Sauter, M., & Regenspurg, S. (2016). Fault-controlled geochemical properties in Lahendong geothermal reservoir Indonesia. *Grundwasser*, 21(1), 29–41. <https://doi.org/10.1007/s00767-015-0313-9>
- Brehme, M., Giese, R., Dokuz, U. E., & Bulut, F. (2021). Fluid pathways identified beneath Narlı Lake (Central Anatolia) show the geothermal potential of former volcanoes. *Scientific Reports*, 11(1). <https://doi.org/10.1038/s41598-021-87743-5>
- Brehme, M., Moeck, I., Kamah, Y., Zimmermann, G., & Sauter, M. (2014). A hydrotectonic model of a geothermal reservoir - A study in Lahendong, Indonesia. *Geothermics*, 51, 228–239. <https://doi.org/10.1016/j.geothermics.2014.01.010>
- Brehme, M., Scheytt, T., Çelik, M., & Dokuz, U. E. (2010). Hydrochemical characterisation of ground and surface water at Dörtöyl/Hatay/Turkey. *Environmental Earth Sciences*, 63(6), 1395–1408. <https://doi.org/10.1007/s12665-010-0810-1>
- Brehme, M., Zurich, E., Blöcher, G., Deon, F., Cacace, M., Moeck, I., Wiegand, B., Kamah, Y., Regenspurg, S., Zimmermann, G., Sauter, M., & Huenges, E. (2016). *Characterizing permeability structures in geothermal reservoirs-A case study in Lahendong*. <https://www.researchgate.net/publication/297860814>
- Bushi, A., Mgejwa, N., & Mkangala, A. (2016). Songwe Geothermal Prospect Infill Study, June-July 2016. *Geology and Geothermal Summary Report*.
- Corti, G., van Wijk, J., Cloetingh, S., & Morley, C. K. (2007). Tectonic inheritance and continental rift architecture: Numerical and analogue models of the East African Rift system. *Tectonics*, 26(6). <https://doi.org/10.1029/2006TC002086>
- Dalampakis, P., Papachristou, M., & Neofotistos, P. (2022). Geothermal resources assessment using temperature–depth relationships in the fault-controlled hydrothermal system of Aristino-Traianoupolis area, Northern Greece. *Geothermal Energy*, 10(1). <https://doi.org/10.1186/s40517-022-00232-4>
- Delvaux, D. (2001). Karoo rifting in western Tanzania: precursor of Gondwana break-up? *Contributions to Geology and Palaeontology of Gondwana in Honour of Helmut Wopfner*, 111–125.

- Delvaux, D. F., & Hanon, M. (1991). Neotectonics of the Mbeya area, SW Tanzania.. 87–97.
- Delvaux, D., Kraml, M., Sierralta, M., Wittenberg, A., Mayalla, J. W., Kabaka, K., & Makene, C. (2010a). Surface Exploration of a Viable Geothermal Resource in Mbeya Area, Sw Tanzania. Part I: Geology of the Ngozi-Songwe Geothermal System. *Proceedings World Geothermal Congress, April*, 25–29.
- Delvaux, D., Kraml, M., Sierralta, M., Wittenberg, A., Mayalla, J. W., Kabaka, K., & Makene, C. (2010b). Surface Exploration of a Viable Geothermal Resource in Mbeya area, SW Tanzania. Part I: Geology of the Ngozi-Songwe Geothermal System. In *Proceedings World Geothermal Congress*.
- Didas, M. M., Armadillo, E., Hersir, G. P., Cumming, W., & Rizzello, D. (2022). Regional thermal anomalies derived from magnetic spectral analysis and 3D gravity inversion: Implications for potential geothermal sites in Tanzania. *Geothermics*, 103. <https://doi.org/10.1016/j.geothermics.2022.102431>
- EAGER. (2018). *Enhanced resource modeling at Songwe*.
- Ebinger, C. J. (1989a). Tectonic development of the western branch of the East African rift system. *Geological Society Of America Bulletin*, 7606(7), 885–903. [https://doi.org/10.1130/0016-7606\(1989\)101<0885](https://doi.org/10.1130/0016-7606(1989)101<0885)
- Ebinger, C. J. (1989b). Tectonic development of the western branch of the East African rift system. *Geological Society of America Bulletin*, 101(7), 885–903. [https://doi.org/10.1130/0016-7606\(1989\)101<0885:TDOTWB>2.3.CO;2](https://doi.org/10.1130/0016-7606(1989)101<0885:TDOTWB>2.3.CO;2)
- Ebinger, C. J., Deino, A. L., Drake, R. E., & Tesha, A. L. (1989). Chronology of volcanism and rift basin propagation: Rungwe volcanic province, East Africa. *Journal of Geophysical Research*, 94(B11). <https://doi.org/10.1029/jb094ib11p15785>
- Ellis, A. J., & Wilson, S. H. (1960a). The geochemistry of alkali metal ions in the Wairakei hydrothermal system. *New Zealand Journal of Geology and Geophysics*, 3(4), 593–617. <https://doi.org/10.1080/00288306.1960.10420148>
- Ellis, A. J., & Wilson, S. H. (1960b). The geochemistry of alkali metal ions in the Wairakei hydrothermal system. *New Zealand Journal of Geology and Geophysics*, 3(4), 593–617. <https://doi.org/10.1080/00288306.1960.10420148>
- Espinoza-Ojeda, O. M., Rivera-Calderón, E., & Tonally Sánchez-Sánchez, P. (2022). Numerical simulation to estimate the conductive thermal state model – Mexican EGS zones as study cases. <https://doi.org/10.1007/s12145-022-00766-y/Published>
- Fernandez-Alonso, M., Cutten, H., De Waele, B., Tack, L., Tahon, A., Baudet, D., & Barritt, S. D. (2012). The Mesoproterozoic Karagwa-Ankole Belt (formerly the NE Kibara Belt): The result of prolonged extensional intracratonic basin development punctuated by two short-lived far-field compressional events. *Precambrian Research*, 216–219, 63–86. <https://doi.org/10.1016/J.PRECAMRES.2012.06.007>
- Fontijn, K., Williamson, D., Mbede, E., & Ernst, G. G. J. (2012). The Rungwe Volcanic Province, Tanzania - A volcanological review. In *Journal of African Earth Sciences* (Vol. 63, pp. 12–31). <https://doi.org/10.1016/j.jafrearsci.2011.11.005>
- Fournier, R. O. (1977). Chemical geothermometers and mixing models for geothermal systems. *Geothermics*, 5(1–4), 41–50. [https://doi.org/10.1016/0375-6505\(77\)90007-4](https://doi.org/10.1016/0375-6505(77)90007-4)
- Frey, M., Bär, K., Stober, I., Reinecker, J., van der Vaart, J., & Sass, I. (2022). Assessment of deep geothermal research and development in the Upper Rhine Graben. In *Geothermal Energy* (Vol. 10, Issue 1). Springer Science and Business Media Deutschland GmbH. <https://doi.org/10.1186/s40517-022-00226-2>
- Gascuel, V., Bédard, K., Comeau, F. A., Raymond, J., & Malo, M. (2020). Geothermal resource assessment of remote sedimentary basins with sparse data: lessons learned from Anticosti Island, Canada. *Geothermal Energy*, 8(1). <https://doi.org/10.1186/s40517-020-0156-1>
- GeothermEx, & Colin Harvey. (2013). Geothermal Exploration Best Practices. www.geothermex.com.
- Giggenbach. (1988a). Geothermal solute equilibria. Derivation of Na-K-Mg-Ca geothermometers. *Geochimica et Cosmochimica Acta*, 52(12), 2749–2765. [https://doi.org/10.1016/0016-7037\(88\)90143-3](https://doi.org/10.1016/0016-7037(88)90143-3)
- Giggenbach, W. F. (1988b). Geothermal solute equilibria. Derivation of Na-K-Mg-Ca geothermometers. *Geochimica et Cosmochimica Acta*, 52(12), 2749–2765. [https://doi.org/10.1016/0016-7037\(88\)90143-3](https://doi.org/10.1016/0016-7037(88)90143-3)
- Giggenbach, W. F., & Soto, R. C. (1992). Isotopic and chemical composition of water and steam discharges from volcanic-magmatic-hydrothermal systems of the Guanacaste Geothermal Province, Costa Rica. *Applied Geochemistry*, 7(4), 309–332. [https://doi.org/10.1016/0883-2927\(92\)90022-U](https://doi.org/10.1016/0883-2927(92)90022-U)
- Harkin, D. A., & Harpum, J. R. (1978). Geological Map of Tukuyu (QDS 244). In *Tech. Rep. Geological Survey of Tanganyika, Dodoma*.
- Hawkins, A. J., & Tester, J. W. (2018). Geothermal systems. In *Encyclopedia of Earth Sciences Series* (pp. 592–596). Springer Netherlands. <https://doi.org/10.1016/b978-0-12-814946-1.00002-5>
- Henley, R. W. (1995). Geothermal fluids: Chemistry and exploration techniques. *Journal of Geochemical Exploration*, 52(3), 382–383. [https://doi.org/10.1016/0375-6742\(95\)90013-6](https://doi.org/10.1016/0375-6742(95)90013-6)
- Henley, R. W., & Ellis, A. J. (1983). Geothermal Systems Ancient and Modern : A Geochemical Review. 19.
- Hinz, N., Cumming, B., & Sussman, D. (2018a). Exploration of fault-related deep-circulation geothermal resources in the western branch of the East African Rift System: examples from Uganda and Tanzania.

- Hinz, N., Cumming, B., & Sussman, D. (2018b). Exploration of fault-related deep-circulation geothermal resources in the western branch of the East African Rift System: examples from Uganda and Tanzania. *In: Proceedings of the 7th African Rift Geothermal Conference 2018. Kigali, Rwanda. 16 p., November.*
- Hinz, N., Sussman, D., Heath, J., & Cumming, B. (2018). Additional Detailed Geologic Mapping at Songwe for General Manager. *Tanzania Geothermal Development Company T79-D02 Version: Final.*
- Hochstein, M. P. (1988). Assessment and modelling of geothermal reservoirs (small utilization schemes). *Geothermics*, 17(1), 15–49. [https://doi.org/10.1016/0375-6505\(88\)90004-1](https://doi.org/10.1016/0375-6505(88)90004-1)
- Hochstein, M. P., Hochstein, M. P., Temu, E. P., & Moshly, C. M. A. (2000). Geothermal Resources of Tanzania. *Geothermal View project Aluto volcanic geothermal system View project Geothermal Resources of Tanzania.* <https://www.researchgate.net/publication/303407596>
- Hochstein, M. P., Temu, E. P., & Moshly, C. M. A. (2000). Geothermal resources of Tanzania. *Proceedings World Geothermal Congress, Japan*(May 28–June 10, 2000), 1233–1238. [https://doi.org/10.1016/0375-6505\(70\)90412-8](https://doi.org/10.1016/0375-6505(70)90412-8)
- Huddleston-Holmes, C., & Hayward, J. A. (2011). The potential of geothermal energy Characterisation of sedimentary geothermal prospects in Western and South Australia View project. <https://www.researchgate.net/publication/228591316>
- IEA. (2024). Electricity 2024 Analysis and Forecast to 2026. <https://iea.blob.core.windows.net/assets/18f3ed24-4b26-4c83-a3d2-8a1be51c8cc8/Electricity2024-Analysisandforecastto2026.pdf>
- Jalilinasrabadly, S., Itoi, R., Gotoh, H., & Tanaka, T. (2010). The Natural State Numerical Model of Takigami Geothermal Reservoir, Oita, Japan. In *PROCEEDINGS, Thirty-Fifth Workshop on Geothermal Reservoir Engineering.*
- Jalilinasrabadly, S., Tanaka, T., Itoi, R., & Goto, H. (2021). Numerical simulation and production prediction assessment of Takigami geothermal reservoir. *Energy*, 236. <https://doi.org/10.1016/j.energy.2021.121503>
- James. (1959). Kopie von subito e.V., geliefert für Helmholtz-Zentrum Potsdam Deutsches GeoForschungsZentrum (FOR01XS0010). *J. Phys. Soc. Japan*, 85(114605).
- Johnson, S. P., Cutten, H. N. C., Muhongo, S., & De Waele, B. (2003). Neoproterozoic magmatism and metamorphism of the western granulites in the central domain of the Mozambique belt, Tanzania: U–Pb zircon geochronology and PT estimates. *Tectonophysics*, 375(1–4), 125–145. <https://doi.org/10.1016/J.TECTO.2003.06.003>
- Jones, D. J. R. (2020). A summary of the East Africa Rift Temperature and Heat flow Model (EARTH).
- Kalberkamp, U., Schaumann, G., Ndonge, P. B., Chiragwile, A. S., Mwano, M. J., & GEOTHERM, working group. (2010). Surface Exploration of a Viable Geothermal Resource in Mbeya Area, SW Tanzania. Part III: Geophysics Ulrich. *Proceedings World Geothermal Congress, April.*
- Kees Mokveld, & Steven von Eije. (2018). *Final Energy report Tanzania Commissioned by the Netherlands Enterprise Agency.*
- Kilembe, E. A., & Rosendahl, B. R. (1992). Structure and stratigraphy of the Rukwa rift. *Tectonophysics*, 209(1–4), 143–158. [https://doi.org/10.1016/0040-1951\(92\)90016-Y](https://doi.org/10.1016/0040-1951(92)90016-Y)
- Koptev, A., Calais, E., Burov, E., Leroy, S., & Gerya, T. (2015). Dual continental rift systems generated by plume–lithosphere interaction. *Nature Geoscience*, 8(5), 388–392. <https://doi.org/10.1038/ngeo2401>
- Kraml, M., Mnjokava, T. T., Mayalla, W. J., Kabaka, K., & GEOTHERM, G. working. (2010). Surface Exploration of a Viable Geothermal Resource in Mbeya Area, SW Tanzania Part II: Geochemistry. *Proceedings World Geothermal Congress.*
- Kraml, M., Mnjokava2, T. T., Mayalla, J. W., Kabaka, K., & Working Group, G. (2010). Surface Exploration of a Viable Geothermal Resource in Mbeya Area, SW Tanzania Part II: Geochemistry. In *Proceedings World Geothermal Congress.*
- Kuznik, F., Roushdy, M., Salem, A.-B. M., WSEAS (Organization), & North Atlantic University Union. (2013). *Advances in modern mechanical engineering: proceedings of the 4th international conference on fluid mechanics and heat & mass transfer (FLUIDSHEAT '13), Dubrovnik, Croatia, June 25-27, 2013.* 277.
- Lambiasi, J. J. (1989). The Framework of African Rifting During the Phanerozoic. In *Journal of African Earth Sciences* (Vol. 8).
- Lee, K. C. (1996). Classification of Geothermal Resources, an engineering Approach. <https://pangea.stanford.edu/ERE/pdf/IGAstandard/SGW/1996/Lee.pdf>
- Macfarlane, A. (1966). Geological Map of Itumba (QDS 258). In *Tech. Rep. Mineral Resources Division, Dodoma.*
- Macharia, M. W., Gachari, M. K., Kuria, D. N., & Mariita, N. O. (2017). Low cost geothermal energy indicators and exploration methods in Kenya. *Journal of Geography and Regional Planning*, 10(9), 254–265. <https://doi.org/10.5897/jgrp2017.0643>
- Makundi, J. S., & Kifua, G. M. (1985a). Geothermal Features of the Mbeya Prospect in Tanzania. *Geothermal Resources Council*, 9, 451–454.
- Makundi, J. S., & Kifua, G. M. (1985b). Geothermal Features of the Mbeya Prospect in Tanzania. *Geotherm. Resour. Council*, 9, 451–454.

- Malek, A. E., Adams, B. M., Rossi, E., Schiegg, H. O., & Saar, M. O. (2022). Techno-economic analysis of Advanced Geothermal Systems (AGS). *Renewable Energy*, 186, 927–943. <https://doi.org/10.1016/j.renene.2022.01.012>
- Marini Luigi. (2016). Fluid Geochemistry of the Lake Rukwa – Lake Nyasa area, *Ngozi and Songwe Geothermal Prospects, Tanzania*.
- McAliley, W. A., & Li, Y. (2019). Methods to invert temperature data and heat flow data for thermal conductivity in steady-state conductive regimes. *Geosciences (Switzerland)*, 9(7). <https://doi.org/10.3390/geosciences9070293>
- Minissale, A., Donato, A., Procesi, M., Pizzino, L., & Giammanco, S. (2019). Systematic review of geochemical data from thermal springs, gas vents and fumaroles of Southern Italy for geothermal favourability mapping. *Earth-Science Reviews*, 188(July 2018), 514–535. <https://doi.org/10.1016/j.earscirev.2018.09.008>
- Mnjokava, T. T. (2007). Interpretation of Exploration Geochemical Data for Geothermal Fluids from the Geothermal Field of the Rungwe Volcanic Area, SW Tanzania. In *UNU-GTP Reykjavik, Iceland* (Issue 14).
- Mnjokava, T. T. (2012). *GEO THERMAL EXPLORATION IN TANZANIA-STATUS REPORT*. <http://www.tanzania.go.tz/energyf.html>
- Mnjokava, T. T. (2013). Geothermal Exploration in Tanzania, Status Report. <https://rafladan.is/bitstream/handle/10802/5410/UNU-GTP-SC-17-1003.pdf?sequence=1>
- Mnjokava, T. T. (2014). Geothermal Exploration in Tanzania, Status Report. <https://rafladan.is/bitstream/handle/10802/9213/UNU-GTP-SC-19-1004.pdf?sequence=1>
- Mnjokava, T. T. (2015). Geothermal Development in Tanzania, Status Report. https://www.ctc-n.org/sites/www.ctc-n.org/files/resources/01017_0.pdf
- Mulibo, G. D., & Nyblade, A. A. (2016). The seismotectonics of Southeastern Tanzania: Implications for the propagation of the eastern branch of the East African Rift. *Tectonophysics*, 674, 20–30. <https://doi.org/10.1016/j.tecto.2016.02.009>
- Mutabazi, E. (2023). 3D Thermal Modelling of the Lithosphere in SW Tanzania: Implication for Geothermal Resource Exploration.
- Nicholson, Keith. (1993). Geothermal fluids: Chemistry and exploration techniques. In *Springer-Verlag Berlin Heidelberg*. [https://doi.org/10.1016/0375-6742\(95\)90013-6](https://doi.org/10.1016/0375-6742(95)90013-6)
- Nyblade, A. A., Pollack, H. N., Jones, D. L., Podmore, F., & Mushayandebvu, M. (1990). Terrestrial heat flow in east and southern Africa. *Journal of Geophysical Research*, 95(B11). <https://doi.org/10.1029/jb095ib11p17371>
- Nzaro. (1970). *Geothermics (i970)-Special Issue~ 2 U. N. Symposium on the Development and Utilization of Geothermal Resources, Pisa 1970*. 2, 1039–1043.
- Ochieng, L. (2016). Overview of Geothermal Surface Exploration Methods.
- Omenda, P., Mangi, P., Ofwona, C., & Mwangi, M. (2021). Country Update Report Kenya Omenda 2021.
- O'sullivan, J. (2014). *Geothermal Reservoir Modelling: Uses and Limitations*.
- Pandey, S. N., Vishal, V., & Chaudhuri, A. (2018). Geothermal reservoir modeling in a coupled thermo-hydro-mechanical-chemical approach: A review. *Earth-Science Reviews*, 185, 1157–1169. <https://doi.org/10.1016/J.EARSCIREV.2018.09.004>
- Parkhurst, D. L., & Appelo, C. a. J. (2013). Description of Input and Examples for PHREEQC Version 3 — A Computer Program for Speciation , Batch-Reaction , One-Dimensional Transport , and Inverse Geochemical Calculations. U.S. Geological Survey Techniques and Methods, book 6, chapter A43, 497 p. *U.S. Geological Survey Techniques and Methods, Book 6, Chapter A43*, 6-43A.
- Pisarskii, B. I., Konev, A. A., Levi, K. G., & Delvaux, D. (1998). Alkaline carbon dioxide hydrotherms and strontium-containing travertines in the Songwe River valley (Tanzania). *Geologiya i Geofizika*, 7, 934–941.
- Pradhipta, Y. D., Sutopo, S., Pratama, H. B., & Adiprana, R. (2019). Natural state modeling of Mataloko Geothermal field, Flores Island, East Nusa Tenggara, Indonesia using TOUGH2 simulator. *IOP Conference Series: Earth and Environmental Science*, 254(1). <https://doi.org/10.1088/1755-1315/254/1/012027>
- Quennell, A. M., McKinlay, A. C. M., Aitken, W. G., & Harris, J. F. (1959). *Summary of the geology of Tanganyika*.
- Rachmat, S., Adrianto, & Syihab, Z. (2019). Natural State Modeling for a Geothermal System using Artificial Intelligence. *International Journal of Science and Research*. <https://doi.org/10.21275/SR201201102622>
- Reed, M., & Nicolas, S. (1984). Calculation of pH and mineral equilibria in hydrothermal waters with application to geothermometry and studies of boiling and dilution. *Geochimica et Cosmochimica Acta*, 48, 1479–1492.
- Roberts, E. M., O'Connor, P. M., Gottfried, M. D., Stevens, N., Kapalima, S., & Ngasala, S. (2004a). Revised stratigraphy and age of the Red Sandstone Group in the Rukwa Rift Basin, Tanzania. *Cretaceous Research*, 25(5), 749–759. <https://doi.org/10.1016/j.cretres.2004.06.007>
- Roberts, E. M., O'Connor, P. M., Gottfried, M. D., Stevens, N., Kapalima, S., & Ngasala, S. (2004b). Revised stratigraphy and age of the Red Sandstone Group in the Rukwa Rift Basin, Tanzania. *Cretaceous Research*, 25(5), 749–759. <https://doi.org/10.1016/j.cretres.2004.06.007>

- Roberts, E. M., O'Connor, P. M., Stevens, N. J., Gottfried, M. D., Jinnah, Z. A., Ngasala, S., Choh, A. M., & Armstrong, R. A. (2010). Sedimentology and depositional environments of the Red Sandstone Group, Rukwa Rift Basin, southwestern Tanzania: New insight into Cretaceous and Paleogene terrestrial ecosystems and tectonics in sub-equatorial Africa. *Journal of African Earth Sciences*, 57(3), 179–212. <https://doi.org/10.1016/j.jafrearsci.2009.09.002>
- Rosendahl, B. R., Reynolds, D. J., Lorber, P. M., Burgess, C. F., McGill, J., Scott, D., Lambiasi, J. J., & Derksen, S. J. (1986). *Structural expressions of rifting: lessons from Lake Tanganyika, Africa*. <https://www.lyellcollection.org>
- Semkiwa, P., Kalkreuth, W., Utting, J., Mayagilo, F., Mpanju, F., & Hagemann, H. (1998). The geology, petrology, palynology and geochemistry of Permian coal basins in Tanzania. 1. Namwele-Mkomolo, Muze and Galula coalfields. *International Journal of Coal Geology*, 36(1–2), 63–110. [https://doi.org/10.1016/S0166-5162\(97\)00020-7](https://doi.org/10.1016/S0166-5162(97)00020-7)
- Seyedrahi-Niaq, M., Doulati Ardejani, F., Noorollahi, Y., Jalili Nasrabadi, S., & Hekmatnejad, A. (2021). An unsaturated three-dimensional model of fluid flow and heat transfer in NW Sabalan geothermal reservoir. *Geothermics*, 89. <https://doi.org/10.1016/j.geothermics.2020.101966>
- Sircar, A., Shah, M., Dwijen Vaidya, ;, Sahajpal, S., Chaudhary, ; Anjali, & Dhale, S. (2015). Geothermal : Updates Overview of Geothermal Surface Exploration Methods. <https://www.researchgate.net/publication/317167510>
- Stern, R. J. (1994). Arc Assembly and Continental Collision in the Proterozoic East African orogen: Implications the Consolidation of Gondwanaland for. In *Annu. Rev. Earth Planet. Sci* (Vol. 22). www.annualreviews.org/online
- Sussman, D., Cumming, B., & Disclaimer, J. H. (2018). Enhanced Resource Modelling at Songwe for General Manager, *Tanzania Geothermal Development Company T74-D05*.
- Sutopo, Prabata, W., & Pratama, H. B. (2019). The development study of Karaha–Talaga Bodas geothermal field using numerical simulation. In *Geothermal Energy* (Vol. 7, Issue 1). SpringerOpen. <https://doi.org/10.1186/s40517-019-0139-2>
- SWECO. (1978). Reconnaissance of geothermal resources. In *Report for the Ministry of Water, Energy and Minerals of Tanzania, SWECO, Stockholm, Sweden and VIRKIR, Reykjavik, Iceland*.
- Tang, B., Zhu, C., Xu, M., Chen, T., & Hu, S. (2019). Thermal conductivity of sedimentary rocks in the Sichuan basin, Southwest China. *Energy Exploration and Exploitation*, 37(2), 691–720. <https://doi.org/10.1177/0144598718804902>
- Teklemariam, M. (2005). *Paper to be presented at Workshop for Decision Makers on Geothermal Projects and Management, organized by UNU-GTP and KengGen in Overview of Geothermal Resources Utilization and Potential in East African Rift System*.
- Theunissen, K., Klerkx, J., Melnikov, A., & Mruma, A. (1996). Mechanisms of inheritance of rift faulting in the western branch of the East African Rift, Tanzania. *Tectonics*, 15(4), 776–790. <https://doi.org/10.1029/95TC03685>
- Truesdell, A., & Jones, B. (1974a). WATEQ: A computer program for calculating chemical equilibrium of natural waters. *U.S. Geological Survey*, 2(2), 233–248.
- Truesdell, A., & Jones, B. (1974b). WATEQ: A computer program for calculating chemical equilibrium of natural waters. *U.S.G.S. J. Res*, 2, 233–248.
- Vereina, O. B. (2005). Numerical Modelling of the Natural State of the Mutnovsky Geothermal Reservoir (Kamchatka, Russia). In *Proceedings World Geothermal Congress*.
- Wilson, S. (1961). pH of natural hydrothermal solution. *Geochimica et Cosmochimica Acta*, 25, 233–235.
- Yang, F., Wang, M., Feng, J., Zhang, Y., Zhang, D., Feng, D., & Lu, T. (2022). A study on modeling a deep sand geothermal field in South China. *Energy Reports*, 8, 794–803. <https://doi.org/10.1016/j.egyr.2022.02.046>

ACKNOWLEDGEMENTS

I would like to express my deepest gratitude to my promotor Prof.dr. Giovanni Bertotti, Prof. dr. David Bruhn and Dr. Maren Brehme for their exceptional guidance, unwavering support and insightful feedback throughout my PhD journey. I would also like to express my gratitude to Dr. Alexandros Daniilidis who generously offered knowledge, expertise and invaluable feedback during my PhD journey. I also could not have undertaken this journey without my defence committee Prof. dr. Phil Vardon, Prof.dr. Hans de Bresser, Prof.dr. Sebastian Geiger and Dr. Elisante Mshiu who generously provided knowledge and expertise.

Special thanks to my fellow researchers Sitti Nur Asnin and Epiphania Mutabazi for their valuable collaboration, discussions and technical assistance that were essential in the success of this research.

I wish to express my gratitude to my family and friends for their unwavering love, encouragement and understanding throughout this challenging process.

Additionally, this endeavour would not have been possible without generous support from the Netherlands Government who sponsored my research through the NUFFIC Tanzania-Dutch Energy Capacity Building project (NICHE-TZA-260). I am grateful to Dr. Dinand Alkema who facilitated the finances, Dr. Robert Hack and Prof. Dr. Freek van der Meer, who were instrumental for the success of the project. I am also grateful to Energi Simulation represented by Dr. Maren Brehme at ETH Zurich by the support for this study through access to equipment and essential resources that made my research possible.

To all those who contributed in any way to this thesis, I extend my sincere thanks.

CURRICULUM VITAE

Martha Phineas NNKO

13-01-1982 Born in Ulanga, Tanzania

EDUCATION

1996-1999 Certificate of Secondary Education
Kifungilo Secondary School, Lushoto, Tanzania

2000-2002 Advanced Certificate of Secondary Education
Msalato Secondary School, Dodoma, Tanzania

2003-2007 Bachelor of Science in Electromechanical Engineering
University of Dar es Salaam, Tanzania

2008-2010 Master of Science in Engineering Management
University of Dar es Salaam, Tanzania

2018-2025

Doctor of Philosophy

Delft University of Technology, Netherlands

Thesis: Predicting temperature patterns and flow behaviour of
poorly constrained geothermal fields: the case of Songwe
extensional basin (Tanzania)

Promoters: Prof.dr. G. Bertotti, Prof.dr. D. Bruhn, Dr. M. Brehme

PROFESSIONAL EXPERIENCES

2011-2013	Projects Engineer, Power generation projects Tanzania Electric Supply Company, Dar es Salaam, Tanzania
-----------	---

2014-2017 Assistant lecturer, Mechanical & Industrial Engineering
Department, University of Dar es Salaam, Tanzania

